Université de Montréal

Les vésicules extracellulaires dérivées de plaquettes améliorent la fonction lymphatique

Par

Laurent Vachon

Département des Sciences Biomédicales, Faculté de Médecine

Mémoire présenté en vue de l'obtention du grade de Maîtrise en Sciences (M.Sc.) Biomédicales, option Sciences Cardiovasculaires

Août 2021

Université de Montréal

Département des Sciences Biomédicales, Faculté de Médecine

Ce mémoire intitulé

Les vésicules extracellulaires dérivées de plaquettes améliorent la fonction lymphatique

Présenté par

Laurent Vachon

A été évalué(e) par un jury composé des personnes suivantes

Guillaume Lettre
Président-rapporteur

Catherine Martel
Directrice de recherche

Davide Brambilla
Membre du jury

Résumé

Les plaquettes sont essentielles au développement lymphatique dès l'embryogenèse et maintiennent la séparation lympho-sanguine au cours de la vie. Elles participent directement à la lymphangiogenèse et à la réparation des vaisseaux en plus d'améliorer l'intégrité lymphatique *in vitro*. En présence d'apolipoprotéine A-I (apoA-I), les plaquettes consolident les connexions intercellulaires en adhérant à l'endothélium lymphatique. Toutefois, les plaquettes sont absentes de la lymphe, contrairement à leurs vésicules extracellulaires (pEVs) exprimant un protéome similaire. De plus, leur concentration dans la lymphe s'accentue en condition d'inflammation chronique, par exemple lors de l'athérosclérose. En ayant caractérisé les effets de ces vésicules sur l'intégrité lymphatique durant ma maîtrise, nous montrons que les pEVs sont rapidement internalisées par les LECs et aident à préserver l'intégrité lymphatique des effets délétères des constituants de la lymphe tels que les EVs dérivées des globules rouges (rbEVs). *In vitro*, des concentrations physiologiques de pEVs limitent la production d'espèces réactives d'oxygène (ROS) et diminuent la nécrose des cellules. Comme les pEVs injectées dans le derme de la peau sont prises en charge par les cellules endothéliales des vaisseaux lymphatiques collecteurs et qu'elles voyagent jusqu'aux ganglions afférents, nous croyons qu'une partie des pEVs circulantes dans la lymphe serait cruciale pour le maintien d'une fonction lymphatique adéquate lors de maladies chroniques inflammatoires telles que l'athérosclérose.

Mots-clés : vésicules extracellulaires, plaquettes, globules rouges, lymphe, cellule endothéliale lymphatique, dysfonction lymphatique, athérosclérose.

Abstract

Platelets have a protective role in lymphatic function both at the embryogenic stage and throughout life by maintaining blood-lymphatic separation. In addition, platelets enhance the integrity of lymphatic endothelial cells (LECs) *in vitro* and appear to exert a shielding effect on the lymphatic endothelium by consolidating the connexion between lymphatic endothelial cells when incubated with apolipoprotein A-I (apoA-I). Whereas platelets are absent from lymph, platelet extracellular vesicles (pEVs) are abundantly circulating within lymphatic vessels, and their level increases during chronic inflammation such as atherosclerosis. Having characterized their effect on lymphatic integrity during my Master internship, we show that pEVs are rapidly internalized by LECs, which in turn help preserve the integrity of the lymphatic endothelium when harmful blood constituent such as red blood cell EVs (rbEVs) are infiltrating lymph. *In vitro*, physiological concentrations of pEVs are limiting the production of reactive oxygen species (ROS) by lymphatic endothelial cells and decreasing their necrosis rate. Furthermore, pEVs injected in the skin interstitium travel through the collecting lymphatics and are rapidly internalized by LECs, which in turn might help preserve the integrity of the lymphatic endothelium. Lymph pEVs might be critical for the maintenance of a proper lymphatic function during chronic inflammatory settings such as atherosclerosis.

Keywords : Extracellular vesicles, platelet, red blood cells, lymph, lymphatic endothelial cells, lymphatic dysfunction, atherosclerosis.

Table des matières

Liste des figures

Liste des sigles et abréviations

ABCA1/ABCG1 : *ATP-binding cassette transporter A1/G1*

ADCY9 : adénylate cyclase 9

ADP : adénosine diphosphate

APC : cellule présentatrice d'antigène

Apo: apolipoprotéine

ATP : adénosine triphosphate

LECs : cellules endothéliales lymphatiques

CMH : complexe majeur d'histocompatibilité

CETP : protéine de transfert des esters de cholestérol

eNOS : *endothelial NO synthase*

ESCRT : complexe de tri endosomal requis pour le transport

FITC : *fluorescein isothiocyanate*

GWAS : *genome-wide association study*

HDL : lipoprotéine de haute densité

HDL-C : lipoprotéine de haute densité avec cholestérol

IL : interleukine

LCAT : *lecithin-cholesterol acyltranferase*

LDL : lipoprotéine de basse densité

LDLR : récepteur aux lipoprotéines de basse densité

LPS : lipopolysaccharides bactérien

LRP : protéine associée aux récepteurs des lipoprotéines de basse densité

MCV : maladies cardiovasculaires

mRCT : transport inverse du cholestérol des macrophages

NK : cellule tueuse naturelle

NO : oxyde nitrique

NTA : *nanoparticle tracking analysis*

OVA : ovalbumine

PAMP : motif moléculaire associé aux pathogènes

PE : phényléphrine

PEG : polyéthylène glycol

PS : phosphatidylsérine

pEVs : vésicules extracellulaires dérivées de plaquettes

rbEVs : vésicules extracellulaires dérivées des globules rouges

ROS : espèces réactives d'oxygène

SR-B1 : *scavenger receptor class B type 1*

SEM : microscopie électronique à balayage

TEM : microscopie à transmission d'électrons

TNFα : *tumor necrosis factor alpha*

EVs : vésicules extracellulaires

VEGF : *vascular endothelial growth factor*

VLDL : lipoprotéine de très basse densité

Remerciements

J’aimerais d’abord remercier ma directrice, Dre **Catherine Martel**, de m’avoir accueilli à bras ouverts dans son laboratoire et pour m’avoir accompagné lors de mes balbutiements en recherche à l’hiver 2019. Son soutien, sa générosité et sa joie de vivre ont rendu mon parcours inoubliable. Merci pour toutes les opportunités et pour m’avoir toujours encouragé.

Merci à mes collègues et amis, **Amal Deis**, **Damien Garçon**, **Gabriel Jean**, **Maya Farhat**, **Nada Amri**, **Nolwenn Tessier**, **Stéphanie Jarry** et **Rémi Bégin** pour m’avoir appris tant de choses et prêté main forte dans les jours les plus laborieux.

Je remercie mes parents extraordinaires, **Nancy Rousseau** et **André Vachon** ainsi que mes frères **Philippe** et **Nicolas Vachon** pour leur amour et soutien inconditionnel. Merci également à mes chères grands-mères **Suzanne Prince** et **Rita Baillargeon** et feus grands-pères **Gaëtan Vachon** et **Jean-Claude Rousseau** de m’avoir toujours aimé et supporté.

Je ne serais pas qui je suis aujourd’hui sans mes amis de longue date **Jérémy Pelletier** et **Marc-André Brossard**. Vous m’avez appris la résilience et avez su me donner la motivation qu’il me fallait à travers votre amitié.

Merci à **Marie Dubeau** d'avoir su comment semer le bonheur en moi, pour m’avoir accompagné dans les moments les plus sombres, pour m’avoir aimé inconditionnellement et sans qui je ne serais pas la meilleure version de moi-même.

Enfin, je remercie **Dr Guillaume Lettre et Dr Davide Brambilla** pour avoir accepté de faire partie du comité de révision et pour le temps qu’ils consacrent à la correction du mémoire.

Chapitre 1 : INTRODUCTION

1. Introduction

1.1 Le système lymphatique

Développé parallèlement au système vasculaire sanguin durant la lymphangiogenèse, le système lymphatique est présent dans la majorité des organes incluant le cerveau, longtemps considéré comme une exception au réseau lymphatique conventionnel[1,2].

Possédant trois grandes fonctions, le système lymphatique est d'abord au cœur de la réponse immune. La lymphe transportant antigènes, bactéries, vésicules extracellulaires (EVs) et cellules immunes jusqu'aux ganglions, le système lymphatique permet la migration des cellules immunes et la modulation de la réponse immunitaire par le transfert d'antigènes aux cellules dendritiques et via l'activation des lymphocytes T[3]. Les cellules dendritiques périphériques expriment davantage le récepteur de chimiokines CCR7 après la rencontre avec un motif moléculaire associé aux pathogènes (PAMP), augmentant la réponse du ligand CCL21 produit par les cellules endothéliales lymphatiques (LECs)[4,5]. Les cellules dendritiques et autres cellules présentatrices d'antigènes (APC) voyagent ensuite aux ganglions et activent les lymphocytes T débutant ainsi la réponse immune adaptative. L'apport continu d'antigènes aux cellules T naïves permet également l'éducation des cellules T et le maintien de la tolérance périphérique[6].

Le système lymphatique est essentiel à l'homéostasie des tissus. Le réseau récolte d'abord l'ultrafiltrat plasmatique à travers des capillaires via des jonctions communicantes et propulse ensuite la lymphe jusqu'aux ganglions via des vaisseaux lymphatiques collecteurs équipés de jonctions serrées et bordés des cellules musculaires lymphatiques contractiles (Figure 1)[7,8]. Ces cellules musculaires lymphatiques sont constituées de cellules musculaires lisses et striées, mais une récente étude propose une dérive unique de certaines cellules musculaires lymphatiques, distincte des voies de différenciation des cellules progénitrices connues[9,10]. Les cellules musculaires lymphatiques assurent la propulsion de la lymphe par des contractions intrinsèques[4]. La propulsion des fluides interstitiels via ce système également constitué de valves permet un flux

unidirectionnel et le retour de la lymphe en circulation sanguine prévenant ainsi la formation d'œdème[11].

Dans l'intestin, les capillaires lymphatiques aussi appelés lactéaux sont présents dans les villosités intestinales et permettent l'absorption des vitamines liposolubles et des lipides intestinaux tel que le cholestérol sous forme de chylomicrons[8,12]. Une fois la lymphe déversée en circulation sanguine, les chylomicrons sont rapidement pris en charge par le foie via le récepteur aux lipoprotéines de basse densité (LDLR) et leurs protéines associées (LRP)[13]. Ces lipides hépatiques peuvent ensuite se conjuguer aux apolipoprotéines pour former les lipoprotéines essentielles au transport des lipides dans le plasma, soit le HDL, le LDL, les IDL et les VLDL[14].

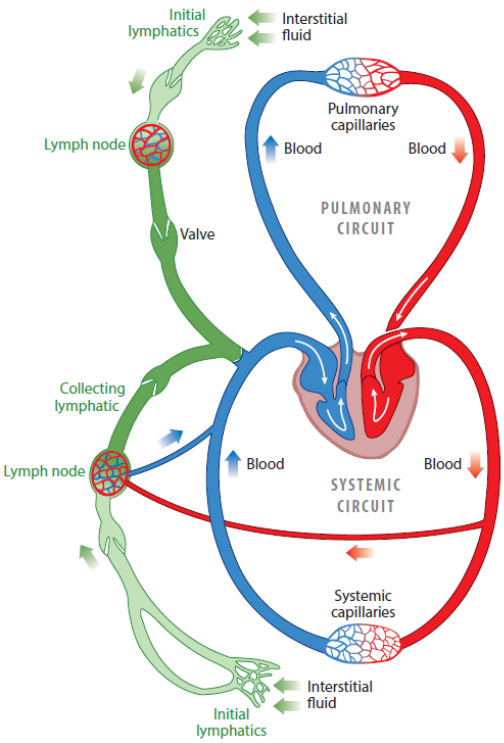

Figure 1 : Le système lymphatique

Les capillaires lymphatiques initiaux absorbent l'ultrafiltrat plasmatique. La lymphe est ensuite propulsée jusqu'aux ganglions par les vaisseaux lymphatiques collecteurs, munis de valves et de cellules musculaires lymphatiques permettant un flux unidirectionnel. La lymphe retourne en circulation sanguine via la veine sous-clavière. (Adapté de Moore et al. Annu Rev Fluid Mech. 2018 1;50 :459-482)[7]

1.2 Le transport inverse du cholestérol

L'intérêt scientifique marqué pour le système lymphatique dans les dernières années a également permis l'identification du rôle essentiel des vaisseaux lymphatiques dans le transport inverse du cholestérol des macrophages (mRCT) permettant notamment le retrait du cholestérol présent dans les lésions athérosclérotiques[15].

Le mRCT implique la lipoprotéine de haute densité (HDL) ainsi que sa composante principale l'apolipoprotéine A-1 (apoA-1). Afin de capter le cholestérol, cette-dernière peut interagir avec les macrophages via les récepteurs *ATP-binding cassette transporter A1* (ABCA1), ABCG1 ou *scavenger receptor class B type 1* (SR-B1)[16]. Une fois le cholestérol transféré, la molécule de HDL porte le nom de HDL-cholestérol (HDL-C) et convertit le cholestérol en ester de cholestérol via l'enzyme *lecithin-cholesterol acyltranferase* (LCAT)[17]. Le HDL-C retourne ainsi au foie où il est pris en charge par les récepteurs SR-B1 du foie[18]. D'une part, les esters de cholestérol sont désestérifiés pour excrétion dans la bile et les selles[18]. D'autre part, le HDL-C hépatique peut être pris en charge par la protéine de transfert des esters de cholestérol (CETP) permettant le transfert des esters de cholestérol du HDL-C vers les lipoprotéines contenant l'apolipoprotéine B (apoB). Parmi ces lipoprotéines, on y retrouve entre-autre la lipoprotéine de basse densité (LDL) ainsi que la lipoprotéine de très basse densité (VLDL)[18].

Comme le HDL en circulation sanguine est connu pour mobiliser le cholestérol hors de la paroi des vaisseaux sanguins via le mécanisme du mRCT, la concentration de HDL est importante pour un transport efficace[16]. L'augmentation des niveaux de HDL sanguin ainsi que la diminution des niveaux de LDL via l'inhibition du CETP devaient ainsi théoriquement pouvoir traiter l'athérosclérose[19]. Cependant, son inhibition pharmacologique via des molécules telles que le Torcetrapib ou le Dalcetrpib n'a pas permis de diminuer la survenue d'accidents cardiovasculaires[20,21]. Ce n'est que quelques années plus tard que des études *genome-wide association study* (GWAS) ont permis de démontrer l'efficacité de la molécule Dalcetrapib chez une certaine partie de la population présentant un polymorphisme du gène de l'adénylate cyclase 9 (ADCY9)[22].

En 1981, Dr Lemole proposait que l'un des facteurs critiques dans l'apparition de l'athérosclérose était la lymphostase[23]. Il a depuis été démontré dans ce sens que le cholestérol contenu dans la plaque athérosclérotique ne peut être mobilisé sans une fonction lymphatique appropriée[15]. En effet, en 2013 Martel et al. ont montré via un modèle de transplant d'aorte et de cholestérol tritié que l'inhibition par un antagoniste de la voie du *vascular endothelial growth factor receptor 3* (VEGFR3) empêchait la repousse des vaisseaux lymphatiques de l'aorte et la sortie du cholestérol hors de la plaque[15]. Cette voie singulière du mRCT démontre que les capillaires lymphatiques situés dans l'adventice des vaisseaux sanguins guident le HDL-C hors de la plaque athérosclérotique jusqu'au foie pour sa prise en charge et son excrétion. Une dysfonction du système lymphatique pourrait donc être à l'origine du développement de la maladie.

1.3 La dysfonction lymphatique

Les cellules endothéliales lymphatiques expriment les récepteurs VEGFR-2 et VEGFR-3 liant le VEGF-C et le VEGF-D en circulation. Plus spécifiquement, le VEGF-C et le VEGF-D possèdent de très longues séquences N- et C-terminales qui doivent être clivées pour activation[24]. Très similaire au VEGF-C au niveau moléculaire, le VEGF-D lie davantage le VEGFR-2 possédant la double fonction de promouvoir à la fois l'angiogenèse et la lymphangiogenèse[25]. Cependant, les souris déficientes en VEGF-D ne développent aucun phénotype lymphatique particulier, témoignant donc de l'absence d'implication majeure du facteur dans le développement du système lymphatique murin[26]. Quant au VEGF-C, il est spécifiquement impliqué dans le processus de lymphangiogenèse par liaison à son récepteur VEGFR-3, de sorte que les souris déficientes en VEGF-C ou en VEGFR-3 ne sont pas un modèle viable en raison de l'incapacité des vaisseaux lymphatiques à migrer et à proliférer[27,28].

Une mutation du domaine tyrosine kinase du VEGFR-3 est à l'origine de la maladie de Milroy, considérée comme l'un des tout premiers cas de lymphœdème congénital répertorié[29]. Le lymphœdème occasionne un mauvais drainage de l'ultrafiltrat plasmatique et l'accumulation de fluide dans les tissus mous. Ce dernier peut apparaître sous deux formes. La forme primaire est d'étiologie génétique et peut être présente à la naissance ou apparaître plus tard au cours de la

vie[30]. La forme secondaire est la cause la plus répandue d'œdème et peut être due à une obstruction ou à un dommage des vaisseaux lymphatiques, notamment lors d'une chirurgie[31].

Un phénotype opposé à celui de la maladie de Milroy, soit une surexpression du VEGFR-3 ou de ses ligands, cause une lymphangiogenèse accrue et peut être observé lors de cancers ou en conditions inflammatoires. Par exemple, une augmentation de la lymphangiogenèse apparaît dans un modèle murin de cancer ovarien, mais ces vaisseaux ne sont toutefois pas fonctionnels[32]. De manière similaire, la maladie de Crohn est une maladie intestinale inflammatoire auto-immune caractérisée par une lymphangiogenèse accrue et notamment associée à une dysfonction de l'activité contractile des vaisseaux lymphatiques[33,34].

Il a également été rapporté que la fonction lymphatique est affectée dans les modèles de souris hypercholestérolémiques déficientes en apolipoprotéine E, un modèle très étudié pour le développement de plaque athérosclérotique dans les artères[35]. Les facteurs de risques prédisposant à l'athérosclérose comme l'âge et une diète riche en gras continue ont également été associés à un défaut des vaisseaux lymphatiques collecteurs, soulignant l'importance de ces vaisseaux dans les maladies inflammatoires chroniques[36,37]. Ce n'est que récemment qu'il a été démontré à l'aide d'un modèle de souris $Ldlr^{-/-}$;$hApoB100^{+/+}$ que cette dysfonction lymphatique n'était non seulement pas dépendante des niveaux de cholestérol circulant, mais qu'elle apparaissait également avant les premiers signes de lésion athérosclérotique[38]. De plus, la dysfonction observée touche initialement les vaisseaux lymphatiques collecteurs sans changer la capacité d'absorption de l'ultrafiltrat plasmatique des capillaires lymphatiques initiaux[38]. Le traitement de ces souris avec un agoniste du VEGFR-3, soit le VEGF-C 152s a également permis de restaurer la fonction lymphatique et de prévenir la formation de plaque athérosclérotique via la stimulation des contractions lymphatiques[39].

Similairement, les souris athérosclérotiques *Ldlr*$^{-/-}$ traitées avec l'apoA-I ont également une fonction lymphatique améliorée et une réduction de la perméabilité[40]. *In vitro*, l'apoA-I permet une meilleure adhésion des plaquettes à l'endothélium lymphatique humain. Cette action permettrait de renforcer les jonctions intercellulaires tout en limitant l'agrégation plaquettaire *ex vivo*, ce qui permettrait non seulement de limiter la dysfonction lymphatique, mais également les

évènements thrombotiques[40]. Comme les plaquettes ne circulent pas dans la lymphe, mais que leurs vésicules extracellulaires sont bien présentes, ces dernières pourraient ainsi réguler l'intégrité et la fonction lymphatique[41].

1.4 Les vésicules extracellulaires

Les vésicules extracellulaires (EVs) sont des vésicules dotées d'une enveloppe lipidique sécrétées par toutes les cellules dans l'espace extracellulaire[42]. Elles ont comme principale fonction la communication intercellulaire reposant sur le contenu varié de leur cargo contenant lipides, protéines et acides nucléiques[42]. On regroupe les EVs en trois principales catégories, soit les exosomes, les microvésicules et les corps apoptotiques. Ces classifications se distinguent par leur processus de biogenèse, leur voie d'excrétion, leur taille, leur contenu et leur fonction[43]. Toutefois, la distinction entre les différentes catégories d'EVs reste difficile en pratique, notamment puisque la variation de la composition en protéines membranaires entre les différentes classifications reste mal comprise[42,44].

Les EVs sont produites en conditions physiologiques, mais également en conditions pathologiques, puisque leur production est régulée par le micro-environnement extracellulaire. La production s'active en condition d'hypoxie, de stress oxydatif, d'apoptose, de sénescence et d'inflammation[45,46]. On retrouve les EVs dans plusieurs fluides corporels comme le sang et la lymphe et leur implication dans le processus de communication intercellulaire est bien connue particulièrement dans les maladies cardiovasculaires ou les cancers[41,47]. Leur cargo complexe (ADN, ARNm, ARN non codant, lipides, protéines, protéases et nucléases) et leur capacité à réguler les processus physiologiques font des EVs de potentiels biomarqueurs diagnostiques remarquables.

1.4.1 Les exosomes

Les exosomes sont en fait des vésicules intraluminales issues du bourgeonnement interne de la membrane endosomale lors de la formation d'endosomes multivésiculaires riches en cholestérol[48,49]. Ils sont excrétés par les cellules une fois la fusion de l'endosome avec la surface de la cellule complétée (figure 2). La biogenèse des exosomes peut également impliquer la

machinerie du complexe de tri endosomal requis pour le transport (ESCRT)[48,50]. L'implication du ESCRT confère à ces vésicules un protéome particulier qui inclut des tétraspanines tels que CD9, CD63 et CD81 qui peuvent également être exprimés par d'autres types d'EVs[48,51]. Les exosomes arborent également certaines protéines plus conservées comme Tsg101, Alix, HSP70, HSP90 indépendamment de leur origine cellulaire[42,52]. D'un diamètre approximatif de 30 à 100 nm, les exosomes forment la plus petite catégorie de vésicules extracellulaires[48,53]. L'origine cellulaire mais également le micro-environnement sont des facteurs déterminant quant à la fonction des exosomes. Notamment, des exosomes dérivées de cellules soumises à un stress oxydatif peuvent générer un signal protecteur inhibant le stress oxydatif et la mort des cellules réceptrices[54,55]. Dans les cancers, les exosomes peuvent à la fois favoriser la progression de la tumeur ou activer une réponse antitumorale. Par exemple, des exosomes du cancer du sein peuvent différencier des cellules souches mésenchymateuses dérivées du tissu adipeux en myofibroblastes participant à l'angiogenèse de la tumeur [56,57]. À l'opposé, des exosomes de cancers pancréatiques ou de carcinomes hépatocellulaires peuvent contenir protéine appelée Hsp70 pouvant directement activer les cellules tueuses naturelles (NK) initiant l'apoptose de cellules tumorales[58,59].

1.4.2 Les microvésicules

Les microvésicules, aussi connues sous le nom d'ectosomes, ont un diamètre allant de 100 à 1000 nm et sont produites par les cellules en conditions physiologiques[53]. Cette production de microvésicules est augmentée en conditions d'hypoxie, de stress oxydatif, de dommage cellulaire ou d'inflammation[45,60,61]. Ces vésicules sont formées via le bourgeonnement de protrusions cytoplasmiques suivi par la scission de la membrane (figure 2)[45]. Le processus de formation est initié par un influx calcique intracellulaire amenant le détachement des protéines membranaires du cytosquelette. Il est suivi par un remodelage du cytosquelette par le clivage du réseau d'actine[45]. Suivant l'influx de calcium, les microvésicules se séparent de la membrane plasmique au niveau des radeaux lipidiques (calvéole) et peuvent exprimer à leur surface la phosphatidylsérine (PS) via l'activation de floppase, flippase et scramblase contrôlant l'asymétrie des phospholipides[45]. La PS n'est toutefois pas un marqueur ubiquitaire des microvésicules, puisqu'il a été démontré que certaines microvésicules ne le présentent pas à leur surface[45,62,63]. Par exemple, il est connu que les plaquettes puissent produire deux populations d'EVs distinctes,

exprimant ou non la PS[64,65]. En effet, une induction de la floppase et une inhibition de la flippase augmente la translocation de la PS à la surface des vésicules[66]. Une inhibition des récepteurs P2Y12 impliqués dans la liaison de l'adénosine diphosphate (ADP) et la sensibilité d'activation des plaquettes aux autres agonistes par la molécule ticagrelor permet d'inhiber la production de pEVs présentant la PS[65]. Ces dernières seraient davantage impliquées dans l'inflammation et le processus de coagulation[64,67]. Ainsi, inhiber la production de pEVs présentant la PS aurait des bienfaits antithrombotiques et anti-inflammatoire[64,67].

1.4.3 Les corps apoptotiques

Les corps apoptotiques possèdent un diamètre allant de 1 à 5 µm (Figure 2). Générées à partir de cellules apoptotiques, ces vésicules longtemps considérées comme des débris cellulaires ont un cargo varié pouvant entre autres inclure des organelles[53]. Les premières étapes de formation débutent avec la pycnose (condensation de la chromatine) suivie par la caryorrhexie (fragmentation du noyau) et la distribution aléatoire du contenu cytoplasmique dans les corps apoptotiques en formation[68]. Les corps apoptotiques une fois relâchés dans le milieu extracellulaire sont rapidement phagocytés par les cellules voisines ou les macrophages, prévenant la nécrose secondaire[69,70]. Impliqués dans le transfert horizontal de l'ADN, les corps apoptotiques sont aussi connus pour leur rôle dans la régulation de l'inflammation, de l'auto-immunité et des cancers[71,72]. Les corps apoptotiques peuvent en théorie avoir un effet plus important sur les cellules réceptrices vis-à-vis des autres types d'EVs de par leur large bagage moléculaire.

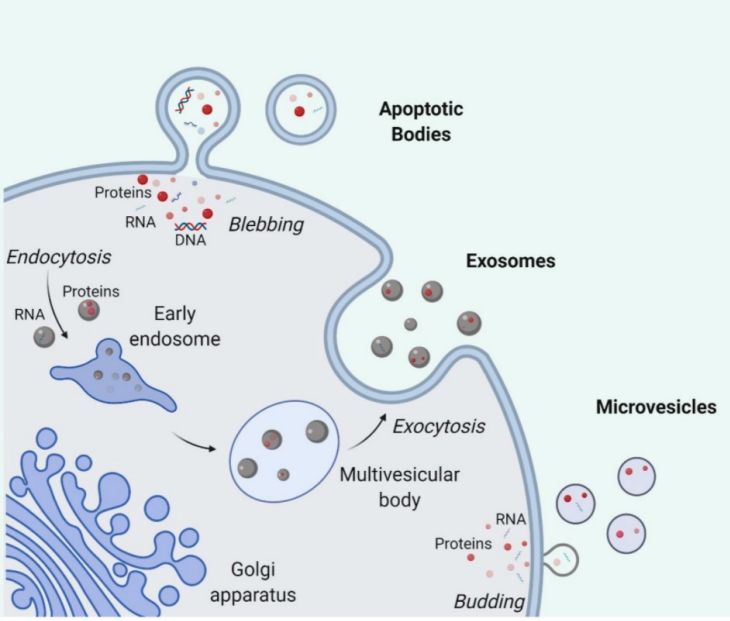

Figure 2 : Biogenèse des vésicules extracellulaires

Les exosomes (30-100 nm) sont formés via le bourgeonnement interne de la membrane endosomale pendant la formation de corps multivésiculaires puis sont relâchés par sa fusion avec la membrane. Les microvésicules (100-1000 nm) sont produites par le bourgeonnement de protrusions cytoplasmiques suivi par une scission de la membrane. Enfin, les corps apoptotiques (1 à 5 µm) sont générés lors de l'apoptose des cellules. Leur contenu est varié et riche en protéines, lipides et acides nucléiques. (Adapté de Dang et al. Cells 2020, 9(10), 2191)[73]

1.5 Isolation et caractérisation des EVs

Le potentiel énorme des EVs comme biomarqueurs est toutefois contrebalancé par les difficultés rencontrées lors de l'isolation et de la caractérisation. Plusieurs méthodes d'isolation ont vu le jour, telles que l'isolation par centrifugations différentielles qui consiste à éliminer les contaminants du surnageant par plusieurs séries de centrifugations à des vitesses croissantes jusqu'à une ultracentrifugation permettant de récolter les vésicules[74]. Cette méthode reste peu couteuse, n'implique pas l'ajout de composés chimiques et permet d'isoler une grande quantité d'EVs.

L'immunoprécipitation est une autre méthode qui consiste à faire passer les EVs à travers des billes magnétiques exprimant un anticorps retrouvé à la surface des EVs[75]. Cette technique est sélective, mais peut être couteuse. Sa grande spécificité peut également présenter un désavantage et faire perdre une partie des EVs d'intérêt qui n'exprimerait pas le marqueur ciblé.

L'isolation par précipitation au polyéthylène glycol (PEG) comme le système ExoQuick (System Biosciences) ou encore par ajout de composés chimiques comme les solvants organiques permet de réduire la solubilité des EVs par la présence de polymères super-hydrophiles (PEG) et d'en récolter le précipité par centrifugation à basse vitesse[76]. Cette technique est couteuse et présente des contaminations de protéines.

Enfin, pour ne nommer que ces quelques exemples, les technologies microfluidiques permettent de diriger un flux dans des appareils munis de microcanaux capables de séparer et purifier des échantillons. Ces appareils munis de structures poreuses ou d'anticorps permettent une isolation rapide avec une grande pureté, mais cette technologie reste couteuse et complexe[77]. Aucune technique n'est parfaite et chacune présente certains avantages et désavantages.

La caractérisation des EVs est également complexe et présente certains défis particulièrement liés à la petite taille des vésicules. Toutefois, la caractérisation des EVs par taille et par catégorie (exosomes, microvésicules ou corps apoptotiques) peut être importante puisque ces vésicules peuvent présenter des fonctions différentes en raison de leur biogenèse et de leur contenu distincts. Une autre caractéristique importante des EVs à vérifier est leur intégrité, puisque certaines EVs peuvent être endommagées à la suite de cycles de gel et dégel et ainsi perdre leur efficacité[78]. La caractérisation des EVs via ses antigènes de surface par cytométrie en flux peut également permettre de retracer l'origine cellulaire et de mieux comprendre l'étiologie d'une maladie, par exemple dans le cas d'inflammation systémique[79]. De plus, la caractérisation peut permettre de déterminer la concentration d'EVs présentent et ainsi déterminer s'il y a eu une induction de relâche d'EVs relative à un stress.

Avec l'utilisation contradictoire des différentes classifications de vésicules extracellulaires et des termes associés en recherche, des lignes directrices ont été émises (*Minimal Information for Studies of Extracellular Vesicles* (MISEV)) par la Société internationale des vésicules

extracellulaires (ISEV) afin d'uniformiser et de renforcer l'étude des EVs[80]. Ainsi, il est recommandé d'employer le terme vésicule extracellulaire au sens large et de référer à leurs caractéristiques physiques telles que la taille, la densité ou autre en plus de caractériser les EVs par de multiples techniques complémentaires.

Par exemple, la cytométrie en flux à haute résolution est une technique qui permet d'analyser et de caractériser des EVs de populations hétérogènes via des anticorps fluorescents spécifiques pour en déterminer la taille, la concentration et l'expression de marqueurs. La cytométrie permet ainsi de déterminer l'expression des protéines de surface et l'origine cellulaire en plus de distinguer les EVs des contaminants et artéfacts[79].

Le *Nanoparticle Tracking Analysis* (NTA) est une autre technique qui permet de mesurer la taille et la concentration des échantillons. Basé sur le principe du mouvement Brownien et utilisant un laser mesurant la vélocité des particules avec l'équation de Stokes-Einstein, le NTA présente toutefois quelques limitations[76,81]. En effet, il reste impossible de distinguer différents types de particules dans une population hétérogène. De plus, il existe une grande variation interinstruments pour de mêmes paramètres donnés dans le même logiciel d'analyse[81].

Permettant de produire une image amplifiée d'un échantillon d'EVs, la microscopie à transmission d'électrons (TEM) permet la caractérisation de la taille, de la morphologie et de la pureté de l'échantillon complémentairement aux autres techniques[82]. Cette technique peut également être couplée au marquage de récepteurs spécifiques avec un anticorps associé à une particule d'or et permet de révéler le phénotype des EVs[82]. Similairement, la microscopie électronique à balayage (SEM) permet de visualiser la topographie des vésicules[83].

1.6 Les EVs dans l'inflammation chronique

Le contenu biologique et l'interaction complexes des EVs avec les cellules réceptrices en font des joueurs clés dans l'inflammation chronique. Les cellules présentatrices d'antigènes (APC) tels que les cellules dendritiques, les macrophages et les lymphocytes B régulent directement la réponse immune via les récepteurs CD4 et CD8 des cellules T et NK[84]. D'autres protéines membranaires telles que le complexe majeur d'histocompatibilité (CMH) de classe I et II, CD80, CD86 ou les molécules d'adhésion comme ICAM régulent également la fonction immune via les APC[84]. Comme

les exosomes et les microvésicules dérivées des APC présentent à leur surface un protéome similaire à celui de leur cellule hôte, elles peuvent ainsi moduler l'activité des lymphocytes T à distance[84,85]. Par exemple, des EVs exprimant CMH II isolées de sérum de souris immunisées contre l'ovalbumine peuvent inhiber la réponse immune spécifique à l'ovalbumine suivant une administration orale ou intradermale de la protéine[86,87]. Ces évidences démontrent que les EVs endogènes dérivées de APC ont principalement une fonction inhibitrice vis-à-vis de la réponse immune. Ces interactions avec les antigènes endogènes et exogènes sont essentielles quant à la prévention de l'inflammation chronique et auto-immune.

D'autres sources d'EVs endogènes peuvent également réguler négativement la réponse immune. Par exemple, les EVs dérivées des trophoblastes chez les souris gestantes sont connues pour réduire la sévérité de l'encéphalite auto-immune chez un modèle de souris atteintes de la sclérose en plaques [88]. Similairement, il est connu que les EVs sériques de femmes en gestation peuvent réduire l'activation des cellules T[88]. De plus, les EVs dérivées de cellules souches mésenchymateuses peuvent aussi réduire le stress oxydatif et aider à la survie du myocarde dans un modèle d'ischémie/reperfusion chez la souris[55].

Les EVs endogènes n'ont toutefois pas uniquement que des fonctions bénéfiques. L'interaction des EVs dérivées de l'endothélium vasculaire est en étroit équilibre avec les EVs dérivées des cellules immunes. L'état inflammatoire de l'endothélium affecte la composition et la concentration des EVs sécrétées. Par exemple, les EVs dérivées de cellules quiescentes d'un endothélium vasculaire peuvent réduire la réponse pro-inflammatoire de macrophages activés par les lipopolysaccharides bactériens (LPS), en partie via le transfert de miARN10a inhibant la voie de signalisation du NF-kB[89]. À l'opposé, dans un environnement inflammatoire les EVs dérivées de l'endothélium vasculaire promeuvent l'angiogenèse via le transfert de miARN aux péricytes, augmentant la production de VEGF et amenant ainsi un remodelage vasculaire pathogénique[90]. En circulation sanguine, le rôle crucial des EVs dérivées des plaquettes, leucocytes, cellules endothéliales et autres a été étudié abondamment vis-à-vis de l'activation immune, endothéliale vasculaire et des cellules musculaires lisses[91]. Toutefois, le rôle de la circulation lymphatique dans le transport de ces EVs fait surface et témoigne de leur importance dans les processus immuns physiologiques et pathologiques. Par exemple. Tessandier et al.

montrent que dans un modèle murin d'arthrite inflammatoire auto-immune, les EVs dérivées des plaquettes s'accumulent dans le liquide synovial des articulations via la lymphe[92].

1.7 Les EVs dans la lymphe

Contrairement à la plupart des cellules, les EVs peuvent circuler dans la lymphe. Considérant le rôle primordial du système lymphatique dans la réabsorption de l'ultrafiltrat plasmatique, la présence d'EVs dans la lymphe est attendue et devrait refléter la composition plasmatique en EVs. En effet, il a récemment été démontré que les vésicules extracellulaires dérivées des plaquettes (pEVs) circulent dans la lymphe et sont plus abondantes lors de l'arthrite inflammatoire[92]. Similairement, la lymphe de souris athérosclérotique arbore de très grandes concentrations d'EVs, notamment dérivées des plaquettes et des globules rouges (rbEVs)[38]. L'augmentation des taux d'EVs plasmatiques circulantes pourrait expliquer l'augmentation des concentrations d'EVs lymphatiques, toutefois d'autres EVs de diverses origines peuvent également se retrouver dans la lymphe[93].

Les vaisseaux lymphatiques collecteurs sont généralement incorporés au tissu adipeux, notamment au niveau du cœur, de l'aorte, de la peau ou des intestins[94-97]. Le tissu adipeux périphérique produit des EVs dérivées de macrophages et d'adipocytes connues pour jouer un rôle dans l'inflammation[98,99]. Sachant que le tissu adipeux et les cellules immunes qu'il contient affectent la fonction lymphatique, il serait probable que les EVs dérivées de ces cellules puissent interagir avec les cellules musculaires ou endothéliales lymphatiques et ainsi moduler l'intégrité des vaisseaux[100,101].

Peu importe l'origine des EVs et l'étiologie de leur entrée dans la lymphe, des EVs qui régulent négativement la fonction et la clairance lymphatique pourraient à leur tour accentuer l'accumulation des vésicules et mener à une dysfonction lymphatique affectant les vaisseaux lymphatiques collecteurs précédant le développement de l'athérosclérose[41].

1.7.1 Les EVs dérivées des plaquettes

Impliquées dans la réponse immune innée et adaptative, la thrombose et l'hémostase, les plaquettes jouent aussi un rôle clé dans la différenciation du système lymphoveineux lors de

l'embryogenèse via l'interaction de CLEC-2 des plaquettes avec la podoplanine des LECs[102-104]. Une étude montre également que les plaquettes améliorent l'intégrité de l'endothélium lymphatique *in vitro* potentiellement via leur adhésion à l'endothélium[40]. Relâchant le VEGF-C via leurs granules alpha, les plaquettes activées participent également à la lymphangiogenèse et à la réparation des vaisseaux lymphatiques[105].

De récentes études chez l'humain montrent que plus de la moitié des EVs en circulation sanguine sont dérivées des plaquettes[106-108]. Produites lors de l'activation des plaquettes, les pEVs peuvent exprimer certains marqueurs des plaquettes tels que CD31, CD41, CD42a, P-sélectine, PF4 et GPIIb/IIIa[109]. Les pEVs sont connues pour jouer un rôle important dans la communication intercellulaire notamment dans la réparation tissulaire, l'angiogenèse, la lymphangiogenèse, la coagulation, l'inflammation et l'athérosclérose[105,108,110-112]. Les bienfaits des pEVs ont été mis en évidence entre autres via leurs pouvoirs anti-apoptotiques, anti-inflammatoires, proangiogénique et prolifératif[110,113,114]. Toutefois, les mécanismes spécifiques par lesquels les pEVs exercent leurs effets restent à éclaircir. Le miR-126-3p enrichi dans les plaquettes, par exemple, est impliqué dans la régénération tissulaire et pourrait être un effecteur clé des pEVs[115].

Les pEVs peuvent toutefois avoir des effets mitigés dans le maintien de l'intégrité endothéliale qui pourrait s'expliquer par la variabilité de leur composition et du contenu biologique de leur cargo. Il a été rapporté d'un côté que les pEVs augmentaient la perméabilité endothéliale sanguine[63]. D'un autre côté, les pEVs protègeraient les microvaisseaux de la thrombine connue pour affecter la perméabilité endothéliale[116]. Sachant que les plaquettes ne sont pas présentent en circulation dans la lymphe, mais que les pEVs sont abondantes dans la circulation sanguine et dans la lymphe de souris athérosclérotiques, la présence de ces vésicules pourrait ainsi affecter le maintien de la fonction et de l'intégrité lymphatique associé à l'athérosclérose[41].

1.7.2 Les EVs dérivées des globules rouges

Les globules rouges sont les particules les plus abondantes en circulation sanguine[117]. Avec la sénescence des globules rouges, les réserves d'adénosine triphosphate (ATP) s'épuisent provoquant une augmentation de la concentration de calcium intracellulaire causée par la baisse d'activité des pompes calciques membranaires provoquant ainsi la relâche de vésicules

extracellulaires dérivées de globules rouges[118]. Les rbEVs peuvent aussi être produites entre autres lorsque lors de l'érythropoïèse ou lorsque les globules rouges sont soumis à des forces de cisaillements[119].

Ces vésicules sont enrichies en diacylglycérol, cholestérol, phosphatidylsérine, CR1, CD55, CD59, acétylcholinestérase et CD235a[120]. Elles favoriseraient notamment la coagulation, participeraient à l'inflammation, au stress oxydatif et induiraient l'activation des cellules endothéliales par un mécanisme de récupération de l'oxyde nitrique (NO), aggravant ainsi la dysfonction endothéliale et l'athérosclérose[121,122].

Dans la plaque athérosclérotique, l'hémoglobine des rbEVs peut être transformée en méthémoglobine ou en ferrylhémoglobine et ainsi capturer le NO présent, aggravant la réponse inflammatoire de l'endothélium sanguin via l'oxydation du LDL[123]. La méthémoglobine peut ensuite réagir avec le H_2O_2 et générer des radicaux endommageant la membrane cellulaire, augmentant sa perméabilité et facilitant l'adhésion des monocytes[123,124]. Les rbEVs exprimant la phosphatidylsérine peuvent aussi interagir avec les macrophages et les cellules de Kupffer générant des anions superoxydes et activant les voies pro-inflammatoires via NFkB et c-Jun entraînant la production de *tumor necrosis factor alpha* (TNFα) et d'interleukine-6 (IL-6) ainsi que la surexpression de VCAM-1 à la surface des cellules endothéliales sanguines[122,125]. Enfin, les rbEVs transportant l'hème peuvent la transférer aux cellules endothéliales sanguines provoquant la production d'espèces réactives d'oxygène (ROS) et l'apoptose *in vivo*[126,127].

L'implication de rbEVs dans la dysfonction endothéliale sanguine est maintenant bien connue et ces dernières sont présentes en plus forte concentration chez les patients développant des maladies cardiovasculaires comme l'infarctus du myocarde avec segment ST élevé[128]. Sachant que la biodisponibilité du NO et des ROS régulent étroitement les contractions des vaisseaux lymphatiques collecteurs, il est ainsi probable que ces vésicules soient également liées à la dysfonction lymphatique associée à l'athérosclérose de par leur implication dans le stress oxydatif et la récupération du NO[129,130].

Considérant que la dysfonction lymphatique empêche un transport inverse du cholestérol efficace associé au développement de l'athérosclérose, la présence de grandes concentrations de

pEVs et de rbEVs dans la lymphe et le sang pourrait aider à comprendre la pathologie et à développer de nouveaux biomarqueurs. Des résultats préliminaires laissent croire que les pEVs peuvent adhérer à l'endothélium lymphatique, limiter la production de ROS et la nécrose des LECs. En contrepartie, les rbEVs augmentent la production de ROS chez les LECs et les amènent à relâcher davantage d'EVs. Les pEVs et les rbEVs pourraient plasmatiques ainsi être absorbés par les capillaires lymphatiques et moduler l'intégrité lymphatique en maintenant ou en altérant respectivement l'intégrité des vaisseaux collecteurs. L'altération pourrait potentiellement affecter la capacité contractile des vaisseaux et ainsi mener à l'accumulation d'EVs dans la lymphe comme il a été observé chez les souris athérosclérotiques[131].

1.8 Résumé des connaissances :

- Le système lymphatique participe à la mobilisation du cholestérol hors de la plaque athérosclérotique
- Le système lymphatique joue un rôle primordial dans l'apparition et l'exacerbation des maladies cardiovasculaires
- Une dysfonction lymphatique est présente avant l'apparition d'une lésion athérosclérotique
- Cette dysfonction lymphatique touche initialement les vaisseaux collecteurs sans affecter la capacité d'absorption des capillaires initiaux
- Le mécanisme à l'origine de cette dysfonction est inconnu, mais les vésicules extracellulaires présentent dans la lymphe pourraient affecter l'intégrité et le transport lymphatique
- Les pEVs et les rbEVs sont présents dans la lymphe de souris saines et en grande concentration dans la lymphe des souris athérosclérotiques
- Les rbEVs peuvent altérer la biodisponibilité du NO essentiel pour la régulation des contractions lymphatiques et pourraient être néfastes
- Les Plaquettes sont impliquées dans la lymphangiogenèse et leurs EVs pourraient maintenir l'intégrité lymphatique

1.9 Hypothèses et objectifs de l'étude :

Nous posons l'hypothèse que les pEVs et les rbEVs pourraient être impliquées dans le maintien et la dysfonction lymphatique associée à l'athérosclérose et jouer un rôle clé dans son développement.

Objectifs :

- Produire et caractériser des pEVs et des rbEVs à partir de sang de patients sains
- Vérifier l'internalisation *in vitro* des EVs dans les cellules endothéliales lymphatiques humaines
- Déterminer les effets des pEVs et des rbEVs sur l'intégrité des cellules endothéliales lymphatiques *in vitro*
- Vérifier la prise en charge et l'internalisation des EVs *in vivo* par le système lymphatique
- Évaluer les effets des pEVs et des rbEVs sur la fonction lymphatique

Chapitre 2. Résultats

Article en préparation pour *Journal of Extracellular Vesicles*

Platelet extracellular vesicles enhance lymphatic function

Vachon L.[1,2], Jean G.[1,2], Tessier N.[1,2], Bégin R.[1,2], Amri N.[1,2], Villeneuve L.[2], Guadarrama Bello D., Garçon D.[1,2], Milasan A.[1,2], Boilard E., Gendron P., Ruiz M., Rak J., Nanci A., Martel C.[1,2]

1. Department of Medicine, Faculty of Medicine, University of Montreal, Montreal, Québec, Canada
2. Montreal Heart Institute, Montreal, Quebec, Canada
3. Bioinformatics Core Facility, Institute for Research in Immunology and Cancer (IRIC), Université de Montréal, Montreal, Quebec, Canada.

Catherine Martel, PhD

Montreal Heart Institute Research Center

5000, Belanger Street, room S5100

Montreal, Quebec (Canada)

H1T 1C8

Telephone: (514) 376-3330 #2977

E-mail: catherine.martel@icm-mhi.org

Abstract:

Platelets have a protective role in lymphatic function both at the embryogenic stage and throughout life by maintaining blood-lymphatic separation. In addition, platelets enhance the integrity of lymphatic endothelial cells (LECs) *in vitro*. Pseudopodia-shaped platelets appear to exert a shielding effect on the lymphatic endothelium by consolidating the connections between lymphatic endothelial cells. Whereas platelets are absent from lymph, platelet extracellular vesicles (pEVs) are abundantly circulating within lymphatic vessels, even in the absence of inflammation. Chronic inflammation increases access of pEVs to lymph but in contrast to platelets *per se*, these lymph pEVs do not readily contribute to coagulation. Here, we show that pEVs are rapidly internalized by LECs, which in turn might help preserve the integrity of the lymphatic endothelium when harmful blood constituents such as red blood cell EVs (rbEVs) infiltrate lymph. *In vitro*, physiological concentrations of pEVs are limiting the production of reactive oxygen species (ROS) by lymphatic endothelial cells and decreasing their necrosis rate. As pEVs injected in the skin interstitium travel through the collecting lymphatic vessels and are either uptaken by lymphatic endothelial cells or continuing their path in lymph to reach the draining lymph nodes, we hypothesize that a specific subset of lymph pEVs might be critical for the maintenance of a proper lymphatic transport during chronic inflammatory diseases such as atherosclerosis.

Keywords: Extracellular vesicles, platelet, red blood cell, lymph, lymphatic endothelial cell, lymphatic dysfunction, inflammation.

Word count: 12 935 words

INTRODUCTION

Until recently, platelets were mostly studied for their key role in hemostasis. In the past decades, these anucleate cells derived from megakaryocytes have been shown to have a protective role in lymphatic function both at the embryogenic stage and throughout life (1-3). Carrying vascular endothelial growth factor-C (VEGF-C) in their alpha granules, activated platelets are crucial during lymphangiogenesis and lymphatic repair (4). VEGF-C/VEGF receptor-3 (VEGFR-3) signalling plays key roles during multiple stages of lymphatic vascular development and subsequent lymphatic transport. Although VEGFR-3 is initially expressed in both blood and lymphatic endothelial cells (BECs and LECs, respectively), it becomes restricted to LECs in embryos at 12.5 days postcoitus during mouse embryogenesis (5). Importantly, the departure of lymphatic endothelial progenitor cells from the embryonic veins is dependent on VEGF-C (6). VEGF-C binding was shown to lead to VEGFR-3 autophosphorylation (7) and transduces signals that promote LEC survival, proliferation, and migration (8, 9). Treatment of a mix of both blood and lymphatic endothelial cells with a VEGFR-3-specific ligand, VEGF-C 156s, led to phosphoinositide 3-kinase (PI3K)- dependent phosphorylation of Akt and protein kinase C (PKC)-dependent activation of mitogen-activated protein kinase (MAPK) (8). Further, VEGF-C/VEGFR-3 binding to LECs induces activation of PI3K/Akt and results in phosphorylation of P70S6K, PLCγ1, Erk1/2 and endothelial nitric oxygen species (eNOS) (10), thus regulating the pumping activity of collecting lymphatic vessels (11). When injected before the administration of a pro-atherogenic regimen with VEGF-C 152s, an analogue of VEGF-C 156s that solely binds to VEGFR3, *Ldlr*$^{-/-}$ mice were protected from excessive plaque formation and in long-term, had a more stable plaque (12). The sustained contraction capacity of the collecting lymphatic vessels and the enhanced expression of VEGFR-3 and FOXC2 observed in the VEGF-C-152s-treated mice contributed to the clearance of harmful components contained in peripheral tissues such as the atherosclerotic lesion (12). Pseudopodia-shaped platelets would also be able to consolidate the interactions between neighbouring lymphatic endothelial cells (LECs) (13). They would exert a shielding effect on the lymphatic endothelium to help preserve the integrity of LECs when harmful blood constituents such as red blood cell extracellular vesicles EVs (rbEVs) infiltrate lymph.

The lymphatic system has a crucial role in the clearance of extravasated interstitial fluid and macromolecules from peripheral tissues (14). Lymph is thus rich in plasma ultrafiltrates, proteins, lipoproteins, immune cells and extracellular vesicles (EVs). EVs are membrane vesicles released by cells under physiological and pathological conditions and their production is regulated by the extracellular microenvironment (15, 16). In addition to expressing markers pertaining to their cell of origin, EVs transport diverse cargo such as RNA, lipids and proteins, ensuring intercellular communication in inflammatory and non-inflammatory settings (17). Whereas lymph is usually devoid of red blood cells and platelets, platelet EVs (pEVs) and red blood cell EVs (rbEVs) have been found to be abundant in the lymph of healthy mice (18). The access of these EVs to lymph is increased in atherosclerosis, a chronic inflammatory condition of the blood vessel wall (18). As EVs could be absorbed by lymphatics whereas their pertaining cells cannot, these findings suggest that EVs are most likely travelling through lymph as messengers to ensure cargo delivery to recipient cells or tissues that otherwise would not by accessible to some cells.

Red blood cells are the most abundant cells in circulation (19). With time, senescent or damaged red blood cells can produce extracellular vesicles (20, 21). Enriched with diacylglycerol, cholesterol, phosphatidylserine, CR1, CD55, CD59 acetylcholinesterase and CD235a, rbEVs have been shown to promote coagulation, inflammation, oxidative stress and induce endothelial cell activation by the scavenging of nitric oxide (NO) which exacerbate endothelial dysfunction and atherosclerosis (22-24). Within the atherosclerotic lesion for instance, the hemoglobin of rbEVs can undergo conformational changes promoting low-density lipoprotein (LDL) oxidation, generatiing reactive oxygen species (ROS) and damaging cell membrane while increasing permeability and monocyte adhesion (25, 26). Since the biodisponibility of NO and ROS tightly regulates lymphatic vessel contractions, rbEVs could be linked to lymphatic dysfunction associated with chronic inflammatory settings such as atherosclerosis due to their ability to scavenge NO and induce oxidative stress (27, 28).

In this manuscript, we show that pEVs can travel through the lymphatics and are rapidly internalized by LECs, which in turn might help preserve the integrity of the lymphatic endothelium. Lymph pEVs might be critical for the maintenance of a proper lymphatic function during chronic inflammatory settings where rbEVs are involved such as atherosclerosis.

METHODS

Production and isolation of human platelet and red blood cell extracellular vesicles

All experiments performed with human specimens were approved by the Montreal Heart Institute Ethic Committee (protocol #2016-2117) and every subject gave informed consent. Human blood from healthy donors was collected with a syringe containing an anticoagulant citrate dextrose (ACD, Sigma cat. #C3821) solution. Blood was transferred into 50 ml tubes (BD Falcon) and centrifuged at 282g for 10 minutes without brakes. Unless otherwise specified, all centrifugations were performed at room temperature. Platelet EVs were produced as described by Rousseau et al. (29). Briefly, the platelet-rich plasma (PRP) was harvested and 1/5 volume of acid citrate dextrose (ACD) and 1/50 volume of EDTA were added. The PRP was then centrifuged at 400g for 5 minutes and the supernatant was harvested and further centrifuged for 5 minutes at 1,300g. The supernatant was discarded, the pellet was resuspended in 2 mL of Tyrode's buffer (pH 6.5) and 13 mL of Tyrode's buffer (pH 7.4) were added to the homogeneous preparation of platelets. Platelets were counted and diluted at 100 x 10^6 platelets/ml with Tyrode's buffer (pH 7.4) containing 5 mM of $CaCl_2$. Next, platelets were stimulated for 2 hours with 0.5 Unit/ml of thrombin (from bovine serum, Sigma) at 37°C. Platelet activation was stopped by addition of 20 mM of EDTA and the preparation was centrifuged twice 10 minutes at 2,000g to eliminate any remnant platelets. The supernatant was collected and centrifuged for 90 minutes at 18,000g (18°C) in swinging buckets (rotor SW-55Ti, Beckman), the supernatant was discarded and the pellet containing pEVs was resuspended in 5 mL of Tyrode's buffer containing 5 mM of $CaCl_2$ (pH 7.4). Platelet EVs were aliquoted and stored at -80°C prior utilization. When fluorescent pEVs were required, human platelets were incubated in presence of CellVue™ Claret Far Red Fluorescent (Sigma cat. #MINClaret-1KT) according to the manufacturer's protocol before two consecutive centrifugations at 18 000 g for 90 min at 4 °C. Pellet was resuspended in 20 uL of 0.22 um-filtered phosphate buffer saline (PBS) 1X.

Red blood cell EVs were produced and isolated following the first blood centrifugation of 10 minutes at 282g, after the PRP and the buffy coat were removed (29). A total of 200 uL of the red blood cell fraction was incubated for 10 minutes with 50 mL of filtered double-distilled water. A volume of 5.5 mL of filtered-PBS 10X (Growcells cat. #75801-000) was added to stop the hypotonic reaction. Red blood cell EVs were then aliquoted and stored at -80°C until further use.

Nanoparticle Tracking Analysis

To determine the sizes of pEVs and rbEVs, Nanoparticle Tracking Analysis (NTA) was performed using a NanoSight LM10 with a 642 nm laser (Malvern Instruments Ltd, Malvern, UK), using software version 2.3, screen gain 4 and camera level 10. Three, 1-minute videos were recorded per sample diluted 1:20 in PBS with analysis screen gain 10 and detection threshold 4. Temperature ranged from 20 to 23.5 °C.

Scanning Electron Microscopy

Platelet and red blood cell EVs were incubated in a glutaraldehyde solution 2.5 % (v/v) for 30 minutes at 4°C and washed in PBS (0.1 M) pH 7.4. The pellet was incubated for 30 minutes in aqueous osmium tetroxide 1% at 4°C, followed by dehydration with graded ethanol (50% and 100%). Then, 10 µl of each sample were deposited on coverslips and allowed to dry. Samples were finally coated with 5 nm carbon using an EM ACE600 carbon coater (Leica Microsystems Inc., Canada). A Regulus 8220 ultrahigh-resolution field emission scanning electron microscope (Hitachi, Ltd., Japan) operated at 1 kV was used to observe the morphology of platelet and red blood cell EVs.

Lymphatic endothelial cell culture

Human dermal microvascular lymphatic endothelial cells isolated from adult donors (HMVEC-dLyAd) (Lonza cat. #CA10064-286) were cultured in Endothelial Cell Growth Media MV2

(Promocell cat. #10175-256) from passages 5 to 7. LECs were pretreated with or without recombinant human tumour necrosis factor alpha (TNF-α, 1 ng/mL) (R&D cat. #201-TA) in EV-depleted complete media for 24 hours prior treatment. The media was removed and pEVs ($1x10^6$/mL) and/or rbEVs ($2x10^6$/mL) were added in EV-depleted complete media for 24 hours. Following treatments, the supernatant was centrifuged for 5 minutes at 430g before being aliquoted and stored at -80°C for further analysis. LECs were washed with complete media and harvested using Tryspin EDTA (Fisher cat. #MT25052CI).

EVs internalization *in vitro*

Platelet ($1x10^6$/mL) and/or red blood cell ($2x10^6$/mL) EVs were stained with CFSE (eBioscience) and incubated on a confluent layer of LECs for 2, 16 or 24 hours in phenol-free and EV-depleted growth medium. LECs were washed with phenol-free and EVs-depleted medium and stained with wheat germ agglutinin (WGA, AF555, Thermo Fisher cat. #W32464) and DAPI (BioShop cat. #DAP444.5) for 7.5 minutes at 37°C. Live cells were washed three times with phenol-free and EVs-depleted medium before Confocal Microscopy imaging using an LSM 710 Confocal Microscope (Zeiss) equipped with a 63/1.4 oil dic objective. Z-stacks were deconvoluted with Huygens Professional (Scientific Volume Imaging, SVI, Netherlands) using a theoretical spread function (PSF).

Transwell permeability assay

LECs were seeded in Transwell inserts (0.4 um) (Corning cat. #3470 and Greiner Bio-one cat. #662640) in a 24-wells plate and treated with $1x10^6$ pEVs/mL, $2x10^6$ rbEVs/mL or both subtypes in phenol-free and EV-depleted medium for 24 hours. TNF-α (10 ng/mL) (R&D cat. #201-TA) was used as positive control of increased permeability. During cell culture and EV treatment, phenol-free and EV-depleted media was used on both sides of the insert. Permeability was assessed by the addition of ovalbumin (AF488) (50 ng/mL) (Invitrogen cat. #34781) for 20 minutes at room temperature followed by bottom-plate fluorescence reading with the plate reader Synergy 2.

Characterization of human lymphatic endothelial cells by flow cytometry

Samples were processed with a flow cytometer (BD FACSCelesta, BD Biosciences, San Jose, CA, USA) in the BVR12 configuration (4 Blue/3 red/5 Violet) equipped with a 20 mW blue laser (488 nm), a 40 mW red laser (640 nm), and a 50 mW violet laser (405 nm). LECs were stained with anti-VEGFR-3 (PE) (BioLegend cat. #356204), anti-LYVE-1 (Dylight 650 APC) (Invitrogen cat. #PA5-22782), anti-podoplanin (PerCP Cy5.5) (BioLegend cat. #337012) and anti-CD31 (APC Cy7) (BD Biosciences cat. #563653) antibodies (BD Biosciences cat. #563653), or with propidium iodide (PI, VWR cat. #89139-066) and Annexin V (BD Biosciences cat. #560506) in Annexin V binding buffer (10 mM Hepes pH 7.4, 140 mM NaCl, and 2.5 mM $CaCl_2$ (BD Biosciences cat. #556454)). Cells were then centrifuged at 430g for 5 minutes at 4°C and resuspended in the appropriate FACS buffer. Finally, in some instance, 4',6-diamidino-2-phenylindole 10 nM (DAPI, BioShop cat. #DAP444.5) was added to stain nuclear DNA before flow cytometry analysis.

Quantification of human platelet, red blood cell and lymphatic endothelial cell EVs by flow cytometry

For the EV analysis, the 450/40 bandpass filter (BV421, violet laser) was manually swapped after CS&T calibration with a 1 mm-thick magnetron sputtered 405/10 bandpass filter (Chroma Technology, Bellows Falls, VT, USA), which is referred herein as V-SSC. Platelet, red blood cell and lymphatic endothelial cell EVs were stained for 30 minutes at 37°C respectively with anti-CD62p (PE, Biolegend cat. #304906), anti-CD235a (BV786, BD Biosciences cat. #740984) or anti-VEGFR-3 (PE, Biolegend cat. #356204) antibodies in sterile polystyrene tubes (Falcon cat. #CA60819-820) in a 0.22 um-filtered buffer (10 mM Hepes pH 7.4, 140 mM NaCl, and 2.5 mM $CaCl_2$) containing 1 □M of a membrane dye carboxyfluorescein diacetate succinimidyl ester (CFSE, Thermo Scientific, Waltham, MA, USA) and 10 □M D-Phe-Pro-Arg-chloromethylketone (PPACK, Cayman Chemical, Ann Arbor, MI, USA). Count beads (Apogee Flow System cat. #1426) were added to determine the concentration of EVs according to the following calculation found in supplemental figure 1.

FACS plots and histograms are showing all parameters in height (indicated as –H), as recommended for EV detection (30). The flow cytometer was calibrated for EV detection using

the Apogee Mix (#1493, Apogee Flow Systems, Hemel Hempstead, UK), a mixture of non-fluorescent silica beads (180, 240, 300, 590, 880, and 1300 nm) and FITC-fluorescent latex beads (110 and 500 nm), and count beads. For EV analysis, events were acquired at a flow rate of 12 µL/minute, which is the lowest flow rate on the FACSCelesta. The flow rate during acquisition was kept to the minimum to avoid swarming effects and coincident detection (31). After acquisition, data analysis was performed with FlowJo v10.5 (Flowjo, Ashland, OR, USA).

Characterization of mouse plasma and lymph extracellular vesicle by flow cytometry

Plasma and lymph were collected from autologous 10 to 15 week-old anesthetized C57BL/6 wild-type mice as previously described (32) and centrifuged at 2,400g or 1,200g, respectively, for 10 minutes at 4°C. In sterile 5 mL polystyrene tubes (Falcon cat. #CA60819-820), plasma and lymph were incubated for 30 minutes at 37°C in a 0.22 µm-filtered Annexin binding buffer 1X (BD Biosciences cat. #556454) containing 1 µM CFSE (Thermo Scientific, Waltham, MA, USA) and 10 µM PPACK (Cayman Chemical, Ann Arbor, MI, USA). Count beads (Apogee Flow System cat. #1426) and with three different antibody panels to further characterize the EV membrane-bound markers (Panel 1: anti-mouse MHCI (BV711, BD Biosciences cat. #743539), CD45 (APC, BioLegend cat. #103112), CD41 (AF700) (BioLegend cat. #133925BLG), CLEC2 (PE, BioLegend cat. #146104), annexin V (PerCP Cy5.5, BioLegend), TER119 (BV510, BD Biosciences cat. #640936) and CD62p (BV605, BD Biosciences cat. #740358) ; Panel II: anti-mouse MHCI (BV711, BD Biosciences cat. #743539), CD45 (BV510, BD Biosciences cat. #563891), CD31 (APC, BioLegend cat. #102509), CD62e (BV605, BD Biosciences cat. #745251), Podoplanine (PeCy7, BioLegend cat. #127411BLG) and VEGFR3 (PE, R&D Systems cat. #FAB743P)). Panel III: anti-mouse MHCI (BV711, BD Biosciences cat. #743539), CD45 (APC, BioLegend cat. #103112), CD11c (PeCy7, Tonbo Biosciences cat. #10051-456), F4/80 (PE, BioLegend cat. #123109), CD3e (BV650, BD Biosciences cat. #564378), CD19 (BV510, BD Biosciences cat. #562956), LY6C (BV605, BD Biosciences cat. #563011), LY6G (PerCP Cy5.5, BD Biosciences cat. #560602) and CD11b (AF700, BioLegend cat. #101222); As mentioned above, count beads (Apogee Flow System cat. #1426) were added to each mix to determine the concentration of EVs and control samples were also assessed.

Acquisitions were made using a FSC-PMT-equipped FACSAria Fusion (BD Biosciences, San Jose, CA, USA) flow cytometer and a 405/10 bandpass filter for side scatter detection (V-SSC) and data analysis was performed with FlowJo v10.5 (Flowjo, Ashland, OR, USA).

Sorting of mouse plasma and lymph extracellular vesicle by flow cytometry

For EV sorting, plasma and lymph were collected from mice, processed and incubated with CFSE and anti-mouse MHCI antibody (BV711, BD Biosciences cat. #743539) as described above. $CFSE^{+}MHCI^{+}$ events included within the EV gate were sorted using a FSC-PMT-equipped FACSAria Fusion (BD Biosciences, San Jose, CA, USA) flow cytometer and a 405/10 bandpass filter. The sorted events represent total EVs of cellular origin. Again, the EV gate was set using the ApogeeMix and absolute concentrations were determined for each sample, which was aliquoted and kept in -80°C until further lipidomic and proteomic analysis as described below.

Untargeted lipidomic by liquid chromatography quadrupole time-of-flight mass spectrometry (LC-QTOF-MS)

Untargeted lipidomic analyses were performed at the Montreal Heart Institute (MHI) as previously described (33). Lipids were extracted from plasma (90µl), lymph (20 µl) or sorted EVs spiked with the following internal standards (Avanti Polar Lipids Inc): (monoacylglycerosphosphocholine (LPC) 13:0, diacylglycerophosphocholine (PC) 14:0/14:0 and 19:0/19:0, phosphatidylserine (PS) 12:0/12:0, diacylglycerophosphoethanolamine (PE) 17:0/17:0, and diacylglycerophosphoglycerol (PG) 15:0/15:0)). Samples (plasma 1.1 µl , lymph 5 µl , EVs from plasma 1.1 µl, EVs from lymph 5 µl) were injected into a high-performance liquid chromatograph (1290 Infinity HPLC, Agilent Technologies Inc)) coupled to a quadrupole time-of-flight mass spectrometry (6550 accurate system, Agilent Technologies Inc.) equipped with a dual electrospray ionization source and analyzed in both positive and negative mode. The lipid elution was carried out on a Zorbax Eclipse plus column (C18, 2.1 mm × 100 mm, particle size 1.8 µm, Agilent Technologies Inc.) for 83 min at a constant temperature of 40 °C using a gradient of solvent

A (0.2% formic acid and 10 mM ammonium formate in water) and B (0.2% formic acid and 5 mM ammonium formate in methanol/acetonitrile/methyl *tert*-butyl ether [MTBE], 55:35:10 [v/v/v]). Mass spectrometry data analysis was performed with the Mass Hunter Qualitative Analysis software package (version B.07) and a bioinformatics script develop at the MHI platform. Lipids of interest were identified using MS/MS analysis. Statistical qualitative analyzes were carried out by unpaired Student's t-test followed by Benjamini-Hochberg correction (lymph vs plasma) or without correction (EVs) with the program Mass Professional Pro version 12.6.1 (Agilent Technologies Inc.).

Proteomics

Samples were reconstituted in 50 mM ammonium bicarbonate with 10 mM TCEP [Tris(2-carboxyethyl)phosphine hydrochloride; Thermo Fisher Scientific], and vortexed for 1 hour at 37°C. Chloroacetamide (Sigma-Aldrich) was added for alkylation to a final concentration of 55 mM. Samples were vortexed for another hour at 37°C. One microgram of trypsin was added, and digestion was performed for 8 hours at 37°C. Samples were dried down and solubilized in 4% formic acid (FA). Peptides were loaded and separated on a home-made reversed-phase column (150 µm i.d. by 200 mm) with a 56 minutes gradient from 10 to 30% ACN-0.2% FA and a 600 nL/min flow rate on an Easy nLC-1000 connected to an Orbitrap Fusion (Thermo Fisher Scientific, San Jose, CA). Each full MS spectrum acquired at a resolution of 60,000 was followed by tandem-MS (MS-MS) spectra acquisition on the most abundant multiply charged precursor ions for a maximum of 3 seconds. Tandem-MS experiments were performed using collision-induced dissociation (CID) at a collision energy of 30%. The data were processed using PEAKS X Pro (Bioinformatics Solutions, Waterloo, ON) and a Uniprot mouse database (16977 entries). Mass tolerances on precursor and fragment ions were 10 ppm and 0.3 Da, respectively. Fixed modification was carbamidomethyl (C). Variable selected posttranslational modifications were oxidation (M), deamidation (NQ), phosphorylation (STY) along acetylation (N-ter). The qualitative data were visualized with Scaffold 4.0 (protein threshold, 99%, with at least 2 peptides identified and a false-discovery rate [FDR] of 1% for peptides).

Reactive Oxygen Species Production

Cells were seeded in 96 wells plates and stained with chloromethyl-dichlorodihydrofluorescein diacetate, acetyl ester (CM-H_2DCFDA) (10 µM) (Invitrogen cat. #C6827) for 30 minutes at 37 °C following Mahmoud et al. protocol (34). Upon cleavage by intracellular esterase and oxidation by ROS, the molecule becomes highly fluorescent. Its fluorescence intensity was measured using Synergy 2 plate reader every 1.13 minute for one hour. Intracellular ROS production was measured on LECs treated with EVs for 24 hours. The same procedure was used to measure ROS production by pEVs ($1x10^6$/mL) and rbEVs ($2x10^6$/mL) in PBS. Superoxide dismutase (100 U/mL) (Alfa Aesar cat. #AAJ630038PL) was used as a negative control.

Quantitative polymerase chain reaction

Total RNA was extracted from EVs-treated LECs kept in Ribozol™ (VWR cat. #97064-950) using PureLink™ RNA Mini Kit (Invitrogen cat. #12-183-018A) following the manufacturer's protocol. Briefly, RNA concentration was measured using NanoDrop™ 1000 Spectrophotometer (Thermo Fisher) and reverse transcription was done using a High-capacity cDNA Reverse Transcription Kit (Applied Biosystems cat. #4368814). Finally, the qPCR was performed using iTaq Universal SYBR Green Supermix (Biorad cat. #1725121) and QuantStudio™ 3 (Thermo Fisher). Primers are shown in table 1. Relative expression was calculated using comparative method ($2^{-\Delta\Delta CT}$) and normalized with beta-actin (B-act) as housekeeping gene.

RNA-sequencing

Following RNA extraction, EVs-treated LECs were also analyzed with Illumina next-generation sequencing at the Institute for Research in Immunology and Cancer (IRIC) Genomics Platform at the University of Montreal (Montreal, Quebec, Canada). Adaptor sequences and low-quality bases in the resulting FASTQ files were trimmed using Trimmomatic version 0.35 and genome alignments were conducted using STAR version 2.7.1a (35, 36). The sequences were aligned to the human genome version GRCh38, with gene annotations from Gencode version 37 based on

Ensembl 103. As part of quality control, the sequences were aligned to several different genomes to verify that there was no sample contamination. Gene expressions were obtained both as raw readcount directly from STAR as well as computed using RSEM in order to obtain gene and transcript level expression in reads per transcripts per million (TPM) for these stranded RNA libraries (37). DESeq2 version 1.22.2 was then used to normalize gene read counts and compute differential expression between the various experimental conditions. Sample clustering based on normalized log read counts produces a hierarchy of samples. A principal component analysis is also used to validate that samples correlate as expected (38).

EVs internalization *in vivo*

Ten-week-old C57BL/6 wild-type mice were anesthetized and injected with a 10 uL Hamilton syringe in the dermis on both sides of the right footpad for a total of 20 uL containing $1x10^7$ pEVs (or control PBS). Animals were sacrificed 2 hours after and popliteal lymphatic vessels were harvested for immunofluorescence analysis. Briefly, popliteal lymphatic vessels were collected and fixed with paraformaldehyde (4%) for 24 hours. Vessels were incubated overnight in donkey serum (5%) and stained with anti-human CD41a antibody (BD Biosciences cat. #561422) for 4 days at 4°C. Vessels were washed with PBS and incubated with the secondary antibody (Cy3, Jackson Immunoresearch cat. #115-165-003) for 2 hours at room temperature. Popliteal lymphatic vessels were then washed again with PBS and stained with DAPI (BioShop cat. #DAP444.5). Z-Stacks were acquired using an LSM 710 Confocal Microscope (Zeiss) equipped with a 63/1.4 oil dic objective.

Following the same injection protocol, but with CellVue™-stained pEVs (Sigma cat. #MINClaret-1KT), popliteal, inguinal and axillary lymph nodes were collected and incubated in collagenase D (Roche cat. #11088882001) for 25 minutes at 37 °C. Skin from the injection site was removed and digested in Liberase TM (1.75 mg/mL, Roche cat. #5401020001) for 55 minutes at 37°C. EDTA (100 mM, Fisher cat. #BP2482100) was added to stop the digestion. Cells were filtered through a 70 um cell strainer (Falcon cat. #352350) in HBSS (Corning cat. #CA-45000-458) and centrifuged at 430g for 10 minutes at 4°C. Finally, cells were resuspended in Hanks Buffer and stained for 30 minutes at 4°C with anti-mouse CD45 (FITC, Tonbo cat. #10050.902), anti-mouse MHCII (V450,

Tonbo cat. #10051.864) and anti-human CD62p (PE) (BioLegends cat. #304905) antibodies. In parallel, supernatant collected from lymph nodes and skin following tissue digestion was stained with anti-human CD62p antibody (AF700) (Labome cat. #304932) and CFSE (eBioscience cat. #65085-84) for 30 minutes at 37°C. All FACS analyses were performed by flow cytometry as described above (BD FACS Celesta, BD Biosciences).

Statistics

Data are expressed as mean ± standard error of the mean (SEM). Significance was calculated using paired T-test or ratio paired T-test using appropriate corrections in Prism™ 6.0. P-values <0.05 were considered statistically significant.

Results

The composition of EVs in lymph differs from that of plasma and might in turn exert diverse functions

EVs are absorbed by lymphatics whereas in some instance their pertaining cells cannot enter lymphatics (18). Thus, EVs appear to be travelling through lymph as messengers to ensure cargo delivery to recipient cells or tissues that otherwise would not by accessible to some cells. However, recent evidence suggests that the functional roles of these EVs might differ from one interstitial space to another (39). Our first step was thus to compare plasmatic and lymphatic EV content. Untargeted lipidomic analysis revealed that lipid composition in lymph differs from that of plasma (figure 1A). Among these, lysophosphatidylcholines (LPC, lysoPC), also called lysolecithins, were more abundant in plasma than lymph, whereas triglycerides were mostly found in lymph (figure 1C). To determine whether the transport of lipids occurs at least in part through EVs, we also performed untargeted lipidomics on EVs that had previously been sorted by flow cytometry (figure 1B). Further, our results revealed that LPC were upregulated in lymph EVs and phosphatidylcholine (PC) were rather upregulated in plasma EVs (figure 1D).

While rbEVs and pEVs are known to be present in mouse lymph (18), the relative concentration of EV subsets in each fluid in still understudied in healthy animals. Our results reveal that overall, wild-type animals carry more $MHCI^+$ EVs in their lymph compared to their plasma (Fig. 2AB). Among these, $CD41^+$ EVs appear to be weighing in the balance (Fig. 2CD), albeit $CD41^+CLEC\text{-}2^+$ EVs are inversely represented, being more concentrated in plasma (figure 2EF). Abundant in both plasma and lymph, the concentration of rbEVs was however unchanged between the two circulating systems (figure 2GH). EVs from endothelial origin also differ from one fluid to another. Although not statistically significant, we tend to observe more LEC-derived EVs in plasma and more HUVEC-derived EVs in lymph (figure 3CD and EF, respectively). Looking at EVs derived from immune cells, we find expectedly that most EVs are more abundant in lymph compared to plasma (Fig 4). The previous MHC I+ trend found in panel I seem to fade out here for males, explaining the significance for females only throughout the panel II (Fig. 4A). For female mice, our results so far suggest that $CD45^+CD3e^+$, $CD45^+CD11b^+$ EVs and MHCI+LY6G+ EVs are more concentrated in lymph than in plasma (figure 4CD, EF and GH respectively). Please note that explanations regarding non-statistically significative results are purely speculative.

To support our observations, preliminary proteomic analysis of both lymph and plasma protein content reveals protein clusters that could be explained by distinct EVs populations. Notably, histone proteins seem to be more abundant in lymph (Fig. 5D) seconding our flow cytometry results showing more neutrophil-derived EVs in lymph. Known to induce cytotoxic effect on erythrocytes, histone proteins could trigger rbEVs production in lymph in pathological conditions where LECs permeability allows red blood cell crossing, which could in turn worsen lymphatic integrity. Red blood cells are the most abundant cells in circulation (19). rbEVs have been shown to promote coagulation, inflammation, oxidative stress and induce endothelial cell activation by the scavenging of nitric oxide (NO) which exacerbate endothelial dysfunction and atherosclerosis (22-24). Since the biodisponibility of NO and ROS tightly regulates lymphatic vessel contractions, rbEVs could be linked to lymphatic dysfunction associated with chronic inflammatory settings such as atherosclerosis (27, 28).

Platelet and red blood cell EVs are internalized by LECs

Since we previously found that *Ldlr*$^{-/-}$ mice display lymphatic dysfunction before atherosclerosis lesion formation and had higher PLT-EVs and RBC-EVs concentrations in circulating lymph, we sought to investigate their effect on a lymphatic endothelium. We firstly had to produce PLT-EVs and RBC-EVs from healthy human blood. Following ISEV guidelines, we made sure of their integrity and purity by three distinct methods: Flow Cytometry, NTA and SEM (Fig. 6). In order to set an *in vitro* model, we incubated both stained EVs subtypes on LECs for different periods of time. Confocal microscopy revealed that the internalisation of both PLT-EVs and RBC-EVs (Green) within cell membrane (Red) was completed after 24 h of incubation (Fig. 7). These observations allowed us to set the incubation period of EVs on LECs at physiological concentration for following experiments.

Red blood cell EVs are harmful to the lymphatic endothelium

RBC-derived EVs produce a significant amount of ROS, even after addition of superoxyde dismutase (SOD) (Fig. 8A). Following a 24 h RBC-derived EVs incubation on LECs, ROS production by cells is significantly increased whereas it is significantly decreased following platelet-derived EVs incubation (Fig 8C-D).

EVs production by cells is a marker of stress. After incubation of physiological concentration of platelet-derived EVs and/or RBC-derived EVs for 24 h on LECs, supernatant was collected for LEC-derived EVs production analysis. Supernatant was spun down for cell debris cleaning and was stained with CFSE and VEGFR-3 in order to highlight LEC-derived EVs only. The addition of Count Beads allowed the assessment of LEC-derived EVs concentration. Physiological concentration of platelet-derived EVs had no effect on LEC-derived EVs production (Fig 9A) whereas the addition of RBC-derived EVs (Fig 9B) or both subtypes (Fig 9C) significantly increased LEC-derived EVs production. Once more, these results indicate that RBC-derived EVs seem to disrupt lymphatic endothelium integrity.

Platelet EVs decrease LEC ROS production and necrosis

In order to assess the effect of both EVs subtypes on LECs integrity, Reactive oxygen species (ROS) production was measured both by EVs alone and by LECs following incubation of physiological concentration of EVs. On the opposite, Platelet-derived EVs produce very few ROS and see their production reduced to none after SOD addition (Fig 8B). Following a 24 h RBC-derived EVs incubation on LECs, ROS production by cells is significantly increased whereas it is significantly decreased following platelet-derived EVs incubation (Fig 8C-D). Furthermore, Annexin/PI analysis after Platelet-derived EVs incubation on LECs reveals a significant decrease of cell necrosis (Fig 8F). Altogether, these results show a protective role of platelet-derived EVs and a disruptive role of RBC-derived EVs on the lymphatic endothelium.

Co-incubation of both platelet and red blood cell-derived EVs lowers LECs permeability

The assessment of LECs permeability by transwell allowed to measure the effects of EVs towards lymphatic cell junctions. The co-incubation of both p-rbEVs significatively lowered LECs permeability (Fig. 10C). When looking at the individual effect of rbEVs alone, we can see that despite mixed effects of rbEVs (Fig. 10B), the addition of pEVs seemed to tighten LECs junctions and decrease permeability. The co-incubation of p-rbEVs could potentiate pEVs adhesion on the lymphatic endothelium.

Lymphatic markers but not their mRNA are regulated by both platelet and red blood cell-derived EVs

In order to find how LECs integrity is regulated by both platelet and red blood cell-derived EVs, LECs membrane protein expression was examined by flow cytometry following EVs incubation for 24 h. Surprisingly, VEGFR3, LYVE-1 and CD31 protein expression were slightly upregulated after incubation of both EVs subtypes (Fig 11G-I) whereas their mRNA remained unchanged (Fig 12).

These data reveal a potential platelet-erythrocyte interaction. Furthermore, qPCR analysis reveals VCAM-1 mRNA downregulation in presence of PLT-RBC EVs (Fig 12C).

RNA-sequencing reveals hypoxia related genes regulation by red blood cell-derived EVs.

To better explain opposite effects of pEVs and rbEVs, LECs mRNA was sequenced following EVs treatment. As found previously by qPCR, pEVs do not seem to regulate mRNA expression in LECs (data not shown) supporting the hypothesis by which physical pEVs adhesion is beneficial. However, rbEVs seem to lower gene expression involved in hypoxia, such as MIR210HG and ANKRD37 (Fig 13), even when co-incubated with pEVs. This pathway could explain the observed harmful effects of rbEVs on LECs.

Platelet EVs are travelling to the lymphatics *in vivo*

With the aim of looking at EVs effects on lymphatic function, we began by injecting Cellvue™ stained human platelet-derived EVs in the dermis of the footpad of C57BL/6 mice. Immunofluorescent imaging revealed the presence of these EVs way up in the popliteal lymphatic vessel 2 h post injection (Fig 14A) compared to PBS controls (Fig 14B). In order to look at the uptake by the injection site and afferent lymph nodes, footpad skin and popliteal and inguinal lymph nodes were collected 15 min or 2 h following the intradermal injection of EVs or PBS. Axillary lymph nodes were collected as negative control. Flow cytometry revealed the presence of free EVs in popliteal and inguinal lymph nodes as soon as 15 min post injection and a significant increase after 2 h (Fig 15A). Free EVs were also recorded in the injection site, but no significant increase after 2 h was found (Fig 15B). EVs were also found in the injection site skin cells, with no significant increase after 2 h (Fig 15C). When looking at popliteal and inguinal lymph nodes cells, we found an uptake as soon as 15 min with a significant increase after 2 h (Fig 15D). Most cells containing stained EVs were found to express MHCII (Fig 15E-F), showing that most EVs present in afferent lymph nodes were brought by migratory cells. These results indicate that platelet-derived EVs can be uptaken by mice lymphatic system when found in plasmatic ultrafitrate and could modulate LECs integrity.

Discussion:

We herein report that lipidomic analysis also reveals that lymph is enriched in TG compared to plasma in C57BL/6 mice (Figure 1A). Of note, in these TG, the most abundant fatty acid is linoleic acid (18:2, LA). LA is the precursor of acid arachidonic (20:4, AA) as well as gammalinoleic acid (18:3, GLA) which is one abundant fatty acid present in the lymph too. Indeed, AA is known to be a crucial factor for platelet aggregation (40). Moreover, free AA and its metabolites promote and modulate type 2 immune response (41). AA metabolites can also have pro-inflammatory purposes and are equally known for their inflammatory-resolving activity (42). The overall abundance in lymph and implication of AA in the modulation of immune response concur with the main function of the lymphatic system.

Opposingly to TG, plasma is enriched in LPC compared to lymph in C57BL/6 mice (Figure 1A). In humans, plasma LPC reduction has been linked to obesity, type 2 diabetes, and cardiovascular diseases (43) as well as weight loss and activated inflammatory status in cancer patients (44). In lymph, LPC is crucial for intestinal lipid absorption (45). Interestingly in dogs, lymph LPC seems to increase with myocardial ischemia and LPC is found to accumulate in ischemic tissues (46). However, both the accumulation of LPC in ischemic tissue and plasma LPC reduction are linked to LPC increase in circulating LDL through phospholipase A-2 (PLA2) upregulation as reported in type 2 diabetes and cardiovascular diseases (47). Rich in LPC, oxidized LDL has been identified as a proinflammatory lipid involved in pathogenesis of atherosclerosis (48).

EVs are in part responsible for the circulating LPC discrepancy in mice (Figure 1B). As shown in Figure 1D, plasma EVs are enriched in LPC compared to lymph EVs. In activated cells such as activated erythrocytes and platelets, secretory PLA2 generates lysophosphatidic acid (LPA) in EVs membrane (49). Activating multiple signaling pathway in oxidative stress and inflammatory response, LPC and its derivative LPA might be key constituents of EVs derived from activated cells and responsible for lymphatic dysfunction (50). Figure 1D also shows phosphatidylcholine (PC) enrichment in lymph EVs compared to plasma EVs. Nothing surprising, since PC is the most abundant lipid in EVs membrane across numerous human cell lines (51). To back up these findings, we observe significantly more MHC I+ EVs in lymph by flow cytometry (Fig. 2AB). Thus,

the abundance of PC in lymph-derived EVs sorted with CFSE and MHC I could reflect MHC I+ EVs abundance. Notably, MHC I+ CD41+ EVs account for a great proportion of total EVs (Fig. 2 CD). Tessandier et al. showed similar pEVs concentration between lymph and plasma in C57BL/6 healthy mice (39). However, the addition of MHC I+ allows us to discriminate basophil population also expressing CD41 in mice (52). Platelets are known to stimulate lymphangiogenesis (4) and promote vasoregeneration after vascular injury (53). Milasan et al. also showed better lymphatic endothelium integrity after platelet adhesion in vitro (13). Nevertheless, the effects of pEVs on a lymphatic endothelium have been understudied.

On Figure 3, no statistical differences were found between endothelial cell-derived EVs distribution in lymph and plasma in healthy mice. Blood endothelial cell-derived EVs are important in both physiological and pathological conditions, as their phenotype varies. In hypoxic conditions, pro-apoptotic proteins are found in those EVs (54). In TNFα conditions, EVs produced from blood endothelial cells carry pro-inflammatory mRNAs (55). High concentration of those EVs could hereby suggest endothelial dysfunction. Still in TNFα conditions, lymphatic endothelial cell-derived EVs were found to guide migration of cancer cells and promote even more metastasis (56). Since lymphatic dysfunction occurs before the onset of atherosclerosis and LEC-derived EVs seem to promote cellular transport through lymphatics, these EVs could potentially help diagnose lymphatic dysfunction and atherosclerosis development.

When looking at immune cell-derived EVs, concentrations seem higher in female mice lymph compared to plasma (Fig. 4). Cancer-related studies also show the implication of immune cell-derived EVs in tumour metastasis promotion and differentiation (57). Since it was reported that tumour mediated factors are enriched in lymph compared to plasma in metastatic melanoma patients (58), it would have been expected to see an increase of basal immune cell-derived EVs abundance in lymph similarly to what is observed in chronic inflammatory diseases such as atherosclerosis or rheumatoid arthritis(18, 39). The absence of MHC I+ EVs statistical difference between lymph and plasma for male mice is reflected throughout the panel III (Fig. 3). However, since the same samples were used for panel I, similar results to female mice should be expected.

Proteomic analysis reveals the presence of extracellular histone proteins in lymph compared to plasma (Fig. 5D). Histones are known to induce cytotoxic effect on endothelial cells and erythrocytes once secreted by neutrophil, notably (59). LPS-activated macrophage can also produce histones-coated EVs (60). However, endothelial lymphatic cells constitutively express PTX3 (pentraxin 3) (61) known to protect against extracellular histone-cytotoxic effect (62). It might be possible that lymphatic system drains extracellular histones to counteract their deleterious effect on erythrocytes in order to avoid erythrocytes apoptosis and inhibits erythrocyte-derived extracellular vesicles secretion. Furthermore, extracellular histones promote thrombin generation through platelet activation (63). Once again, lymph fluid could drain extracellular histones to avoid deleterious effects from thrombin formation. It could also be possible that the histone proteins cluster found in lymph results from the abundance of neutrophil-derived EVs (Fig. 3GH).

In the light of our results, lipidomic analysis, specialized flow cytometry and preliminary proteomic analysis reveal no peculiar difference between plasma and lymph from healthy mice. However, similar experiments using atherosclerotic mice would give a better insight. Given our hypothesis in which pEVs might be beneficial for lymphatic integrity, their relative abundance in healthy mice lymph supports this premise. Since the amount of EVs found in lymph, notably pEVs and rbEVs, remarkably increases during lymphatic dysfunction associated with chronic inflammatory disease such as atherosclerosis (18), we sought to better define their effect on lymphatic function and integrity.

We firstly characterized pEVs and rbEVs produced from healthy human donors. Using BD FACSCelesta equipped with a 405 nm bandpass filter on the violet laser as side-scatter detector, we were able to assess the purity and concentration of our samples (Fig. 6AB) using the gating strategy shown in supplemental Figure 2. Nanoparticle Tracking Analysis (NTA) allowed us to determine the size distribution of pEVs and rbEVs (Fig. 6 CD). Finally, Scanning Electron Microscopy (SEM) once more attested for the size and purity of our sample, showing slightly smaller rbEVs compared to pEVs and supporting the NTA results (Fig. 6 EF).

The best EVs incubation time to use throughout the study seemed to be 24 h since both EVs subtypes were completely internalized, as shown by deconvoluted images in Figure 7. Similarly, French et al. use a 20 to 24 h incubation period for PLT-EVs but also show rapid interaction of PLT-EVs with megakaryocytes by confocal microscopy as early as 30 min after incubation (64). Correspondingly, Usman et al. show internalisation of RBC-EVs after 24 h in breast cancer CA1a cells (65).

We first showed that RBC-EVs produce ROS and induce ROS production in LECs (Figure 8 A and C) These results are not surprising, since RBC-EVs are known to promote excessive ROS production by neutrophils (66). In endothelial cells, RBC-EVs are associated with increase oxidative stress and can transfer free heme to the cell while also scavenging NO faster than erythrocytes, causing vasoconstriction and endothelial damage (22, 67). Since ROS production is linked with cell necrosis and apoptosis, RBC-EVs association with ROS at physiological concentration could have limited effect and explain the absence of apoptosis induction (Figure 8 E) (68). In a similar way, we found that RBC-EVs stimulate LECs-derived EVs production (Figure 9B). As elevated ROS levels are found in high EVs producing cells such as senescent or tumoral cells, it is likely that the pro-oxidant environment generated by RBC-EVs is involved in enhanced LECs-derived EVs production (69, 70). Permeability is also a good indicator of integrity. In figure 10 B, we see various effects of rbEVs depending on the donor and a clear trend, but no statistical significance. In atherosclerosis, the pathological concentrations of RBC-EVs might show adverse effect on LECs cell death. The use of an antioxidant could help show if the adverse effects of RBC-EVs are mediated by ROS.

Conversely, PLT-EVs reduced ROS production by LECs as well as cell necrosis (Figure 8 D and F). Interestingly, while PLT-EVs in septic individuals possess pro-apoptotic NADPH oxidase activity, we found no effect of PLT-EVs on LECs apoptosis (Sup Figure 3B) (71). Wang et al. showed that PLT-EVs mediate platelet activation and oxidative stress in atherosclerotic plaque in a CD36 and phosphatidylserine dependant matter (72). However, the blood and lymphatic endothelium are quite different, the latest expressing podoplanin able to interact with CD62p. Kitazume et al. reported the ability of CD31 homophilic interactions on LECs membrane to maintain vascular integrity and cell survival (73). Furthermore, PLT-EVs have been shown to prevent rat ostenonecrosis via Akt/Bad/Bcl-2 signaling pathways (74). Inhibition of ROS production but also

homophilic CD31 interactions could explain PLT-EVs ability to prevent cell necrosis (Figure 8F). Opposingly to RBC-EVs, PLT-EVs also did not alter LECs-derived EVs production (Figure 9A), showing no sign of threat to the lymphatic endothelium. These results show beneficial effects of pEVs on lymphatic integrity. Interestingly, even though LECs-derived EVs production is still increased after co-incubation of p-rbEVs (Fig. 9C), permeability assay shows a decrease of LECs permeability after treatment with both subtypes (Fig. 10C). These last results are not only indicating better integrity, but also a potential interaction between pEVs and rbEVs.

Platelet-erythrocyte aggregates were first found in patients with sickle cell anemia (75). Platelet-erythrocyte interactions can enhance CD62p expression and platelet aggregability via exposure of phosphatidylserine on erythrocytes (76). We found that CD31 expression is upregulated on LECs membrane after co-incubation of PLT-RBC EVs (Figure 11 I). Known for improving cell migration, survival and cell junction (77), the observed CD31 enhancement could be beneficial for the lymphatic integrity. Lymphatic markers VEGFR-3 and LYVE-1 also seemed to be upregulated in presence of PLT-RBC EV (Figure 11 G-H). Both respectively implicated in lympangiogenesis and leukocyte trafficking, VEGFR3 and LYVE-1 upregulation at physiological concentration of PLT-RBC EVs could also prove beneficial for lymphatic integrity (78, 79). Although, the presence of PLT-EVs did not seem to inhibit LECs-derived EVs production in presence of both EVs subtypes (Figure 9 C), the co-incubation of PLT-RBC EVs downregulated VCAM-1 (Figure 12 C). Important adhesion molecules in leukocyte recruitment and cellular immune response VCAM-1 inhibition could prevent inflammation (80). While qPCR (Figure 12) and RNA-sequencing did not reveal mRNA change for the corresponding proteins, the pathway surrounding results seems strictly mechanistic and could be justified by the potentiation of PLT-EVs interactions with LECs endothelium by platelet-erythrocyte interactions. Note that the qPCR effect on VCAM-1 is unseen in RNA-Sequencing and could be due to the fact that our qPCR have more statistical power. In plasma, miR-126 mainly derives from activated platelets and correlates with pEVs concentrations (81, 82). In blood endothelial cells, miR-126 regulates angiogenesis and vascular integrity by inhibiting VCAM-1 expression, inhibiting in turn leukocyte adhesion and inflammation (83, 84).

In terms of effect, EVs tend to have high variation between each donor as seen by flow cytometry, but the general tendency remains hence the use of ratio-paired T test for statistical analysis. Even though each donor was considered healthy, donors age ranged between 18 and 40 years old and many other factors could explain variations. This disparity allowed to pin-point two key genes continuously regulated in LECs by EVs using RNA-sequencing analysis, no matter the donor. RNA-sequencing results were also confirmed by qPCR (Sup. Fig. 4). RBC-EVs downregulated MIR210HG, a long non-coding RNA potentiating the metabolic transcription factor hypoxia-inducible factor 1a (HIF-1a) and upregulating the expression of glycolytic enzymes (85). MicroRNA such as MIR210 can also mediate HIF-1a regulation via ROS (86). In our case, under normoxia, studies have found that ROS seem to stabilize HIF-1a (87-89). In a similar way, NO has also been shown to stabilize HIF-1a by impairing its degradation (90, 91). According to our RNA-sequencing data, the resulting outcome of two opposing forces (ROS production and NO scavenging) by RBC-EVs leads MIR210HG to downregulation. MicroRNA directly transferred by RBC-EVs could also target MIR210HG. However, HIF-1a is essential for angiogenesis and induces the transcription of genes regulating cell proliferation and survival (92). Also implicated in VEGF-C expression and lymphangiogenesis, HIF-1a inhibition by RBC-EVs via downregulation of MIR210GH could in turn alter lymphatic function (93). MIR210HG is also highly expressed in cancers such as invasive breast cancer and osteosarcoma where its overexpression facilitates cell invasion and migration via the epithelial-mesenchymal transition pathway (94, 95). However, RBC-EVs incubation on LECs did not alter cell migration via scratch assay (Sup Figure 5B).

Co-incubation of PLT-RBC EVs on LECs also downregulated MIR210HG expression as well as ANKRD37. ANKRD37 is a direct HIF-1a effector highly induced in hypoxia (96). Promoting cell growth by inducing p62 expression, ANKRD37 is required to promote cell proliferation and autophagy in colon cancer (96). Its inhibition might be directly linked to MIR210HG downregulation by RBC-EVc and could have similar effects compromising lymphatic integrity. Transcriptomic would also have been relevant on EVs alone in order to assess if these effects come directly from EVs transcriptome.

Given the beneficial effects of pEVs on LECs integrity, we now aim to assess if pEVs could modulate lymphatic function and integrity in vivo and help treat or prevent lymphatic dysfunction associated with atherosclerosis. We hereby show that pEVs can be uptaken by popliteal lymphatic vessels as early as 2 hours post intradermal injection (fig. 14). Furthermore, pEVs can be found freely in afferent lymph nodes (Fig. 15 A) as well as in lymph node cells (Fig. 15D), whereas no statistical difference can be noted for free and uptaken pEVs at the injection site (Fig. 15 BC). The retention of pEVs in lymph node cells also seems to happen in CD45+ MHC II+ cells, indicating possible internalisation by migrating cells to afferent lymph nodes (Fig. 15F). However, the assessment of lymphatic function after pEVs treatment is limited by the difference of specie. Long-term treatments could induce immune response and alter the results, since a few differences exist between murine and human platelets. Rowley et al. showed by transcriptomic analysis that some human platelet receptors are missing on murine platelets, such as PTAFR, PAR1 and CD68 (97). Further promising experiments are required, starting with pEVs and rbEVs production from mice blood.

Conclusion:

In order to prepare ground for in vivo lymphatic function assessment and its regulation by EVs, we first showed that human PLT-EVs can be uptaken by collecting lymphatics after intradermal injection (Figure 14). After observing no harmful effects of PLT-EVs on LECs *in vitro* and knowing they help inhibiting ROS production and cell necrosis, PLT-EVs could be beneficial to lymphatic function. Opposingly, even only physiological concentrations of RBC-EVs seem to have adverse effects on lymphatic endothelium *in vitro* via ROS production and MIR210HG inhibition. In addition, we show that PLT-EVs can be internalized in vivo by MHC II positive cells and accumulate in lymph nodes (Figure 15E-F). This brings forward the potential role of PLT-EVs in inflammatory response regulation which could in turn affect lymphatic function. Further investigations and proper lymphatic function assessment after murine-produced EVs treatments are necessary in order to understand lymphatic dysfunction onset.

Acknowledgments: We would like to thank the Bioinformatics Core Facility, Institute for Research in Immunology and Cancer (IRIC), Université de Montréal, Montréal, Quebec, Canada, for the RNA-sequencing. Proteomics analyses were performed by the Center for Advanced Proteomics Analyses, a Node of the Canadian Genomic Innovation Network that is supported by the Canadian Government through Genome Canada.

Declaration of Interest Statement:

The authors have no other relevant affiliations or financial involvement with any organization or entity with a financial interest in or financial conflict with the subject matter or materials discussed in the manuscript apart from those disclosed.

References:

1. Ali RA, Wuescher LM, Worth RG. Platelets: essential components of the immune system. Curr Trends Immunol. 2015;16:65-78.

2. Carramolino L, Fuentes J, García-Andrés C, Azcoitia V, Riethmacher D, Torres M. Platelets Play an Essential Role in Separating the Blood and Lymphatic Vasculatures During Embryonic Angiogenesis. 2010;106(7):1197-201.

3. Osada M, Inoue O, Ding G, Shirai T, Ichise H, Hirayama K, et al. Platelet activation receptor CLEC-2 regulates blood/lymphatic vessel separation by inhibiting proliferation, migration, and tube formation of lymphatic endothelial cells. J Biol Chem. 2012;287(26):22241-52.

4. Lim L, Bui H, Farrelly O, Yang J, Li L, Enis D, et al. Hemostasis stimulates lymphangiogenesis through release and activation of VEGFC. Blood. 2019;134(20):1764-75.

5. Kaipainen A, Korhonen J, Mustonen T, van Hinsbergh VW, Fang GH, Dumont D, et al. Expression of the fms-like tyrosine kinase 4 gene becomes restricted to lymphatic endothelium during development. Proc Natl Acad Sci U S A. 1995;92(8):3566-70.

6. Karkkainen MJ, Haiko P, Sainio K, Partanen J, Taipale J, Petrova TV, et al. Vascular endothelial growth factor C is required for sprouting of the first lymphatic vessels from embryonic veins. Nat Immunol. 2004;5(1):74-80.

7. Joukov V, Pajusola K, Kaipainen A, Chilov D, Lahtinen I, Kukk E, et al. A novel vascular endothelial growth factor, VEGF-C, is a ligand for the Flt4 (VEGFR-3) and KDR (VEGFR-2) receptor tyrosine kinases. EMBO J. 1996;15(2):290-98.

8. Makinen T, Jussila L, Veikkola T, Karpanen T, Kettunen MI, Pulkkanen KJ, et al. Inhibition of lymphangiogenesis with resulting lymphedema in transgenic mice expressing soluble VEGF receptor-3. Nat Med. 2001;7(2):199-205.

9. Salameh A, Galvagni F, Bardelli M, Bussolino F, Oliviero S. Direct recruitment of CRK and GRB2 to VEGFR-3 induces proliferation, migration, and survival of endothelial cells through the activation of ERK, AKT, and JNK pathways. Blood. 2005;106(10):3423-31.

10. Coso S, Zeng Y, Opeskin K, Williams ED. Vascular endothelial growth factor receptor-3 directly interacts with phosphatidylinositol 3-kinase to regulate lymphangiogenesis. PloS one. 2012;7(6):e39558.

11. Breslin JW, Gaudreault N, Watson KD, Reynoso R, Yuan SY, Wu MH. Vascular endothelial growth factor-C stimulates the lymphatic pump by a VEGF receptor-3-dependent mechanism. Am J Physiol Heart Circ Physiol. 2007;293(1):H709-18.

12. Milasan A, Smaani A, Martel C. Early rescue of lymphatic function limits atherosclerosis progression in Ldlr(-/-) mice. Atherosclerosis. 2019;283:106-19.

13. Milasan A, Jean G, Dallaire F, Tardif JC, Merhi Y, Sorci-Thomas M, et al. Apolipoprotein A-I Modulates Atherosclerosis Through Lymphatic Vessel-Dependent Mechanisms in Mice. 2017;6(9):e006892.

14. Milasan A, Farhat M, Martel C. Extracellular Vesicles as Potential Prognostic Markers of Lymphatic Dysfunction. Front Physiol. 2020;11:476.

15. Ståhl AL, Johansson K, Mossberg M, Kahn R, Karpman D. Exosomes and microvesicles in normal physiology, pathophysiology, and renal diseases. Pediatr Nephrol. 2019;34(1):11-30.

16. Camussi G, Deregibus MC, Bruno S, Cantaluppi V, Biancone L. Exosomes/microvesicles as a mechanism of cell-to-cell communication. Kidney Int. 2010;78(9):838-48.

17. Doyle LM, Wang MZ. Overview of Extracellular Vesicles, Their Origin, Composition, Purpose, and Methods for Exosome Isolation and Analysis. 2019;8(7):727.

18. Milasan A, Tessandier N, Tan S, Brisson A, Boilard E, Martel C. Extracellular vesicles are present in mouse lymph and their level differs in atherosclerosis. J Extracell Vesicles. 2016;5:31427.

19. Arias CF, Arias CF. How do red blood cells know when to die? R Soc Open Sci. 2017;4(4):160850.

20. Kuo WP, Tigges JC, Toxavidis V, Ghiran I. Red Blood Cells: A Source of Extracellular Vesicles. Methods Mol Biol. 2017;1660:15-22.

21. Morel O, Jesel L, Freyssinet JM, Toti F. Cellular mechanisms underlying the formation of circulating microparticles. Arterioscler Thromb Vasc Biol. 2011;31(1):15-26.

22. Donadee C, Raat NJ, Kanias T, Tejero J, Lee JS, Kelley EE, et al. Nitric oxide scavenging by red blood cell microparticles and cell-free hemoglobin as a mechanism for the red cell storage lesion. Circulation. 2011;124(4):465-76.

23. Li KY, Zheng L, Wang Q, Hu YW. Characteristics of erythrocyte-derived microvesicles and its relation with atherosclerosis. Atherosclerosis. 2016;255:140-4.

24. Pascual M, Lutz HU, Steiger G, Stammler P, Schifferli JA. Release of vesicles enriched in complement receptor 1 from human erythrocytes. J Immunol. 1993;151(1):397-404.

25. Moxness MS, Brunauer LS, Huestis WH. Hemoglobin oxidation products extract phospholipids from the membrane of human erythrocytes. Biochemistry. 1996;35(22):7181-7.

26. Potor L, Bányai E, Becs G, Soares MP, Balla G, Balla J, et al. Atherogenesis may involve the prooxidant and proinflammatory effects of ferryl hemoglobin. Oxid Med Cell Longev. 2013;2013:676425.

27. Bohlen HG, Gasheva OY, Zawieja DC. Nitric oxide formation by lymphatic bulb and valves is a major regulatory component of lymphatic pumping. 2011;301(5):H1897-H906.

28. Gasheva OY, Zawieja DC, Gashev AA. Contraction-initiated NO-dependent lymphatic relaxation: a self-regulatory mechanism in rat thoracic duct. 2006;575(3):821-32.

29. Rousseau M, Belleannee C, Duchez AC, Cloutier N, Levesque T, Jacques F, et al. Detection and quantification of microparticles from different cellular lineages using flow cytometry. Evaluation of the impact of secreted phospholipase A2 on microparticle assessment. PloS one. 2015;10(1):e0116812.

30. Poncelet P, Robert S, Bailly N, Garnache-Ottou F, Bouriche T, Devalet B, et al. Tips and tricks for flow cytometry-based analysis and counting of microparticles. Transfus Apher Sci. 2015;53(2):110-26.

31. Poncelet P, Robert S, Bouriche T, Bez J, Lacroix R, Dignat-George F. Standardized counting of circulating platelet microparticles using currently available flow cytometers and scatter-based triggering: Forward or side scatter? Cytometry A. 2016;89(2):148-58.

32. Milasan A, Dallaire F, Mayer G, Martel C. Effects of LDL Receptor Modulation on Lymphatic Function. Sci Rep. 2016;6:27862.

33. Forest A, Ruiz M, Bouchard B, Boucher G, Gingras O, Daneault C, et al. Comprehensive and Reproducible Untargeted Lipidomic Workflow Using LC-QTOF Validated for Human Plasma Analysis. J Proteome Res. 2018;17(11):3657-70.

34. Mahmoud AM, Wilkinson FL, McCarthy EM, Moreno-Martinez D, Langford-Smith A, Romero M, et al. Endothelial microparticles prevent lipid-induced endothelial damage via Akt/eNOS signaling and reduced oxidative stress. FASEB J. 2017;31(10):4636-48.

35. Dobin A, Davis CA, Schlesinger F, Drenkow J, Zaleski C, Jha S, et al. STAR: ultrafast universal RNA-seq aligner. Bioinformatics. 2012;29(1):15-21.

36. Bolger AM, Lohse M, Usadel B. Trimmomatic: a flexible trimmer for Illumina sequence data. Bioinformatics. 2014;30(15):2114-20.

37. Li B, Dewey CN. RSEM: accurate transcript quantification from RNA-Seq data with or without a reference genome. BMC Bioinformatics. 2011;12:323.

38. Love MI, Huber W, Anders S. Moderated estimation of fold change and dispersion for RNA-seq data with DESeq2. Genome Biol. 2014;15(12):550.

39. Tessandier N, Melki I, Cloutier N, Allaeys I, Miszta A, Tan S, et al. Platelets Disseminate Extracellular Vesicles in Lymph in Rheumatoid Arthritis. 2020;40(4):929-42.

40. Maclouf J, Levy-Toledano S, Savariau E, Hardisty R, Caen JP. Arachidonic acid-induced human platelet aggregation independent of cyclooxygenase and lipoxygenase. Prostaglandins. 1984;28(3):383-98.

41. Barnig C, Cernadas M, Dutile S, Liu X, Perrella MA, Kazani S, et al. Lipoxin A₄ Regulates Natural Killer Cell and Type 2 Innate Lymphoid Cell Activation in Asthma. 2013;5(174):174ra26-ra26.

42. Maderna P, Godson C. Lipoxins: resolutionary road. Br J Pharmacol. 2009;158(4):947-59.

43. Barber MN, Risis S, Yang C, Meikle PJ, Staples M, Febbraio MA, et al. Plasma Lysophosphatidylcholine Levels Are Reduced in Obesity and Type 2 Diabetes. PloS one. 2012;7(7):e41456.

44. Taylor LA, Arends J, Hodina AK, Unger C, Massing U. Plasma lyso-phosphatidylcholine concentration is decreased in cancer patients with weight loss and activated inflammatory status. Lipids in Health and Disease. 2007;6(1):17.

45. Nakano T, Inoue I, Katayama S, Seo M, Takahashi S, Hokari S, et al. Lysophosphatidylcholine for efficient intestinal lipid absorption and lipoprotein secretion in caco-2 cells. J Clin Biochem Nutr. 2009;45(2):227-34.

46. Akita H, Creer MH, Yamada KA, Sobel BE, Corr PB. Electrophysiologic effects of intracellular lysophosphoglycerides and their accumulation in cardiac lymph with myocardial ischemia in dogs. J Clin Invest. 1986;78(1):271-80.

47. Zakiev ER, Sukhorukov VN, Melnichenko AA, Sobenin IA, Ivanova EA, Orekhov AN. Lipid composition of circulating multiple-modified low density lipoprotein. Lipids Health Dis. 2016;15(1):134.

48. Schmitz G, Ruebsaamen K. Metabolism and atherogenic disease association of lysophosphatidylcholine. Atherosclerosis. 2010;208(1):10-8.

49. Fourcade O, Simon M-F, Viodé C, Rugani N, Leballe F, Ragab A, et al. Secretory phospholipase A2 generates the novel lipid mediator lysophosphatidic acid in membrane microvesicles shed from activated cells. Cell. 1995;80(6):919-27.

50. Law S-H, Chan M-L, Marathe GK, Parveen F, Chen C-H, Ke L-Y. An Updated Review of Lysophosphatidylcholine Metabolism in Human Diseases. Int J Mol Sci. 2019;20(5):1149.

51. Zhang H, Freitas D, Kim HS, Fabijanic K, Li Z, Chen H, et al. Identification of distinct nanoparticles and subsets of extracellular vesicles by asymmetric flow field-flow fractionation. Nature Cell Biology. 2018;20(3):332-43.

52. Bakocevic N, Claser C, Yoshikawa S, Jones LA, Chew S, Goh CC, et al. CD41 is a reliable identification and activation marker for murine basophils in the steady state and during helminth and malarial infections. 2014;44(6):1823-34.

53. Mause SF, Ritzel E, Liehn EA, Hristov M, Bidzhekov K, Müller-Newen G, et al. Platelet microparticles enhance the vasoregenerative potential of angiogenic early outgrowth cells after vascular injury. Circulation. 2010;122(5):495-506.

54. Melotte V, Qu X, Ongenaert M, van Criekinge W, de Bruïne AP, Baldwin HS, et al. The N-myc downstream regulated gene (NDRG) family: diverse functions, multiple applications. FASEB J. 2010;24(11):4153-66.

55. Chistiakov DA, Orekhov AN, Bobryshev YV. Extracellular vesicles and atherosclerotic disease. Cell Mol Life Sci. 2015;72(14):2697-708.

56. Brown M, Johnson LA, Leone DA, Majek P, Vaahtomeri K, Senfter D, et al. Lymphatic exosomes promote dendritic cell migration along guidance cues. J Cell Biol. 2018;217(6):2205-21.

57. Srinivasan S, Vannberg FO, Dixon JB. Lymphatic transport of exosomes as a rapid route of information dissemination to the lymph node. Sci Rep. 2016;6:24436.

58. Broggi MAS, Maillat L, Clement CC, Bordry N, Corthésy P, Auger A, et al. Tumor-associated factors are enriched in lymphatic exudate compared to plasma in metastatic melanoma patients. Journal of Experimental Medicine. 2019;216(5):1091-107.

59. Kordbacheh F, O'Meara CH, Coupland LA, Lelliott PM, Parish CR. Extracellular histones induce erythrocyte fragility and anemia. Blood. 2017;130(26):2884-8.

60. Nair RR, Mazza D, Brambilla F, Gorzanelli A, Agresti A, Bianchi ME. LPS-Challenged Macrophages Release Microvesicles Coated With Histones. Front Immunol. 2018;9:1463-.

61. Sironi M, Conti A, Bernasconi S, Fra AM, Pasqualini F, Nebuloni M, et al. Generation and characterization of a mouse lymphatic endothelial cell line. Cell Tissue Res. 2006;325(1):91-100.

62. Daigo K, Takamatsu Y, Hamakubo T. The Protective Effect against Extracellular Histones Afforded by Long-Pentraxin PTX3 as a Regulator of NETs. 2016;7(344).

63. Semeraro F, Ammollo CT, Morrissey JH, Dale GL, Friese P, Esmon NL, et al. Extracellular histones promote thrombin generation through platelet-dependent mechanisms: involvement of platelet TLR2 and TLR4. Blood. 2011;118(7):1952-61.

64. French SL, Butov KR, Allaeys I, Canas J, Morad G, Davenport P, et al. Platelet-derived extracellular vesicles infiltrate and modify the bone marrow during inflammation. Blood Advances. 2020;4(13):3011-23.

65. Usman WM, Pham TC, Kwok YY, Vu LT, Ma V, Peng B, et al. Efficient RNA drug delivery using red blood cell extracellular vesicles. Nature Communications. 2018;9(1):2359.

66. Jank H, Salzer U. Vesicles generated during storage of red blood cells enhance the generation of radical oxygen species in activated neutrophils. ScientificWorldJournal. 2011;11:173-85.

67. Camus SM, De Moraes JA, Bonnin P, Abbyad P, Le Jeune S, Lionnet F, et al. Circulating cell membrane microparticles transfer heme to endothelial cells and trigger vasoocclusions in sickle cell disease. Blood. 2015;125(24):3805-14.

68. Ryter SW, Kim HP, Hoetzel A, Park JW, Nakahira K, Wang X, et al. Mechanisms of cell death in oxidative stress. Antioxid Redox Signal. 2007;9(1):49-89.

69. Benedikter BJ, Weseler AR, Wouters EFM, Savelkoul PHM, Rohde GGU, Stassen FRM. Redox-dependent thiol modifications: implications for the release of extracellular vesicles. Cellular and Molecular Life Sciences. 2018;75(13):2321-37.

70. Burger D, Kwart DG, Montezano AC, Read NC, Kennedy CRJ, Thompson CS, et al. Microparticles Induce Cell Cycle Arrest Through Redox‐Sensitive Processes in Endothelial Cells: Implications in Vascular Senescence. 2012;1(3):e001842.

71. Janiszewski M, do Carmo AO, Pedro MA, Silva E, Knobel E, Laurindo FRM. Platelet-derived exosomes of septic individuals possess proapoptotic NAD(P)H oxidase activity: A novel vascular redox pathway*. Critical Care Medicine. 2004;32(3).

72. Wang H, Wang Z-H, Kong J, Yang M-Y, Jiang G-H, Wang X-P, et al. Oxidized Low-Density Lipoprotein-Dependent Platelet-Derived Microvesicles Trigger Procoagulant Effects and Amplify Oxidative Stress. Molecular Medicine. 2012;18(2):159-66.

73. Kitazume S, Imamaki R, Ogawa K, Komi Y, Futakawa S, Kojima S, et al. Alpha2,6-sialic acid on platelet endothelial cell adhesion molecule (PECAM) regulates its homophilic interactions and downstream antiapoptotic signaling. J Biol Chem. 2010;285(9):6515-21.

74. Tao S-C, Yuan T, Rui B-Y, Zhu Z-Z, Guo S-C, Zhang C-Q. Exosomes derived from human platelet-rich plasma prevent apoptosis induced by glucocorticoid-associated endoplasmic reticulum stress in rat osteonecrosis of the femoral head via the Akt/Bad/Bcl-2 signal pathway. Theranostics. 2017;7(3):733-50.

75. Wun T, Paglieroni T, Tablin F, Welborn J, Nelson K, Cheung A. Platelet activation and platelet-erythrocyte aggregates in patients with sickle cell anemia. J Lab Clin Med. 1997;129(5):507-16.

76. Vallés J, Santos MT, Aznar J, Martínez M, Moscardó A, Piñón M, et al. Platelet-erythrocyte interactions enhance αIIbβ3 integrin receptor activation and P-selectin expression during platelet recruitment: down-regulation by aspirin ex vivo. Blood. 2002;99(11):3978-84.

77. Lertkiatmongkol P, Liao D, Mei H, Hu Y, Newman PJ. Endothelial functions of platelet/endothelial cell adhesion molecule-1 (CD31). Curr Opin Hematol. 2016;23(3):253-9.

78. Baldwin ME, Halford MM, Roufail S, Williams RA, Hibbs ML, Grail D, et al. Vascular Endothelial Growth Factor D Is Dispensable for Development of the Lymphatic System. 2005;25(6):2441-9.

79. Jackson DG. Biology of the lymphatic marker LYVE-1 and applications in research into lymphatic trafficking and lymphangiogenesis. Apmis. 2004;112(7-8):526-38.

80. Schlesinger M, Bendas G. Vascular cell adhesion molecule-1 (VCAM-1)—An increasing insight into its role in tumorigenicity and metastasis. 2015;136(11):2504-14.

81. Willeit P, Zampetaki A, Dudek K, Kaudewitz D, King A, Kirkby NS, et al. Circulating MicroRNAs as Novel Biomarkers for Platelet Activation. 2013;112(4):595-600.

82. Kaudewitz D, Skroblin P, Bender LH, Barwari T, Willeit P, Pechlaner R, et al. Association of MicroRNAs and YRNAs With Platelet Function. 2016;118(3):420-32.

83. Wang S, Aurora AB, Johnson BA, Qi X, McAnally J, Hill JA, et al. The endothelial-specific microRNA miR-126 governs vascular integrity and angiogenesis. Dev Cell. 2008;15(2):261-71.

84. Harris TA, Yamakuchi M, Ferlito M, Mendell JT, Lowenstein CJ. MicroRNA-126 regulates endothelial expression of vascular cell adhesion molecule 1. 2008;105(5):1516-21.

85. Voellenkle C, Garcia-Manteiga JM, Pedrotti S, Perfetti A, De Toma I, Da Silva D, et al. Implication of Long noncoding RNAs in the endothelial cell response to hypoxia revealed by RNA-sequencing. Scientific Reports. 2016;6(1):24141.

86. Movafagh S, Crook S, Vo K. Regulation of Hypoxia-Inducible Factor-1a by Reactive Oxygen Species : New Developments in an Old Debate. 2015;116(5):696-703.

87. Chandel NS, McClintock DS, Feliciano CE, Wood TM, Melendez JA, Rodriguez AM, et al. Reactive oxygen species generated at mitochondrial complex III stabilize hypoxia-inducible factor-1alpha during hypoxia: a mechanism of O2 sensing. The Journal of biological chemistry. 2000;275(33):25130-8.

88. Brunelle JK, Bell EL, Quesada NM, Vercauteren K, Tiranti V, Zeviani M, et al. Oxygen sensing requires mitochondrial ROS but not oxidative phosphorylation. Cell Metabolism. 2005;1(6):409-14.

89. Guzy RD, Hoyos B, Robin E, Chen H, Liu L, Mansfield KD, et al. Mitochondrial complex III is required for hypoxia-induced ROS production and cellular oxygen sensing. Cell Metabolism. 2005;1(6):401-8.

90. Mateo J, García-Lecea M, Cadenas S, Hernández C, Moncada S. Regulation of hypoxia-inducible factor-1alpha by nitric oxide through mitochondria-dependent and -independent pathways. Biochem J. 2003;376(Pt 2):537-44.

91. Metzen E, Zhou J, Jelkmann W, Fandrey J, Brüne B. Nitric oxide impairs normoxic degradation of HIF-1alpha by inhibition of prolyl hydroxylases. Mol Biol Cell. 2003;14(8):3470-81.

92. Lee J-W, Bae S-H, Jeong J-W, Kim S-H, Kim K-W. Hypoxia-inducible factor (HIF-1)α: its protein stability and biological functions. Experimental & Molecular Medicine. 2004;36(1):1-12.

93. Liang X, Yang D, Hu J, Hao X, Gao J, Mao Z. Hypoxia inducible factor-alpha expression correlates with vascular endothelial growth factor-C expression and lymphangiogenesis/angiogenesis in oral squamous cell carcinoma. Anticancer Res. 2008;28(3a):1659-66.

94. Li J, Wu QM, Wang XQ, Zhang CQ. Long Noncoding RNA miR210HG Sponges miR-503 to Facilitate Osteosarcoma Cell Invasion and Metastasis. DNA Cell Biol. 2017;36(12):1117-25.

95. Li XY, Zhou LY, Luo H, Zhu Q, Zuo L, Liu GY, et al. The long noncoding RNA MIR210HG promotes tumor metastasis by acting as a ceRNA of miR-1226-3p to regulate mucin-1c expression in invasive breast cancer. Aging (Albany NY). 2019;11(15):5646-65.

96. Deng M, Zhang W, Yuan L, Tan J, Chen Z. HIF-1a regulates hypoxia-induced autophagy via translocation of ANKRD37 in colon cancer. Exp Cell Res. 2020;395(1):112175.

97. Rowley JW, Oler AJ, Tolley ND, Hunter BN, Low EN, Nix DA, et al. Genome-wide RNA-seq analysis of human and mouse platelet transcriptomes. Blood. 2011;118(14):e101-e11.

A. Untargeted lipidomics lymph vs. plasma

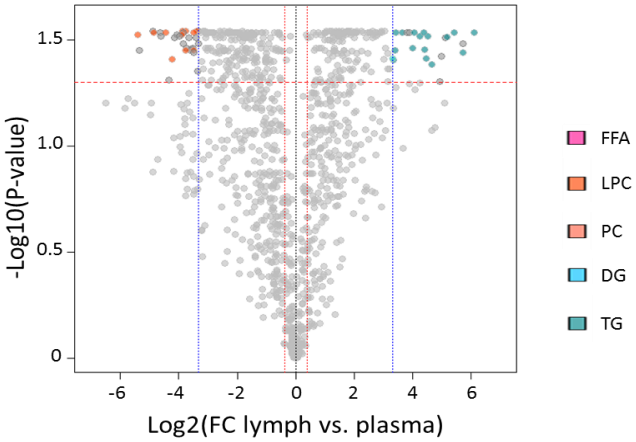

B. Untargeted lipidomics lymph vs. plasma (EVs)

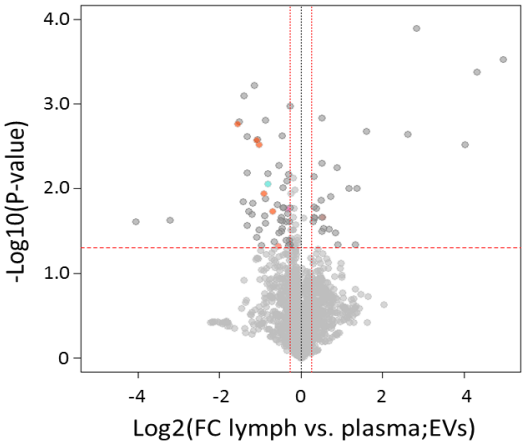

C. Untargeted lipidomics lymph vs. plasma: list of lipids identified

Identification	FC	P-value (corr)	Identification	FC	P-value (corr)
DOWN			*UP*		
LPC(13:0)	0.05	0.029	TG(18:2_18:2_18:2)	68.6	0.029
LPC(16:0)	0.07	0.029	TG(18:3_18:2_22:6)	16.0	0.034
LPC(16:0)	0.10	0.029	TG(18:2_18:3_18:2)	52.6	0.036
LPC(16:1)	0.09	0.035	TG(18:2_18:2_22:6)	10.1	0.039
LPC(17:1)	0.08	0.035	TG(18:2_18:2_20:4)	10.5	0.035
LPC(18:1)	0.07	0.029	TG(22:5_19:0_18:2)	10.8	0.029
LPC(18:2)	0.09	0.029	TG(16:0_18:2_18:3)	30.5	0.05
LPC(18:3)	0.02	0.030	TG(20:1_18:2_22:6)	12.5	0.029
LPC(18:3)	0.05	0.039	TG(16:0_20:4_16:0)	21.4	0.035
LPC(20:4)	0.07	0.029	TG(18:2_19:1_18:2)	25.1	0.041
LPC(22:6)	0.03	0.029	TG(16:0_18:2_16:0)	16.5	0.029
LPC(22:6)	0.07	0.030	TG(18:0_16:0_20:4)	19.0	0.030
			TG(16:0_16:0_16:0)	22.9	0.030
			TG(18:0_18:2_18:1)	43.1	0.029
			TG(18:1_18:2_20:1)	36.2	0.031

D. Untargeted lipidomics lymph vs. plasma (EVs): list of lipids identified

Identification	FC	P-value
DOWN		
LPC(14:0)	0.34	0.0017
LPC(14:0)	0.49	0.003
LPC(16:0)	0.47	0.0027
LPC(18:0)	0.53	0.011
LPC(18:2)	0.62	0.018
FFA C16:1n7	0.79	0.018
PC(16:0_22:6)	0.68	0.047
UP		
PC(36:4)	1.45	0.022

Figure 1: Untargeted lipidomic analysis of lymph, plasma and their EVs shows lipid distribution discrepancies. Matched mice lymph and plasma as well as EVs from both biological fluids were analyzed by LC-QTOF-MS. (**A**) Volcano plot of lymph vs. plasma showed 1200 features obtained following MS data processing. The x axis represents the fold changes (FC, in log2) of MS signal intensities values in lymph vs. plasma and the Y-axis represents the P-Values (in –log10). Using

the following criteria of selection: corrected p<0.05 and FC>10 or <0.1, we selected 55 features significantly discriminating lymph and plasma from which we annotated 29 unique lipids validated using MS/MS analysis as indicated in the volcano by color symbols. The corresponding list of lipids identified are presented in detail in **(C)**. (**B**) Volcano plot of EVs from lymph vs. EVs from plasma showed 1867 features obtained following MS data processing. Using the following criteria of selection: p<0.05 and FC>1.2 or <0.83, we selected 82 features significantly discriminating lymph and plasma from which we annotated 8 unique lipids validated using MS/MS analysis as indicated in the volcano by color symbols. The corresponding list of lipids identified are presented in detail in **(D)**. Abbreviations: FFA: free fatty acid; LPC: lysoglycerophosphatidylcholine; PC: diacylglycerophosphatidylcholine; DG: diacylglycerols; TG: triacylglycerol. The underscore symbol "_" beside the acyl side chain for TGs or PCs refers to acyl chains for which the sn position remains to be ascertained. n=3 (each n is a pool of 2-4 mice)

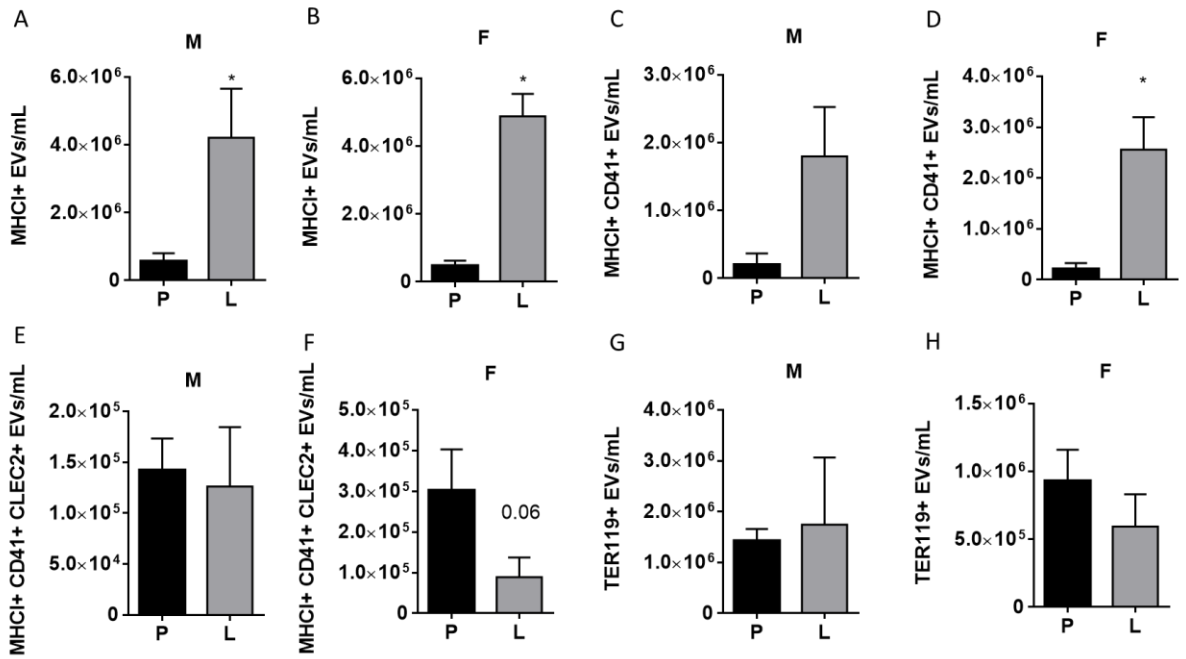

Figure 2: Panel I Flow cytometry results show MHC I+ and CD41+ EVs abundance in mice lymph. Matched mice lymph and plasma samples were analyzed by flow cytometry. Here, samples were stained targetting platelet and red blood cell-derived EVs. Male and female samples were stained with MHC I+ **(A-B)**, MHCI+ and CD41+ **(C-D)**, MHCI I+, CD41+ and CLEC2+ **(E-F)** or Ter119+ **(G-H)**. Count beads (Apogee Flow System cat. #1426) were added to each mix to determine the concentration of EVs in each sample. Acquisitions were made using a FSC-PMT-equipped FACSAria Fusion (BD Biosciences, San Jose, CA, USA) flow cytometer and a 405/10 bandpass filter for side scatter detection (V-SSC). *$p<0.05$; n=5-6

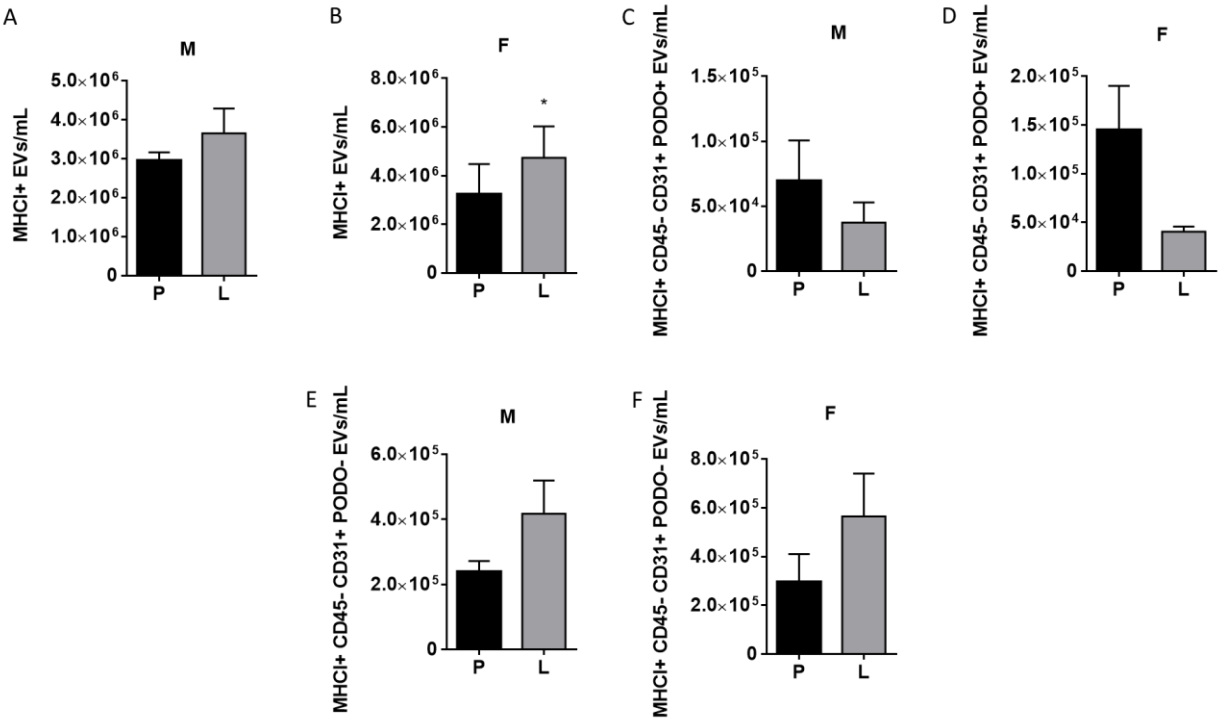

Figure 3: Panel II Flow cytometry results show opposite trends for lymphatic and blood endothelial cell-derived EVs concentration in lymph and plasma. Matched mice lymph and plasma samples were analyzed by flow cytometry. Here, samples were stained targetting endothelial cell-derived EVs. Male and female samples were gated using MHC I+ **(A-B)**, MHC I+, CD45-, CD31+ and Podoplanin+ **(C-D)** or MHC I+, CD45-, CD31+ and Podoplanin- **(E-F)**. Count beads (Apogee Flow System cat. #1426) were added to each mix to determine the concentration of EVs and control samples were also assessed. Acquisitions were made using a FSC-PMT-equipped FACSAria Fusion (BD Biosciences, San Jose, CA, USA) flow cytometer and a 405/10 bandpass filter for side scatter detection (V-SSC) *$p<0.05$; n=6

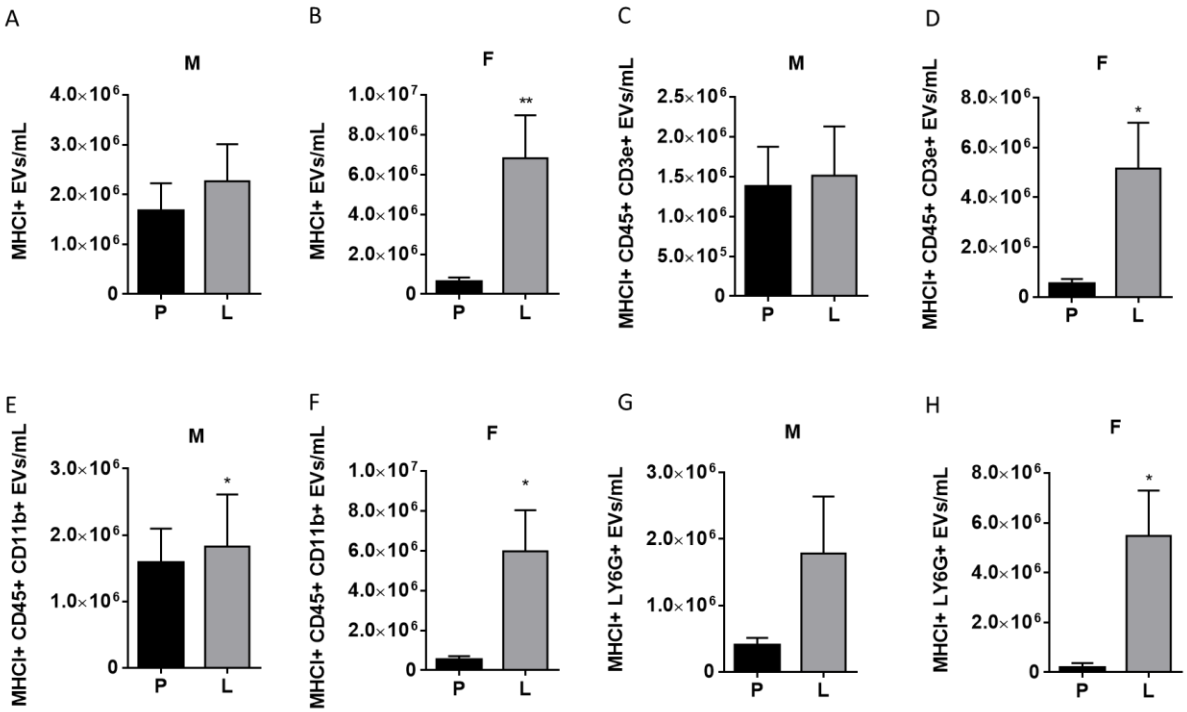

Figure 4: Panel III Flow cytometry results show abundance of immune cell-derived EVs in female mice lymph. Matched mice lymph and plasma samples were analyzed by flow cytometry. Here, samples were stained targetting immune cell-derived EVs. Male and female sample were gated using MHC I+ **(A-B)**, MHC I+, CD45+ and CD3e+ **(C-D)**, MHC I+, CD45+ and CD11b+ **(E-F)** and MHC I+ and LY6G+ **(G-H)**. Count beads (Apogee Flow System cat. #1426) were added to each mix to determine the concentration of EVs and control samples were also assessed. Acquisitions were made using a FSC-PMT-equipped FACSAria Fusion (BD Biosciences, San Jose, CA, USA) flow cytometer and a 405/10 bandpass filter for side scatter detection (V-SSC) *p<0.05, **p<0.01; n=5

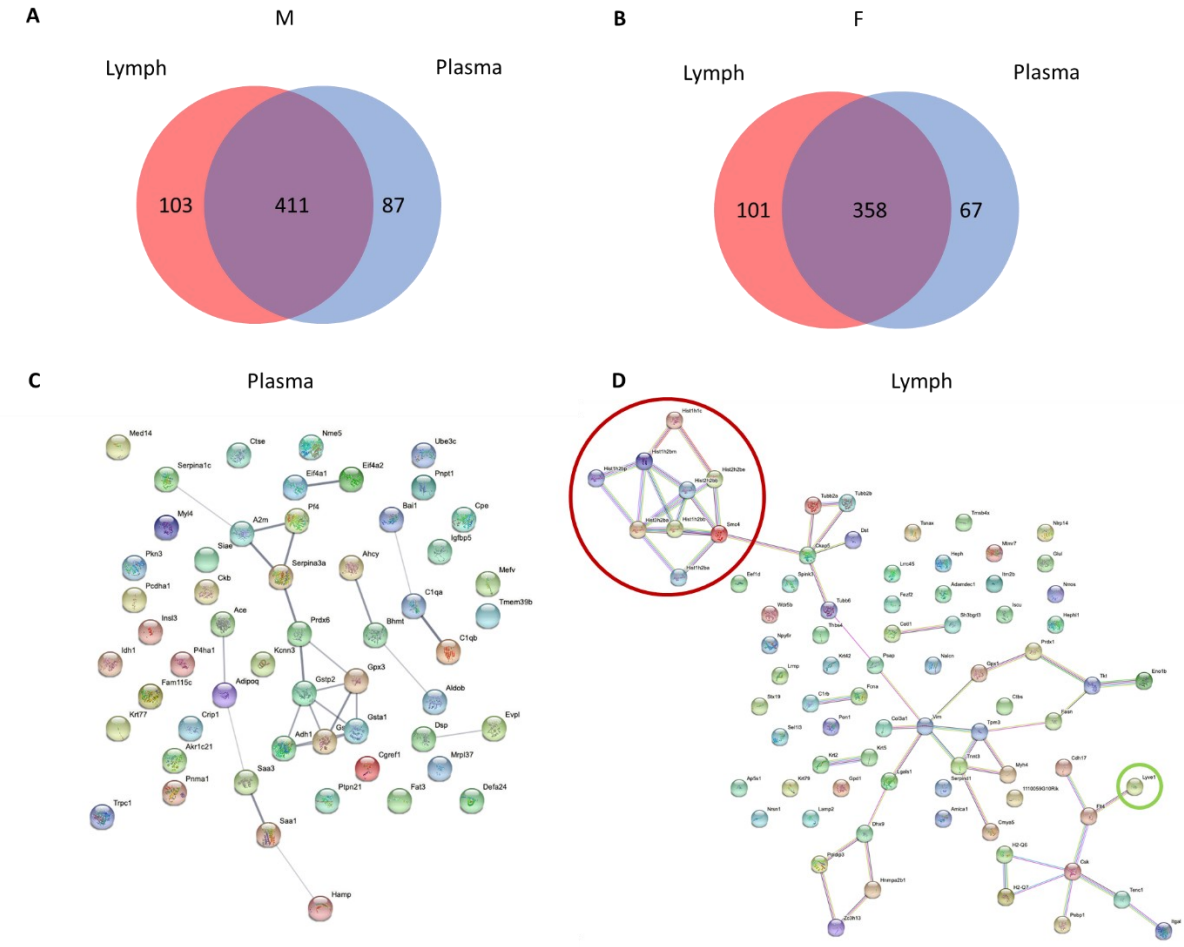

Figure 5: Preliminary proteomic analysis reveals protein distribution discrepancy between mice lymph and plasma. Venn diagram showing plasma and lymph protein content for both male **(A)** and female mice **(B).** Proteomic String Pathway for plasma protein in female mice sample **(C)** and lymph protein in female mice **(D)** with their interaction according to String Pathways analysis. Red circle represents protein cluster. Green circle highlights endothelial-lymphatic specific protein. Plasma and lymph sample are a pool of 3 mice. This map was made with https://string-db.org/ database. n=1

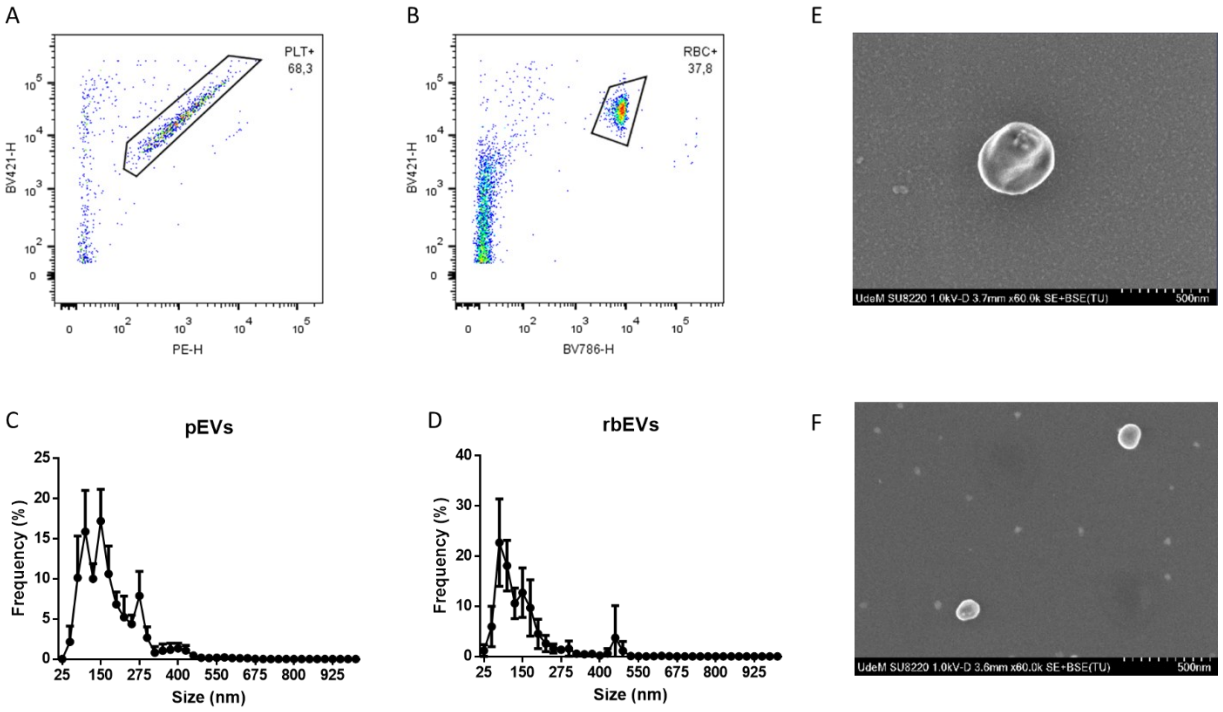

Figure 6: Quantification and characterisation of platelet and red blood cell-derived EVs. Each EVs production was quantified and characterized using BD FACSCelesta equipped with a 405 nm bandpass filter on the violet laser as side scatter detector. CFSE (FITC) and CD62p (PE) positive EVs were identified as platelet-derived Evs **(A)**. CFSE and CD235a (BV786) positive EVs were identified as red blood cell-derived EVs **(B)**. Detailed gating strategy is shown in Supplemental figure 2. Particle size distributions of pEVs **(C)** and rbEVs **(D)** was measured by Nanoparticle Tracking Analysis (NTA) (n=3) (SEM). A Regulus 8220 ultrahigh-resolution field emission scanning electron microscope (SEM) (Hitachi, Ltd., Japan) operated at 1 kV was used to observe the morphology of platelet **(E)** and red blood cell EVs **(F)**.

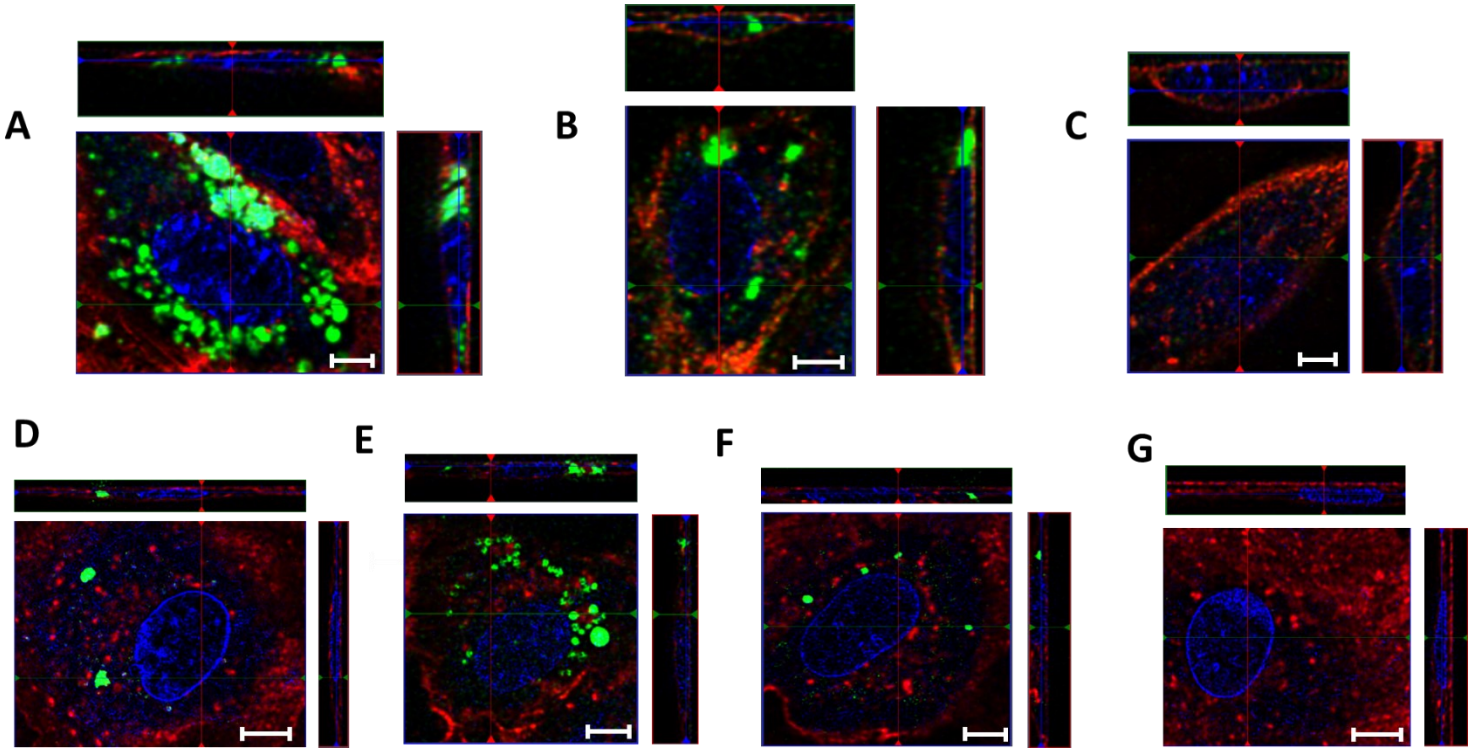

Figure 7: EVs internalisation by LECs over time. Representative images of pEVs (1x10^6/mL) and rbEVs (2x10^6/mL) stained with CFSE (green) and incubated on LECs in EVs-depleted and phenol-free medium. pEVs were incubated on LECs for 2 h **(A)** or 24 h **(B)**. Control cells without EVs are shown in **(C)**. rbEVs were incubated on LECs for 2 h (D), 16 h **(E)** or 24 h **(F)**. Control cells without Evs are shown in **(G)**. Cells were washed and stained with wGA (red) and DAPI (blue). Z-Stacks were acquired using an LSM 710 Confocal Microscope (Zeiss) equipped with a 63/1.4 oil dic objective and images were deconvoluted with Huygens Professional (Scientific Volume Imaging, SVI, Netherlands) using a theoretical spread function (PSF). Scale bar = 5 um. n=3

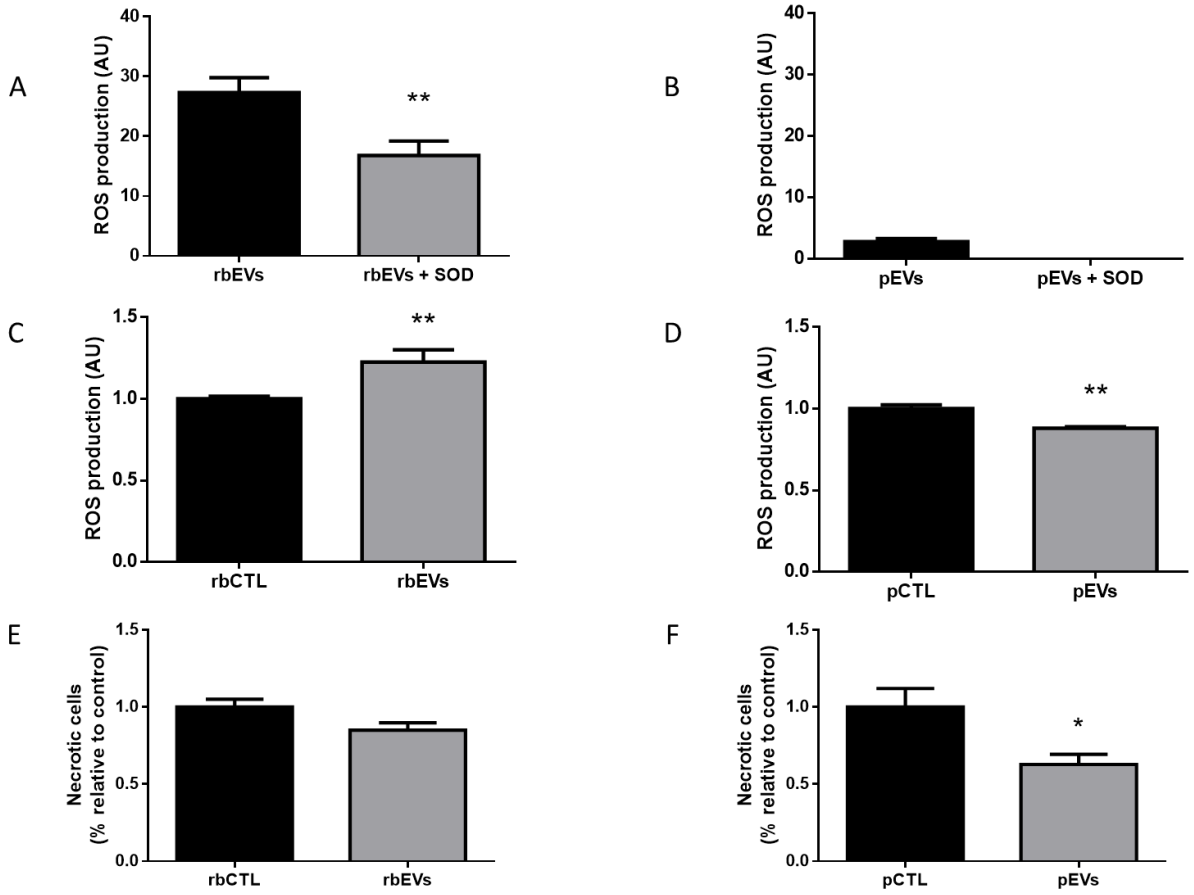

Figure 8: pEVs and rbEVs effect on oxydative stress, ROS production and necrosis. EVs samples were diluted in PBS and stained with CMH2DCF-DA in order to evaluate ROS production by rbEVs **(A)** or pEVs alone **(B)**. Superoxyde dismutase (SOD) (100 U/mL) was used as negative control. Similarly, ROS production by LECs was measured after treatment with rbEVs **(C)** or pEVs **(D)**. In another experiment, LECs were stained with Propidium Iodide and Annexin V antibody in order to analyse necrosis following rbEVs **(E)** or pEVs incubation for 24 h. *p<0.05; **p<0.01; n=6-7

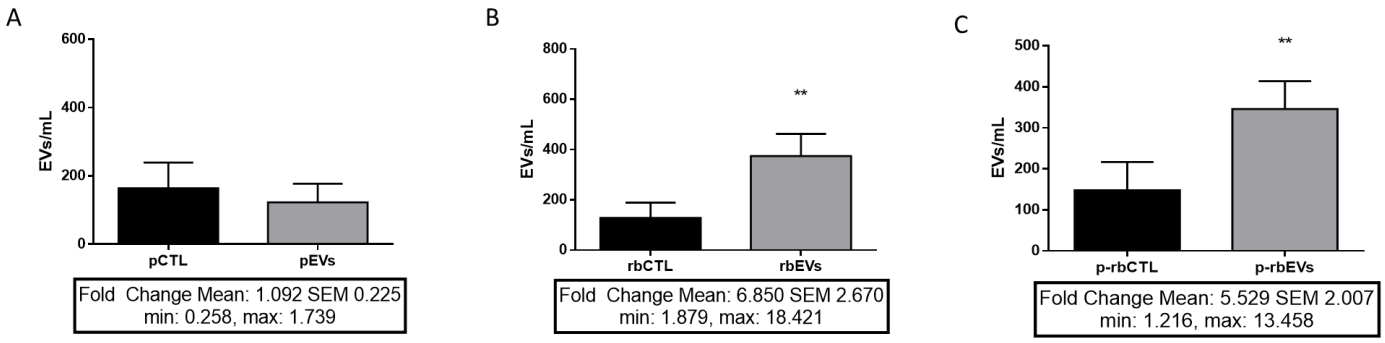

Figure 9: Red blood cell-derived Evs increase LEC-derived Evs production. Following the incubation of pEVs **(A)**, rbEVs **(B)** or both subtypes **(C)** on LECs for 24 h at physiological concentration, supernatant was collected. EVs were stained with CFSE and VEGFR-3 antibody (PE) and analysed using BD FACSCelesta equipped with a 405 nm bandpass fliter on the violet laser. *p<0.05; **p<0.01. n=6

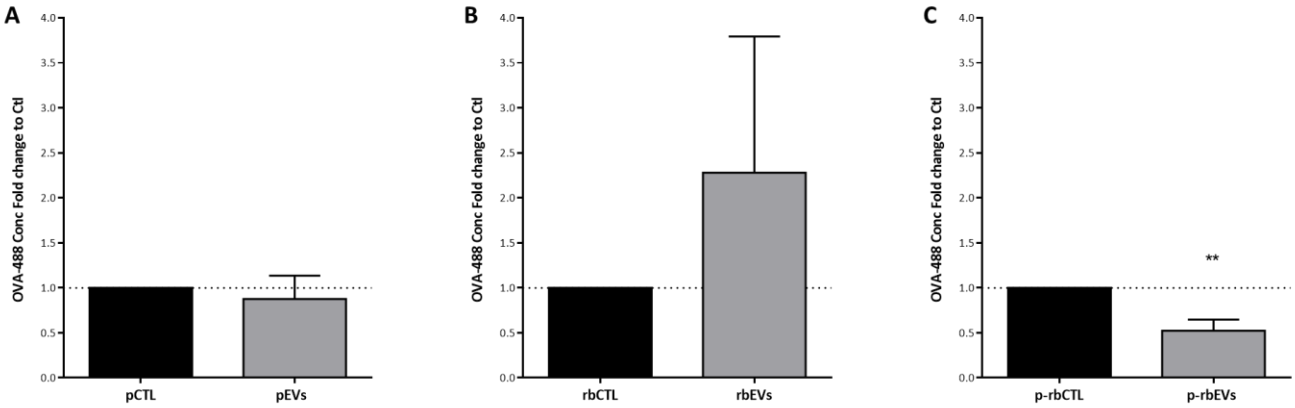

Figure 10: Co-incubation of platelet and red blood cell-derived EVs inhibit LECs permeability. During cell culture and EVs treatment with pEVs **(A**), rbEVs **(B)** or both subtypes **(C)**, phenol-free and EVs-depleted medium was used on both sides of the insert. Permeability was assessed by the addition of Ovalbumin (AF488) (50 ng/mL) (Invitrogen cat. #34781) for 20 minutes at RT followed by bottom-plate fluorescence reading with the plate reader Synergy 2. **p<0.01; n=6

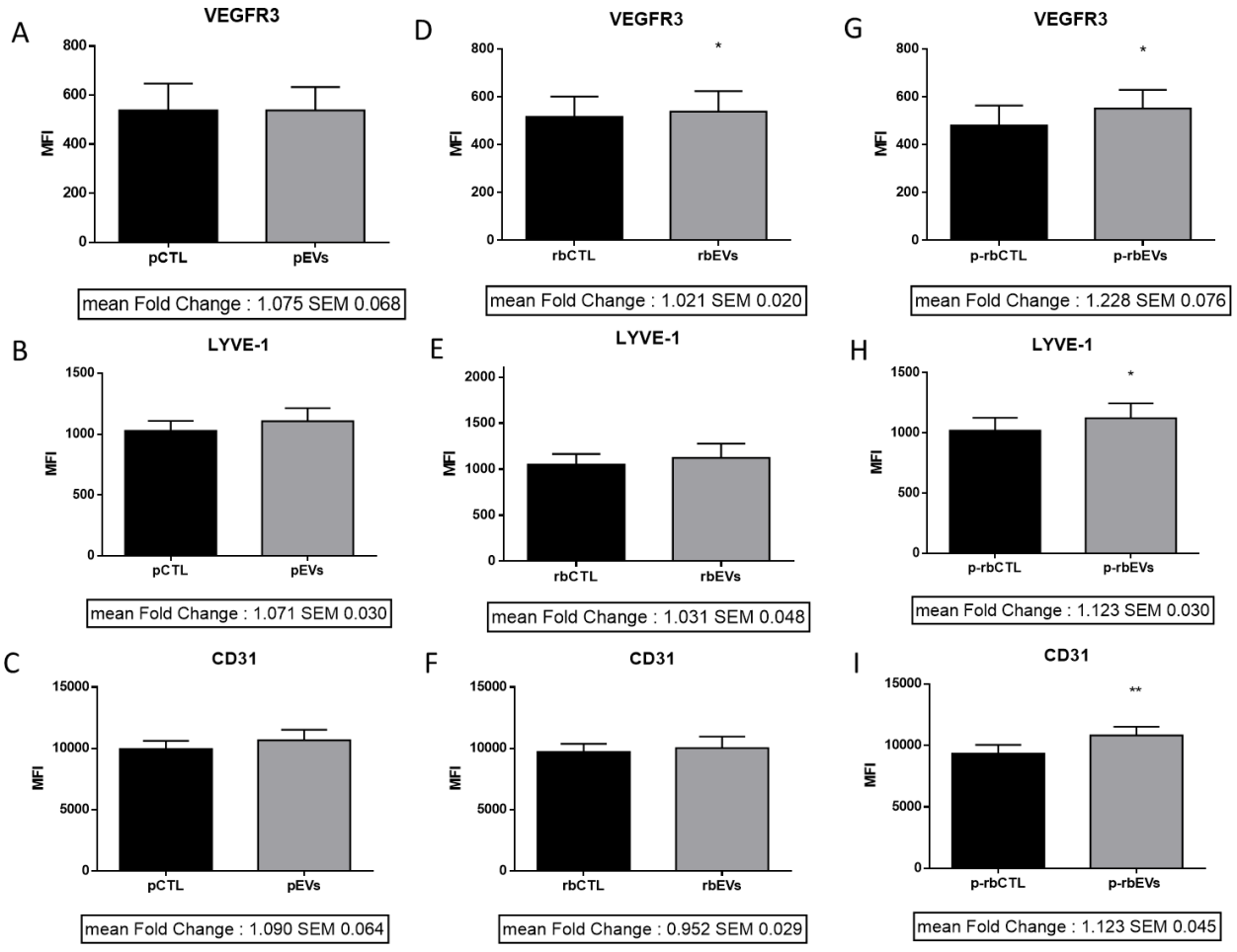

Figure 11: Co-incubation of platelet and red blood cell-derived EVs increase lymphatic markers expression on LECs. LECs were treated for 24 h with pEVs **(A, B, C)**, rbEVs **(D, E, F)**, or both subtypes **(G, H, I)**. Cells were stained using VEGFR3 (PE), LYVE-1 (APC), CD31 antibody (APC Cy-7) and DAPI. Markers expression was analysed by flow cytometry (BD FACSCelesta). **p<0.01; n=9

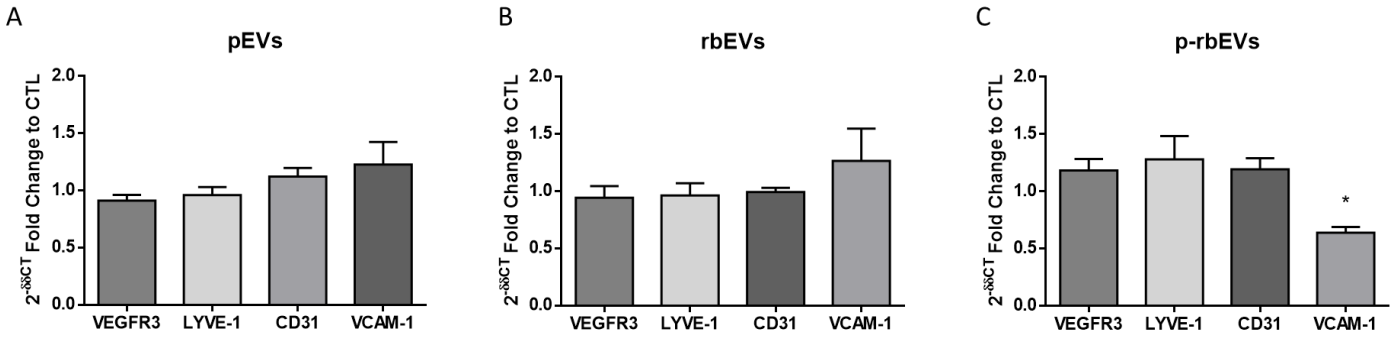

Figure 12: Co-incubation of platelet and red-blood cell-derived EVs regulates VCAM-1 gene expression in LECs. mRNA regulation in LECs was measured by qPCR in VEGFR3, LYVE-1, CD31, and VCAM-1 genes following 24 h incubation of pEVs **(A)**, rbEVs **(B)** or both subtypes **(C)**. *$p<0.05$; (n=5-6).

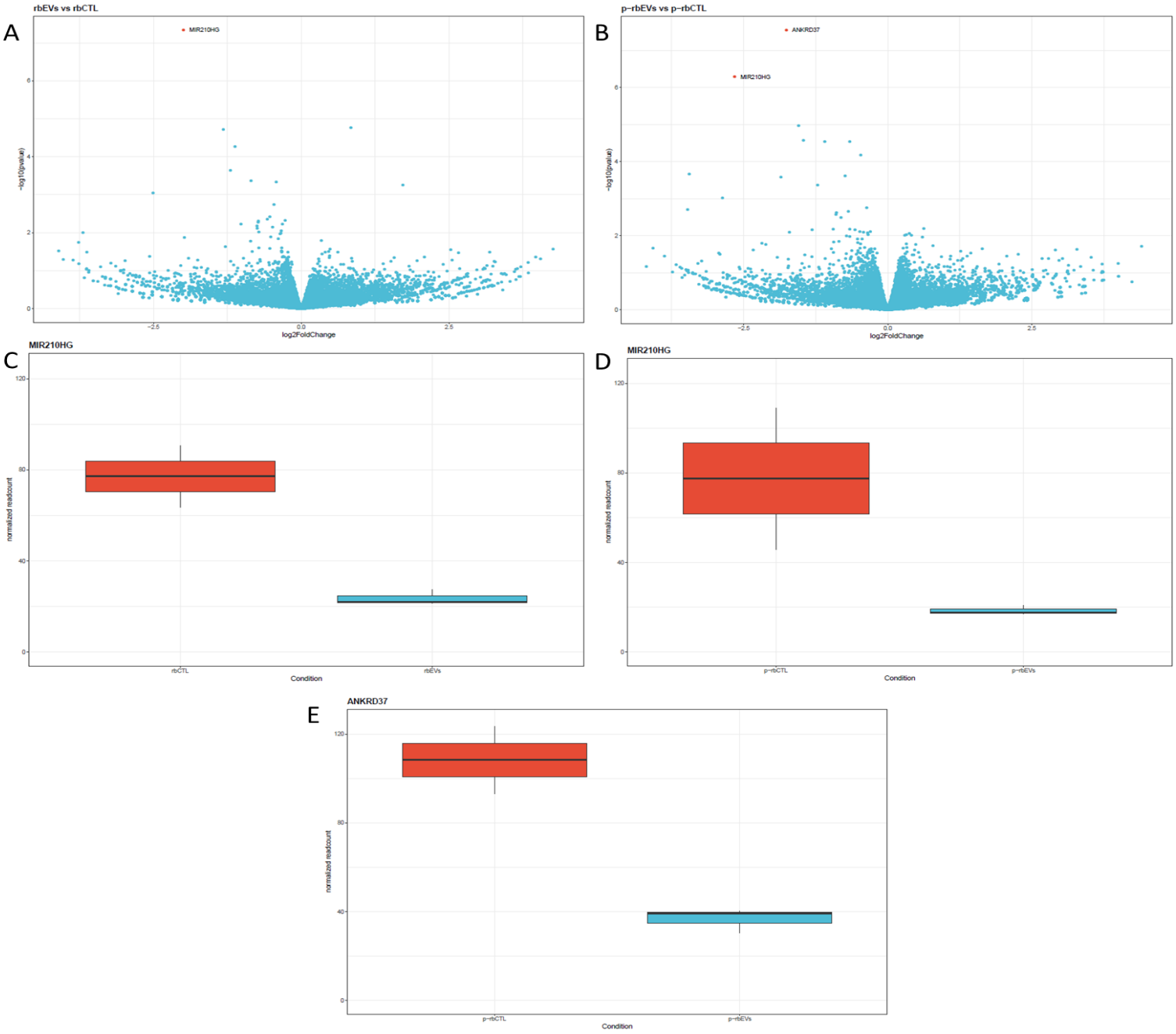

Figure 13: RNA-sequencing reveals hypoxia related genes regulation by red blood cell-derived EVs. Transcriptomic was performed with Illumina next generation sequencing following LECs treatment with pEVs, rbEVs or both subtypes. Volcano-plot representations for rbEVs **(A)** and p-rbEVs treatments **(B)** show labels on significant genes. Expression variation of significant genes (normalized read counts) is shown for MIR210HG after rbEVs incubation **(C)** and both MIR210HG and ANKRD37 after p-rbEVs incubation **(D-E)**. Significant differentially expressed genes (DEGs) have an ajusted p-value lower than 0.05.

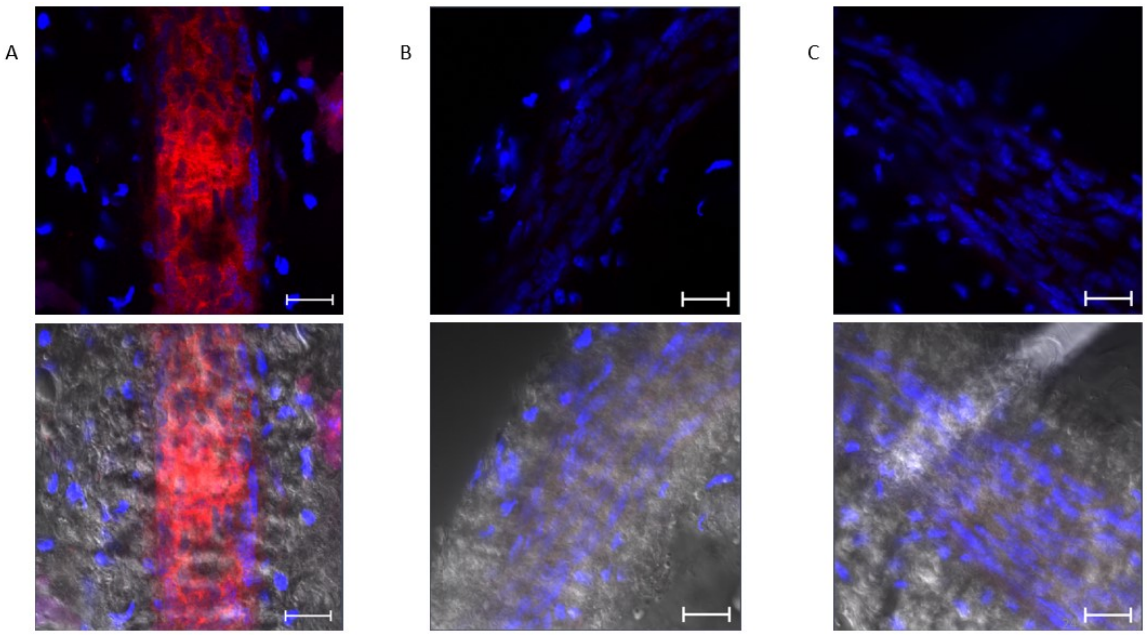

Figure 14: Uptake of pEVs in vivo by popliteal lymphatic vessel. Human platelet-derived EVs ($1x10^7$) **(A)** or PBS **(B)** were injected in the dermis of the footpad in C57BL/6 mice. Popliteal lymphatic vessels were collected 2 h post injection and were fixed in PFA 4 % for 24 h. Vessels were stained with human CD41a antibody (red) and DAPI (blue). Secondary antibody control is shown in **(C)**. Z-Stacks were acquired using an LSM 710 Confocal Microscope (Zeiss) equipped with a 63/1.4 oil dic objective. Corresponding T-PMT images shown below. n=4

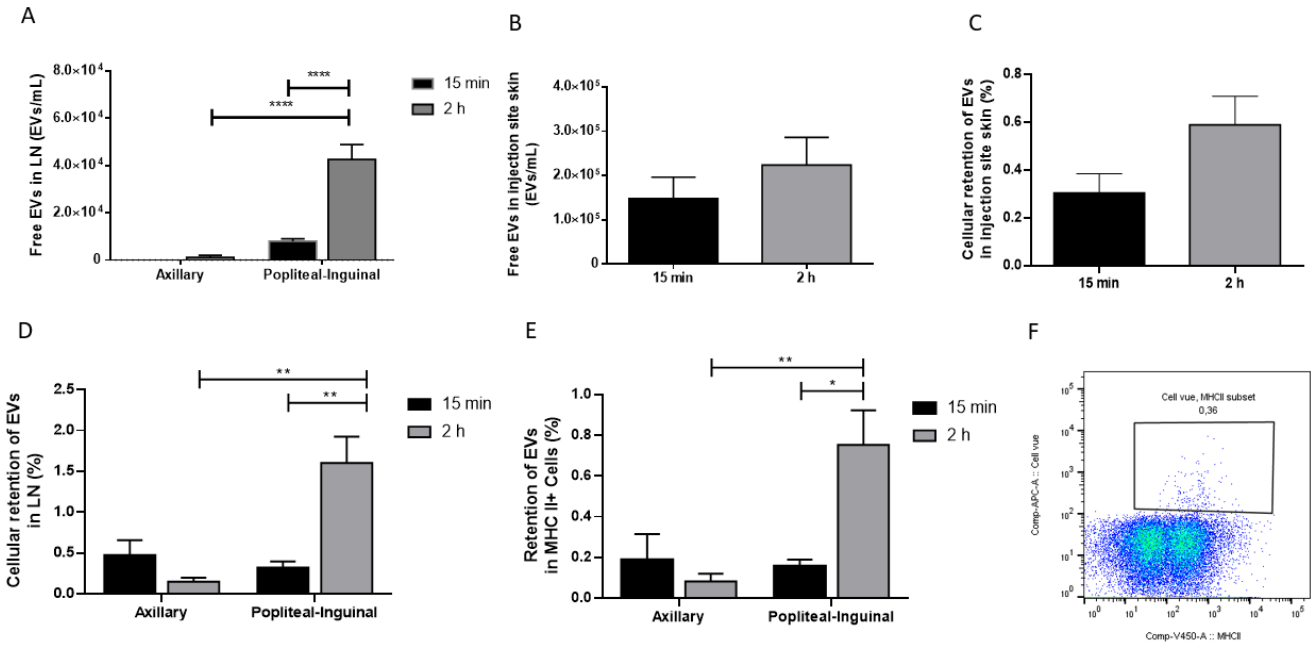

Figure 15: PLT-EVs are uptaken *in vivo* by migratory cells in afferent lymph nodes. Cellvue™ stained Human platelet-derived EVs (1x10^7) were injected in the dermis of the footpad in C57BL/6 mice. Axillary, popliteal and inguinal lymph nodes were collected 15 min or 2 h post injection and digested in collagenase D. Similarly, skin from the injection site was collected and placed in Liberase. Supernatants from LN **(A)** and skin **(B)** digestion were stained with anti-human CD62p (AF700) and CFSE. EVs were analysed using BD FACSCelesta with a 405 nm bandpass filter on the violet laser. Skin cells **(C)** and lymph nodes cells **(D-E)** were stained with anti-mouse CD45, MHCII and anti-human CD62p before analysis with BD FACSCelesta. Gating strategy shows Cellvue™ and MHCII positive cells **(F)**. *p<0.05, **p<0.01, ****p<0.0001; n=3-5

Supplemental Figrues:

Table 1: List of primer sequences used for qPCR analysis

Species	Gene	Gene symbol	Compagnie	RefSeq (NM)	Forward	Reverse
Human	B-ACTIN	hACTB	Sigma	NM_001101.5	GATGTATGAAGGCTTTGGTC	TGTGCACTTTTATTGGTCTC
Human	PDPN	hPDPN	Sigma	NM_006474.5	AGATAAGAAAGATGGCTTGC	AACAACAATGAAGATCCCTC
Human	VEGFR-3	hFLT4	Sigma	NM_182925	AGGTATTACAACTGGGTGTC	TTCCTCAAATGTCTTCATCC
Human	LYVE-1	hLYVE-1	Sigma	NM_006691	TGTCAAAAGGTATGTGAAGG	TCTAAACTTCAGCTTCCAGG
Human	CD31	hPECAM1	BioCorp	NM_000442.5	AAGTGGAGTCCAGCCGCATATC	ATGGAGCAGGACAGGTTCAGTC
Human	ICAM-1	hICAM1	Sigma	NM_000201	ACCATCTACAGCTTTCCG	TCACACTTCACTGTCACC
Human	VCAM-1	hVCAM1	Sigma	NM_001078.4	ACTTGATGTTCAAGGAAGAG	TCCAGTTGAACATATCAAGC
Human	PROX-1	hPROX1	Sigma	NM_001270616	TAGACTTAACTAGGGATACCAC	CATTGCACTTCCCGAATAAG
Human	VE-CADHERIN	hCDH5	Sigma	NM_001795	CGCAATAGACAAGGACATAAC	TATCGTGATTATCCGTGAGG
Human	ZO-1	TJP1	Sigma	NM_003257.5	TTGTCTTCAAAAACTCCCAC	GACTCACAGGAATAGCTTTAG
Human	MIR210HG	MIR210HG	Sigma	NR_038262.1	AGTTCCTGTTGCCAAGCTGA	GGATGGTCCTGTTGGCTGAA
Human	ANKRD37	ANKRD37	Sigma	NM_181726.4	ATTGTGTTGCCGTGCTCAGA	AACCCACGTGACATCAGCAC

$$[EVs] = \left(\left(\frac{nb.EVs}{nb.CB}\, x\, \frac{vol.CB\ x\ [CB\ initial]}{vol.total}\, x\, DF\right) - [EVs\ BG]\right) * 1000$$

Supplemental Figure 1: Determination of EVs concentration in samples

[EVs] = Evs concentration in sample, nb. EVs = amount of Evs of interest during analysis, nb. CB = amount of *Count Beads* during analysis, Vol. CB = volume of *Count Beads* added to sample, [CB initial] = initial concentration of *Count Beads*, vol. total = total volume of the analyzed sample, DF = Dilution Factor of EVs in sample, [EVs BG] = Concentration of EVs in Background tube.

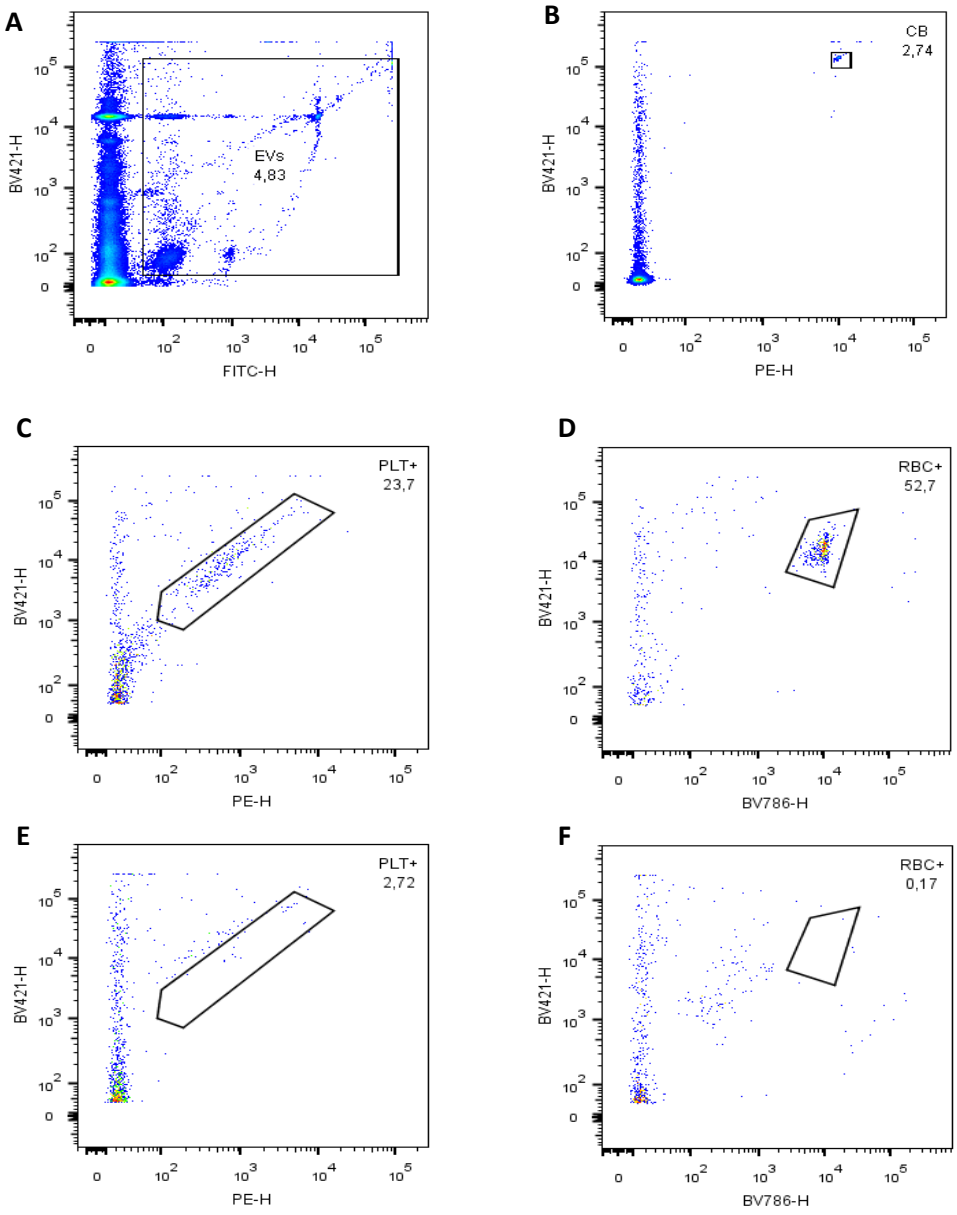

Supplemental Figure 2: Flow cytometry gating strategy for EVs. Megamix calibration beads (Apogee Flow System) ranging from 180 to 1 300 nm were used to identify events with similar size and granularity **(A)**. PE positive Count beads (CB) (1 um) (Apogee Flow System were used to calculate the concentration of events of interest **(B)**. Among the events, those CSFE (FITC) and CD62p (PE) positive were identified as platelet-derived Evs **(C)**. Events CSFE (FITC) and CD235a (BC786) positive were identified as red blood cell-derived Evs **(D)**. The addition of Triton X-100 confirms the gating strategy of PLT-EVs **(E)** and RBC-EVs **(F)**.

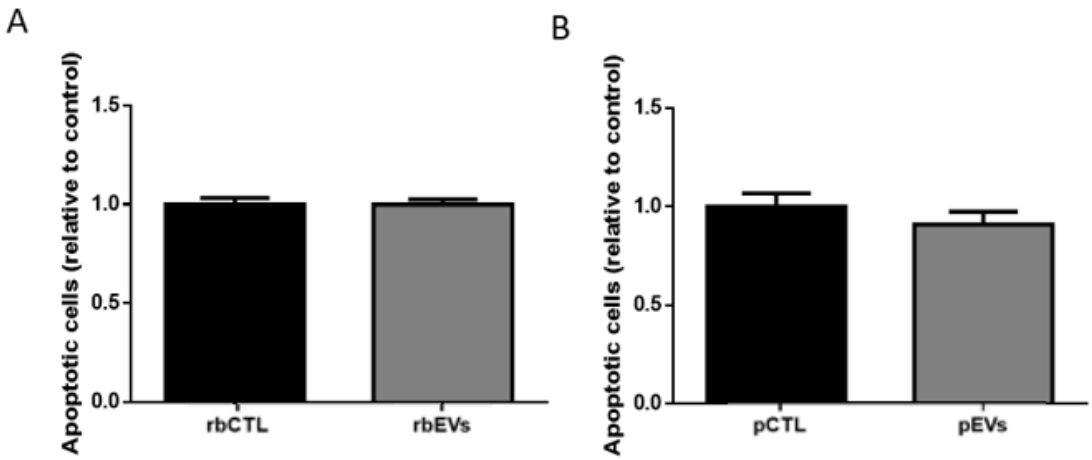

Supplemental Figure 3: Effects of platelet and red blood cell-derived EVs on LECs apoptosis. EVs treated LECs were stained with propidium iodide and Annexin V antibody before flow cytometry analysis using BD FACSCelesta, in order to measure changes in apoptotic cells proportion after RBC-EVs **(A)** or PLT-EVs **(B)** incubation. n=6-7

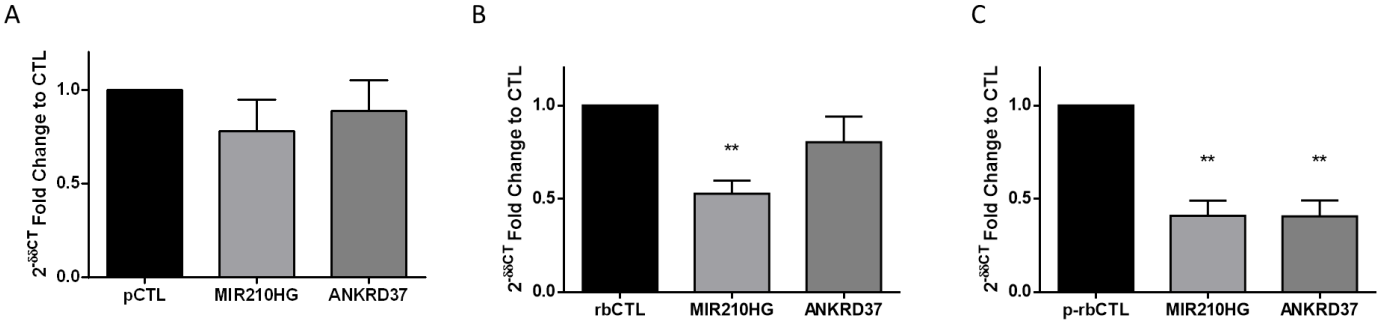

Supplemental Figure 4: Reported RNA-sequencing gene modulation verified by qPCR. The same mRNA sent for RNA-sequencing was used for qPCR analysis, using MIR210HG and ANKRD37 primers. Similar results are observed here. pEVs treatment on LECs does not seem to affect either gene expression **(A)**. rbEVs seem to downregulate MIR210HG expression in LECs **(B)**. Treatment with both subtypes keep downregulating MIR210GH expression as well as ANKRD37 **(C)**. **p<0.01; n=3

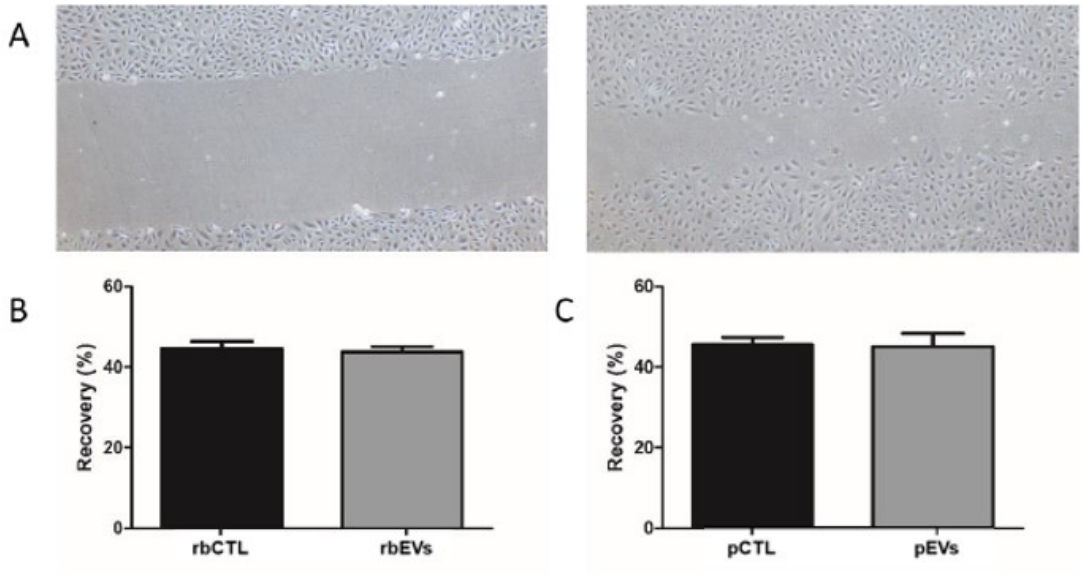

Supplemental Figure 5: Effects of platelet and red blood cell-derived EVs on LECs migration. LECs were seeded in 12 wells plates until they reached confluence of 100 %. Scratching was done with a 1000 uL tip and cells were washed with PBS before EVs incubation. Representative images of scratch assay at 0 h and 24 h **(A)**. Quantification of LECs migration following pEVs **(B)** or rbEVs **(C)** scratch assay. Migration was calculated measuring the percentage of recovered area. Images were analyzed with Image-J. n=6

Chapitre 3. DISCUSSION

3. Discussion :

D'un côté, nos résultats suggèrent que les EVs présentes dans la lymphe peuvent moduler l'intégrité de l'endothélium lymphatique humain. Plus encore, des concentrations physiologiques de rbEVs semblent altérer l'intégrité lymphatique. Ainsi, des concentrations pathologiques de rbEVs pourraient être à l'origine d'une dysfonction lymphatique et d'un mauvais mRCT menant au développement de l'athérosclérose et à l'accumulation d'EVs dans la lymphe. D'un autre côté, nos résultats démontrent également le rôle protecteur des pEVs vis-à-vis de l'endothélium lymphatique et suggèrent une potentielle avenue thérapeutique quant au traitement ou à la prévention de la dysfonction lymphatique. Toutes les expériences jusqu'à présent ont été réalisées en conditions physiologiques. Sachant que les concentrations d'EVs dans la lymphe augmentent lors de maladies inflammatoires chroniques, nous avons également voulu voir ce qu'il en était en conditions d'inflammation.

3.1 EVs et inflammation

L'ajout de TNFα comme prétraitement aux LECs pendant 24 heures a permis de simuler un endothélium en condition inflammatoire. Comme un environnement pro-inflammatoire est connu pour stimuler la production de vésicules extracellulaires, il aurait été attendu que les niveaux basaux d'EVs dérivées de LECs soient augmentés en comparaison avec les taux observés en conditions physiologiques[45,46]. Toutefois, on constate que les niveaux d'EVs produites sont similaires en conditions inflammatoires et que les effets des EVs dérivées de plaquettes et de globules rouges sont les mêmes que rapportés précédemment (Figure sup 1). Comme le milieu est changé entre le prétraitement au TNFα et l'incubation des EVs, les EVs dérivées de LECs probablement produites en plus grande quantité lors du prétraitement sont ainsi enlevées. On constate par ces résultats que l'effet du TNFα n'est potentiellement pas prolongé au-delà du prétraitement. L'ajout de TNFα pendant la période d'incubation des EVs aurait ainsi pu simuler un meilleur environnement pro-inflammatoire. L'expression des marqueurs lymphatiques à la membrane des LECs prétraitées au TNFα a également été observées par cytométrie en flux après

traitement aux pEVs et au rbEVs (Figure sup 2). Encore une fois, les niveaux d'expressions sont similaires aux conditions physiologiques, mais les effets des EVs disparaissent. Il a été montré qu'en présence de TNFα, le LYVE-1 des LECs est dégradé après trois heures et une diminution de CD31 est aperçue après 24 heures[132,133]. Sachant que les pEVs expriment le CD31 et qu'elles peuvent adhérer aux LECs via interactions homologues du CD31, les conditions inflammatoires pourraient nuire à l'internalisation des pEVs, expliquant l'absence d'effet[109]. Augmentant la perméabilité vasculaire sanguine et l'angiogenèse, le TNFα est également connu pour stimuler la lymphangiogenèse via l'induction de la transcription du facteur VEGF-C par la voie du promoteur NF-kB[134,135]. *In vivo*, l'expression du VEGF-C et du VEGFR3 des macrophages et cellules dendritiques est stimulée pendant l'inflammation[136,137]. Ces cellules activées présenteraient ainsi une source de VEGF-C contribuant à la lymphangiogenèse des cellules endothéliales[138]. Sachant que les granules alpha des plaquettes contiennent du VEGF-C, les pEVs en combinaison avec le TNFα pourraient donc potentiellement stimuler la lymphangiogenèse expliquant la légère augmentation du VEGFR3 à la surface des LECs (Figure sup 2A)[105]. Malgré l'absence générale d'effet des EVs vis-à-vis de l'expression des marqueurs lymphatiques à la surface des LECs en conditions inflammatoires, les EVs semblent réguler l'expression de gènes tels qu'observé par qPCR (Figure sup 3). On constate ainsi que les pEVs inhiberaient l'expression de LYVE-1 alors que les rbEVs l'augmenteraient (Figure sup 3A-B). Le récepteur d'acide hyaluronique LYVE-1 étant impliqué dans la migration des leucocytes et le trafic des cellules dans les vaisseaux lymphatiques et les ganglions, ces résultats offrent ainsi un aperçu du pouvoir modulatoire des EVs vis-à-vis de la réponse inflammatoire[139]. De plus, la co-incubation des deux sous-types d'EVs semble stabiliser l'expression du gène LYVE-1, mais aussi augmenter l'expression de Prox-1 (Figure sup 3C). Essentiel à l'induction du phénotype lymphatique des cellules endothéliales, Prox-1 est également augmenté en conditions pro-inflammatoires et est un médiateur de la lymphangiogenèse[140,141]. Sachant que le TNFα induit l'activation des voies NF-kB et qu'il a été démontré que ces dernières stimulent l'expression de Prox-1 et de VEGFR3, il est surprenant de ne pas observer une augmentation de l'expression du gène VEGFR3 avec Prox-1[141,142]. Toutefois, Flister et al. observent *in vivo* que l'activation des voies NF-kB amène une augmentation de l'expression de Prox-1 et de VEGFR3 quatre et deux jours respectivement avant l'apparition de la

lymphangiogenèse[141]. Il se pourrait ainsi que l'incubation des deux sous-types d'EVs sur les LECs potentialise l'activation de la voie NF-kB en parallèle au TNFα, mais que l'augmentation du VEGFR3 ne soit pas encore visible après 24 heures. Il est cependant difficile de tirer des conclusions de ces résultats étant donné que l'effet du prétraitement ne semble pas persister lors des traitements aux EVs. Une analyse transcriptomique permettrait non seulement de confirmer l'effet du TNFα, notamment par l'activation de la voie NF-kB, mais également de mieux comprendre les effets observés. Quoiqu'il en soit, l'absence d'effet des pEVs quant à la production d'EVs dérivées de LECs ainsi que l'inhibition du gène LYVE-1 régulant ainsi négativement la réponse immune démontrent encore une fois un maintien de l'intégrité lymphatique par les pEVs.

3.2 La fonction lymphatique et les pEVs

L'effet des EVs sur la fonction lymphatique n'a pas été testé dans notre étude. Toutefois, on sait maintenant que les pEVs peuvent être pris en charge par les vaisseaux lymphatiques collecteurs après injection intradermale. De plus, une certaine proportion atteint les ganglions afférents, principalement via leur internalisation dans les cellules migratoires exprimant le CMH II. La fonction lymphatique peut être mesurée directement chez les souris par diverses techniques, notamment par l'analyse des fréquences de contractions. En effet, les vaisseaux lymphatiques collecteurs sont recouverts de cellules musculaires lymphatiques possédant un phénotype à la fois lisse et strié, mais une certaine proportion de ces cellules ont une fonction *pacemaker* et initie les contractions intrinsèques[10,143]. Le mécanisme à l'origine de ces contractions est grandement dépendant des niveaux de calcium intracellulaire. Une contraction débute ainsi par l'augmentation des niveaux de calcium cytoplasmique liant le récepteur calmoduline et activant la sous-unité catalytique de la myosine kinase à chaine légère (MLCK) qui peut ainsi phosphoryler la myosine à chaîne légère de 20 kDa (MLK_{20})[144]. D'autre part, le NO peut moduler la relâche et l'absorption du calcium ainsi que les enzymes impliquées[145]. Son équilibre est complexe et sa production peut être augmentée par les forces de cisaillements qui activent l'*endothelial NO synthase* (eNOS)[146]. Dans l'ensemble, le NO s'oppose au calcium intracellulaire et induit une vasodilatation réduisant ainsi la fréquence des contractions[147]. Il a été montré que le NO inhibe l'activation des plaquettes et que les plaquettes activées peuvent générer la molécule, créant

ainsi une boucle de rétroaction négative[148]. En présence de pEVs, les taux de NO sont augmentés chez les cellules myocardiques de lapin[149]. Il serait ainsi pertinent de mesurer les effets des pEVs sur la biodisponibilité du NO pour comprendre leur potentiel effet sur les fréquences de contractions lymphatiques. Sachant que les rbEVs récupèrent le NO et qu'elles sont présentent en grande quantité dans la lymphe de souris athérosclérotiques présentant une dysfonction des vaisseaux lymphatiques collecteurs, l'ajout de pEVs pourrait ainsi hypothétiquement permettre de rétablir l'équilibre de l'oxyde nitrique régulant les contractions lymphatiques.

3.3 L'apoA-I et les pEVs

Afin de potentialiser les effets favorables des pEVs observés dans l'étude, l'ajout de l'apoA-I semble une voie prometteuse. En effet, les bienfaits pléiotropiques de l'apoA-1 sur la fonction lymphatique démontrés par mon équipe pourraient être dépendants des plaquettes[40]. L'apoA-I causant une augmentation de l'adhésion de ces dernières sur les LECs *in vitro*, il se pourrait donc que les mêmes observations soient faites *in vivo* grâce aux pEVs présentes dans la lymphe. Il a été démontré qu'en conditions inflammatoires, la préincubation de l'apoA-I sur les LECs doublait l'expression du gène de la podoplanine[150]. Liant le récepteur CLEC-2 des plaquettes et des pEVs, la surexpression de la podoplanine pourrait à son tour potentialiser l'adhésion des pEVs et aider à maintenir l'intégrité de l'endothélium. De plus, une récente étude démontre que la liaison de l'apoA-I à l'apoA-I *binding protein* (AIBP) des LECs régulerait la lymphangiogenèse en altérant la composition en cholestérol des calvéoles, empêchant ainsi l'inhibition de Cav1 vis-à-vis de la signalisation du VEGFR3[151]. Comme les granules alpha des plaquettes contiennent du VEGF-C, la potentialisation de l'adhésion des pEVs aux LECs via l'apoA-I pourrait à son tour promouvoir la lymphangiogenèse[105].

Notre équipe a également démontré qu'en présence d'apoA-I, les plaquettes adhèrent à l'endothélium et renforcent les jonctions des LECs[40]. Exprimant un protéome similaire à celui des plaquettes, il est possible que les pEVs aient un effet comparable. Les souris *Ldlr*$^{-/-}$; *hApoB100*$^{+/+}$ présentent une dysfonction lymphatique à priori au niveau des vaisseaux lymphatiques collecteurs avant même l'apparition de l'athérosclérose et développent par la suite une hyperperméabilité des mêmes vaisseaux[38]. Il est connu qu'en conditions pathologiques

inflammatoires, comme dans le cas de l'athérosclérose, l'endothélium vasculaire sanguin a une perméabilité augmentée favorisant la migration des cellules immunes en raison d'une dérégulation des niveaux d'expression des molécules d'adhésion, du relargage de cytokines pro-inflammatoires et de facteurs de croissance[152]. Des conditions inflammatoires similaires et la présence de facteurs pro-inflammatoires tels que le TNFα, l'IL-6 ou l'interféron gamma sont aussi connues pour augmenter la perméabilité des vaisseaux lymphatiques[153,154]. Des traitements aux pEVs pourraient ainsi pallier ce défaut de perméabilité en renforçant les jonctions intercellulaires. Toutefois, les pEVs sont connus pour leur rôle à la fois dans la progression et la stabilisation de l'athérosclérose. Ayant un fort potentiel thrombotique, les pEVs peuvent participer à la progression de l'athérosclérose via la formation de thrombose et d'occlusion vasculaire[155]. À l'opposé, les pEVs peuvent également limiter la formation de cellules spumeuses en inhibant l'expression du récepteur CD36 qui participe au transfert du cholestérol vers les macrophages[156]. Comme le pouvoir thrombotique des pEVs est dû en grande partie à l'exposition du PS à leur surface et qu'un traitement aux pEVs pourrait favoriser la survenue d'évènements thrombotiques et la progression de l'athérosclérose, l'ajout de la molécule ticagrelor pendant la production des pEVs pourrait ainsi limiter l'expression de la PS[157]. Inhibant les récepteurs P2Y12 impliqués dans la liaison de l'ADP et dans la sensibilité d'activation des plaquettes, le ticagrelor permettrait non seulement d'inhiber l'expression de la PS et le phénotype thrombotique des pEVs, mais aussi de potentialiser leurs effets favorables[64,65,67].

3.4 Projet pEVs et ApoA-I

Il serait ainsi possible de constater l'effet des pEVs sur la fonction lymphatique avec un projet utilisant des souris *Ldlr*$^{-/-}$; *hapoB100*$^{+/+}$ prédisposées à développer l'athérosclérose, un modèle avec lequel nous avions démontré que le VEGF-C 152s permettait de restaurer la fonction lymphatique et de limiter le développement de la maladie. Similairement aux données publiées par Milasan et al. en 2016, des résultats préliminaires chez les souris C57BL/6 et *Ldlr*$^{-/-}$ mâles et femelles âgées de 10 à 11 semaines montrent bel et bien une fonction lymphatique altérée chez les souris *Ldlr*$^{-/-}$ prédisposées à développer l'athérosclérose (Figure sup 4)[38]. Nous avons ainsi voulu voir si une injection simple de pEVs pouvait moduler la fonction lymphatique, sachant que

les pEVs sont internalisées par les LECs dès deux heures. Deux heures suivant l'injection de pEVs dans le derme de la patte droite des souris, une solution contenant le marqueur *fluorescein isothiocyanate* (FITC) ainsi que du dibutyl phthalate activant la réponse immunitaire a été appliquée topiquement sur leur dos. Afin de laisser migrer les cellules dendritiques internalisant le FITC, les souris n'ont été sacrifiées que 18 heures plus tard et leurs ganglions inguinaux ont été récupérés. La digestion des ganglions dans la collagénase D et le marquage des cellules au CD11c, CD11b et CMH II ont ainsi permis de calculer la concentration de cellules dendritiques ayant migrées de la peau aux ganglions inguinaux. Par cette technique couplant la capacité d'absorption ainsi que le transport lymphatique, on constate qu'une injection simple de pEVs après un total de 20 heures ne parvient pas à restaurer la fonction lymphatique des souris *Ldlr*$^{-/-}$ mâles et femelles présentant une fonction lymphatique altérée (Figure sup 4 C-D). Similairement, la capacité contractile des vaisseaux lymphatiques collecteurs poplités des souris a été évaluée deux heures suivant l'injection de pEVs dans le derme de la patte. La peau de la patte a été retirée, puis l'ovalbumine fluorescente (OVA) (AF647) de 45 kDa a été injectée dans le derme. Son poids moléculaire permet son absorption par les capillaires lymphatiques, mais empêche sa fuite une fois dans les vaisseaux collecteurs en raison des jonctions serrées. Après une période d'équilibre de cinq minutes, une vidéo de dix minutes a été enregistrée à l'aide du microscope à fluorescence AxioZoom 5.6 (Zeiss). La phényléphrine (PE) a ensuite été injectée dans le derme en suivant la même procédure afin de stimuler les contractions lymphatiques intrinsèques et afin d'évaluer la réactivité des vaisseaux. Encore une fois, la fonction lymphatique altérée chez les souris *Ldlr*$^{-/-}$ est visible de par leurs fréquences de contractions plus basses que chez les souris C57BL/6 (Figure sup 5 C-D). Encore ici, une injection simple de pEVs ne parvient pas non plus à restaurer la capacité contractile des vaisseaux collecteurs.

L'une des limitations ici est sans aucun doute que l'espèce d'origine des pEVs diffère de l'espèce du receveur. Quelques différences existent entre les plaquettes humaines et murines. Plus spécifiquement, Rowley et al. ont montré par analyse transcriptomique que certains récepteurs des plaquettes humaines n'étaient pas exprimés par les plaquettes des souris[158]. En effet, le récepteur PTAFR est absent, réfutant les observations précédemment publiées selon lesquelles le PAF n'active pas les plaquettes murines[159,160]. De plus, marqueur de la translocation lysosomale

en réponse à l'activation des plaquettes, le récepteur CD68 n'est également pas[161]. Enfin, le récepteur PAR1 essentiel à la signalisation via la thrombine chez les plaquettes humaines est aussi absent des plaquettes de souris, expliquant pourquoi les plaquettes des souris déficientes en *Par1* sont toujours activées par la thrombine[162]. Malgré ces différences, les pEVs humaines ne semblent pas avoir activées la réponse immune des souris, puisque l'on n'observe aucune différence de fonction lymphatique 20 heures après l'injection du véhicule ou des pEVs (Figure sup 4). Devant les contraintes éthiques que présenterait l'injection de pEVs chez des patients humains, il serait pertinent de tester si les bienfaits des pVEs humaines persistent sur un endothélium lymphatique murin *in vitro* avant d'aller plus loin.

Une fois ces vérifications faites, des traitements à doses multiples de pEVs et/ou d'apoA-I suivi par une la prise d'une diète riche en gras permettrait de vérifier plusieurs hypothèses. Premièrement, on pourrait ainsi constater si les pEVs améliorent la fonction lymphatique et peuvent prévenir la formation d'athérosclérose chez les souris en comparaison avec les souris traitées avec le véhicule. Deuxièmement, on pourrait constater si réellement l'apoA-I permet de potentialiser les bienfaits des pEVs comme nous l'avions démontré avec les plaquettes *in vitro*. L'étude pourrait également inclure des pEVs préalablement produites en présence de la molécule ticagrelor qui inhibe l'exposition de la PS à la surface des vésicules, mais uniquement une fois leurs effets sur les LECs caractérisés *in vitro*. La perméabilité lymphatique pourrait être mesurée via l'injection du colorant bleu d'Evans, suivi par la quantification des zones présentant une fuite autour des vaisseaux lymphatiques collecteurs. La fonction lymphatique pourrait également être mesurée par l'injection d'une protéine fluorescente comme l'ovalbumine dans le derme des souris, suivi par le calcul des fréquences de contractions des vaisseaux lymphatiques collecteurs observées directement au microscope à fluorescence. La capacité d'absorption des vaisseaux ainsi que la lymphangiogenèse pourraient à leur tour être mesurées respectivement directement au niveau des oreilles par la prise en charge du bleu d'Evans par les capillaires lymphatiques initiaux ainsi que par l'évaluation de la morphologie des vaisseaux par immunofluorescence. Enfin, la mesure de la capacité de migration des cellules dendritiques par l'application cutanée d'une solution de FITC (FITC *painting*) suivi par la quantification du colorant dans les cellules

dendritiques des ganglions à l'aide d'un cytomètre en flux permettrait d'évaluer le transport lymphatique dans son ensemble.

Pour la suite du projet, le contenu des pEVs, mais plus précisément leur contenu en miARN devrait également être étudié davantage. Les miARN sont des micros séquences d'ARN qui modulent la production de protéines. Ils sont des joueurs clés dans la régulation des fonctions cellulaires et sont considérés comme des biomarqueurs dans plusieurs pathologies. Leur identification et celle des protéines qu'ils régulent peuvent permettre d'identifier de nouvelles cibles thérapeutiques. Comme les plaquettes jouent un rôle crucial dans la pathogenèse de l'athérosclérose et de l'infarctus du myocarde, plusieurs études se sont penchées sur les potentiels rôles des miARN relâchés par les plaquettes et leurs vésicules. Plus de 500 miARN sont retrouvés dans les plaquettes[163]. Par exemple, une étude montre une diminution de l'expression d'ICAM-1 par des cellules endothéliales microvasculaires (HMEC-1) en présence de pEVs via la relâche de miR-320b inhibant ainsi le recrutement des leucocytes[164]. L'un des miARN hautement exprimés par les plaquettes est le miR-223, impliqué dans la thrombopoïèse et l'expression de P2Y12[163,165]. Plus encore, le miR-126 plasmatique dérive principalement des plaquettes, corrèle avec les concentrations de pEVs et est un marqueur de l'activation plaquettaire[166,167]. Dans les cellules endothéliales, l'expression du miR-126 module l'angiogenèse, l'intégrité vasculaire et inhibe l'expression de VCAM-1 qui à son tour inhibe l'adhésion des leucocytes et régule l'inflammation[168-170]. Similairement au miR-126, il a été montré que des patients souffrant d'un infarctus du myocarde avec segment ST élevé ont des niveaux diminués de miR-22, miR-320b et miR-185 dans leurs plaquettes, soit des miARN impliqués dans l'activation des plaquettes via la thrombine[164]. Enfin le miR-9, impliqué dans la différenciation des mégakaryocytes, est également impliqué dans la réponse au TNFα dans les vaisseaux lymphatiques mésentériques chez le rat et induit l'augmentation de l'expression du VEGFR3 indiquant un potentiel rôle dans la lymphangiogenèse[171,172].

3.5 Projet translationnel

Il ne faut toutefois pas oublier que la lymphe transporte biens d'autres EVs d'origines différentes qui pourraient présenter un potentiel thérapeutique bien plus grand ou encore faire de meilleurs

biomarqueurs. C'est pourquoi nous avons mis en place un projet translationnel visant à démontrer la présence d'une dysfonction lymphatique avant l'apparition de l'athérosclérose chez l'humain en corrélation avec la caractérisation de leurs EVs plasmatiques et de leurs paramètres biochimiques. Dans cette étude, des patients sains et des patients avec une histoire familiale de maladie cardiovasculaire (MCV) chez un parent de premier degré (paramètre connu pour augmenter les risques de MCV de 60 à 75%) seront suivis pendant cinq ans. De plus, ces données pourront être couplées au score de risque polygénique de développer une MCV, soit une estimation génétique prédisant le risque de développer la maladie ciblée, afin d'identifier des variants génétiques d'intérêts. Nos résultats préliminaires suggèrent que les sujets avec antécédents familiaux de MCV présentent des signes de dysfonction lymphatique. De plus, des disparités ont été observées lors de la caractérisation de leurs EVs plasmatiques. En effets, les patients avec antécédents familiaux de MCV auraient moins d'EVs au potentiel protecteur et davantage d'EVs néfastes. Plus spécifiquement, ces patients semblent avoir une diminution des niveaux de pEVs et d'EVs dérivées de cellules myéloïdes progénitrices (CD14+ LYVE-1+) ainsi qu'une augmentation des taux d'EVs dérivées des lymphocytes T. Participant à la coagulation, l'activation des monocytes et l'activation des cellules endothéliales, les EVs de lymphocytes T témoignent potentiellement d'un état pro-inflammatoire supérieur chez ces patients[173,174]. De plus, la présence moins importante d'EVs dérivées de cellules myéloïdes progénitrices CD14+ LYVE-1+ pourrait témoigner d'une lymphangiogénèse diminuée ou inadéquate[175]. La caractérisation plus en profondeur de ces EVs ainsi que de leurs effets sur l'endothélium lymphatique *in vitro* dans notre laboratoire en plus de leur analyse en corrélation avec le score de risque polygénique pourront potentiellement permettre d'identifier l'origine de la dysfonction lymphatique associée à l'athérosclérose. Ces découvertes permettront ensuite d'identifier de nouveaux biomarqueurs et de nouvelles cibles de thérapeutiques.

Chapitre 4. CONCLUSION

4. Conclusion

Ayant précédemment démontré que le transport lymphatique est altéré chez les jeunes souris prédisposée à développer l'athérosclérose, l'ensemble de nos données confirme donc l'hypothèse selon laquelle les EVs présentes dans lymphe circulante peuvent moduler l'intégrité lymphatique. Plus encore, les pEVs présentes dans la lymphe participeraient au maintien de l'intégrité de l'endothélium lymphatique. En effet, n'utilisant que des concentrations physiologiques de pVEs, nos résultats démontrent une adhésion rapide des vésicules sur les CELs en plus d'une inhibition de la production de ROS ainsi que de la nécrose cellulaire.

Les pEVs semblent ainsi une avenue thérapeutique prometteuse qu'il faudra continuer d'explorer. Notre laboratoire ayant déjà démontré qu'il existe une synergie entre l'apoA-I et les plaquettes, il faudra donc assurément tester si l'apoA-I permettrait de potentialiser les effets des pEVs pour ultimement pallier ou prévenir la dysfonction lymphatique observée à priori au niveau des vaisseaux lymphatiques collecteurs précocement au développement de l'athérosclérose. En joignant ces résultats au projet translationnel en cours dans notre laboratoire, nous espérons potentiellement permettre l'identification de nouveaux biomarqueurs ou de nouvelles stratégies qui permettront d'améliorer la dysfonction lymphatique menant à la régression ou la prévention de maladies inflammatoires chroniques telles que l'athérosclérose.

Références bibliographiques

1. He, W.*, et al.* The anatomy and metabolome of the lymphatic system in the brain in health and disease. *Brain Pathol* **30**, 392-404 (2020).
2. Aspelund, A.*, et al.* A dural lymphatic vascular system that drains brain interstitial fluid and macromolecules. *J Exp Med* **212**, 991-999 (2015).
3. Trevaskis, N.L., Kaminskas, L.M. & Porter, C.J. From sewer to saviour - targeting the lymphatic system to promote drug exposure and activity. *Nat Rev Drug Discov* **14**, 781-803 (2015).
4. Jones, D. & Min, W. An overview of lymphatic vessels and their emerging role in cardiovascular disease. *Journal of Cardiovascular Disease Research* **2**, 141-152 (2011).
5. Dieu, M.C.*, et al.* Selective recruitment of immature and mature dendritic cells by distinct chemokines expressed in different anatomic sites. *J Exp Med* **188**, 373-386 (1998).
6. Huang, F.P.*, et al.* A discrete subpopulation of dendritic cells transports apoptotic intestinal epithelial cells to T cell areas of mesenteric lymph nodes. *J Exp Med* **191**, 435-444 (2000).
7. Moore, J.E., Jr. & Bertram, C.D. Lymphatic System Flows. *Annu Rev Fluid Mech* **50**, 459-482 (2018).
8. Cifarelli, V. & Eichmann, A. The Intestinal Lymphatic System: Functions and Metabolic Implications. *Cell Mol Gastroenterol Hepatol* **7**, 503-513 (2019).
9. Muthuchamy, M., Gashev, A., Boswell, N., Dawson, N. & Zawieja, D. Molecular and functional analyses of the contractile apparatus in lymphatic muscle. *Faseb j* **17**, 920-922 (2003).
10. Kenney, H.M.*, et al.* Lineage tracing reveals evidence of a popliteal lymphatic muscle progenitor cell that is distinct from skeletal and vascular muscle progenitors. *Sci Rep* **10**, 18088-18088 (2020).
11. Mortimer, P.S. & Levick, J.R. Chronic peripheral oedema: the critical role of the lymphatic system. *Clin Med (Lond)* **4**, 448-453 (2004).
12. Iqbal, J. & Hussain, M.M. Intestinal lipid absorption. **296**, E1183-E1194 (2009).
13. Hussain, M.M.*, et al.* Clearance of chylomicron remnants by the low density lipoprotein receptor-related protein/alpha 2-macroglobulin receptor. *J Biol Chem* **266**, 13936-13940 (1991).
14. Ramasamy, I. Recent advances in physiological lipoprotein metabolism %J Clinical Chemistry and Laboratory Medicine (CCLM). **52**, 1695-1727 (2014).
15. Martel, C.*, et al.* Lymphatic vasculature mediates macrophage reverse cholesterol transport in mice. *J Clin Invest* **123**, 1571-1579 (2013).
16. Rosenson, R.S.*, et al.* Cholesterol Efflux and Atheroprotection. **125**, 1905-1919 (2012).
17. Ouimet, M., Barrett, T.J. & Fisher, E.A. HDL and Reverse Cholesterol Transport. **124**, 1505-1518 (2019).
18. Annema, W. & Tietge, U.J. Regulation of reverse cholesterol transport - a comprehensive appraisal of available animal studies. *Nutr Metab (Lond)* **9**, 25 (2012).
19. Tall, A.R. CETP inhibitors to increase HDL cholesterol levels. *N Engl J Med* **356**, 1364-1366 (2007).

20. Joy, T.R. & Hegele, R.A. The failure of torcetrapib: what have we learned? *Br J Pharmacol* **154**, 1379-1381 (2008).
21. Kosmas, C.E., DeJesus, E., Rosario, D. & Vittorio, T.J. CETP Inhibition: Past Failures and Future Hopes. *Clin Med Insights Cardiol* **10**, 37-42 (2016).
22. Tardif, J.-C*., et al.* Pharmacogenomic Determinants of the Cardiovascular Effects of Dalcetrapib. **8**, 372-382 (2015).
23. Lemole, G.M. The Role of Lymphstasis in Atherogenesis. *The Annals of Thoracic Surgery* **31**, 290-293 (1981).
24. Rauniyar, K., Jha, S.K. & Jeltsch, M. Biology of Vascular Endothelial Growth Factor C in the Morphogenesis of Lymphatic Vessels. **6**(2018).
25. Leppänen, V.-M*., et al.* Structural determinants of vascular endothelial growth factor-D receptor binding and specificity. *Blood* **117**, 1507-1515 (2011).
26. Baldwin, M.E*., et al.* Vascular Endothelial Growth Factor D Is Dispensable for Development of the Lymphatic System. **25**, 2441-2449 (2005).
27. Karkkainen, M.J*., et al.* Vascular endothelial growth factor C is required for sprouting of the first lymphatic vessels from embryonic veins. *Nat Immunol* **5**, 74-80 (2004).
28. Dumont, D.J*., et al.* Cardiovascular failure in mouse embryos deficient in VEGF receptor-3. *Science* **282**, 946-949 (1998).
29. MILROY, W.F. CHRONIC HEREDITARY EDEMA: MILROY'S DISEASE. *Journal of the American Medical Association* **91**, 1172-1175 (1928).
30. Connell, F., Brice, G. & Mortimer, P. Phenotypic Characterization of Primary Lymphedema. **1131**, 140-146 (2008).
31. Rockson, S.G. Lymphedema. *Am J Med* **110**, 288-295 (2001).
32. Jeon, B.H*., et al.* Profound but dysfunctional lymphangiogenesis via vascular endothelial growth factor ligands from CD11b+ macrophages in advanced ovarian cancer. *Cancer Res* **68**, 1100-1109 (2008).
33. von der Weid, P.Y., Rehal, S. & Ferraz, J.G. Role of the lymphatic system in the pathogenesis of Crohn's disease. *Curr Opin Gastroenterol* **27**, 335-341 (2011).
34. Pedica, F., Ligorio, C., Tonelli, P., Bartolini, S. & Baccarini, P. Lymphangiogenesis in Crohn's disease: an immunohistochemical study using monoclonal antibody D2-40. *Virchows Archiv* **452**, 57-63 (2008).
35. Lim, H.Y*., et al.* Hypercholesterolemic mice exhibit lymphatic vessel dysfunction and degeneration. *Am J Pathol* **175**, 1328-1337 (2009).
36. Zolla, V*., et al.* Aging-related anatomical and biochemical changes in lymphatic collectors impair lymph transport, fluid homeostasis, and pathogen clearance. *Aging Cell* **14**, 582-594 (2015).
37. Blum, K.S*., et al.* Chronic high-fat diet impairs collecting lymphatic vessel function in mice. *PLoS One* **9**, e94713 (2014).
38. Milasan, A., Dallaire, F., Mayer, G. & Martel, C. Effects of LDL Receptor Modulation on Lymphatic Function. *Sci Rep* **6**, 27862 (2016).
39. Milasan, A., Smaani, A. & Martel, C. Early rescue of lymphatic function limits atherosclerosis progression in Ldlr(-/-) mice. *Atherosclerosis* **283**, 106-119 (2019).
40. Milasan, A*., et al.* Apolipoprotein A-I Modulates Atherosclerosis Through Lymphatic Vessel-Dependent Mechanisms in Mice. **6**, e006892 (2017).

41. Milasan, A.*, et al.* Extracellular vesicles are present in mouse lymph and their level differs in atherosclerosis. *J Extracell Vesicles* **5**, 31427 (2016).
42. Doyle, L.M. & Wang, M.Z. Overview of Extracellular Vesicles, Their Origin, Composition, Purpose, and Methods for Exosome Isolation and Analysis. **8**, 727 (2019).
43. Zaborowski, M.P., Balaj, L., Breakefield, X.O. & Lai, C.P. Extracellular Vesicles: Composition, Biological Relevance, and Methods of Study. *BioScience* **65**, 783-797 (2015).
44. Ko, S.Y. & Naora, H. Extracellular Vesicle Membrane-Associated Proteins: Emerging Roles in Tumor Angiogenesis and Anti-Angiogenesis Therapy Resistance. *Int J Mol Sci* **21**(2020).
45. Ståhl, A.L., Johansson, K., Mossberg, M., Kahn, R. & Karpman, D. Exosomes and microvesicles in normal physiology, pathophysiology, and renal diseases. *Pediatr Nephrol* **34**, 11-30 (2019).
46. Camussi, G., Deregibus, M.C., Bruno, S., Cantaluppi, V. & Biancone, L. Exosomes/microvesicles as a mechanism of cell-to-cell communication. *Kidney Int* **78**, 838-848 (2010).
47. Caby, M.P., Lankar, D., Vincendeau-Scherrer, C., Raposo, G. & Bonnerot, C. Exosomal-like vesicles are present in human blood plasma. *Int Immunol* **17**, 879-887 (2005).
48. van Niel, G., D'Angelo, G. & Raposo, G. Shedding light on the cell biology of extracellular vesicles. *Nat Rev Mol Cell Biol* **19**, 213-228 (2018).
49. Möbius, W.*, et al.* Immunoelectron microscopic localization of cholesterol using biotinylated and non-cytolytic perfringolysin O. *J Histochem Cytochem* **50**, 43-55 (2002).
50. van der Vorst, E.P.C., de Jong, R.J. & Donners, M.M.P.C. Message in a Microbottle: Modulation of Vascular Inflammation and Atherosclerosis by Extracellular Vesicles. **5**(2018).
51. Hessvik, N.P. & Llorente, A. Current knowledge on exosome biogenesis and release. *Cell Mol Life Sci* **75**, 193-208 (2018).
52. Hong, S.B.*, et al.* Potential of Exosomes for the Treatment of Stroke. *Cell Transplant* **28**, 662-670 (2019).
53. Gustafson, D., Veitch, S. & Fish, J.E. Extracellular Vesicles as Protagonists of Diabetic Cardiovascular Pathology. **4**(2017).
54. El Andaloussi, S., Mäger, I., Breakefield, X.O. & Wood, M.J.A. Extracellular vesicles: biology and emerging therapeutic opportunities. *Nature Reviews Drug Discovery* **12**, 347-357 (2013).
55. Arslan, F.*, et al.* Mesenchymal stem cell-derived exosomes increase ATP levels, decrease oxidative stress and activate PI3K/Akt pathway to enhance myocardial viability and prevent adverse remodeling after myocardial ischemia/reperfusion injury. *Stem Cell Research* **10**, 301-312 (2013).
56. Cho, J.A., Park, H., Lim, E.H. & Lee, K.W. Exosomes from breast cancer cells can convert adipose tissue-derived mesenchymal stem cells into myofibroblast-like cells. *Int J Oncol* **40**, 130-138 (2012).
57. Vong, S. & Kalluri, R. The role of stromal myofibroblast and extracellular matrix in tumor angiogenesis. *Genes Cancer* **2**, 1139-1145 (2011).
58. Gastpar, R.*, et al.* Heat shock protein 70 surface-positive tumor exosomes stimulate migratory and cytolytic activity of natural killer cells. *Cancer Res* **65**, 5238-5247 (2005).

59. Lv, L.H.*, et al.* Anticancer drugs cause release of exosomes with heat shock proteins from human hepatocellular carcinoma cells that elicit effective natural killer cell antitumor responses in vitro. *J Biol Chem* **287**, 15874-15885 (2012).
60. Hugel, B., Martínez, M.C., Kunzelmann, C. & Freyssinet, J.M. Membrane microparticles: two sides of the coin. *Physiology (Bethesda)* **20**, 22-27 (2005).
61. VanWijk, M.J., VanBavel, E., Sturk, A. & Nieuwland, R. Microparticles in cardiovascular diseases. *Cardiovasc Res* **59**, 277-287 (2003).
62. Connor, D.E., Exner, T., Ma, D.D. & Joseph, J.E. The majority of circulating platelet-derived microparticles fail to bind annexin V, lack phospholipid-dependent procoagulant activity and demonstrate greater expression of glycoprotein Ib. *Thromb Haemost* **103**, 1044-1052 (2010).
63. Boulanger, C.M., Loyer, X., Rautou, P.-E. & Amabile, N. Extracellular vesicles in coronary artery disease. *Nature Reviews Cardiology* **14**, 259-272 (2017).
64. Gasecka, A*., et al.* P2Y12 antagonist ticagrelor inhibits the release of procoagulant extracellular vesicles from activated platelets. *Cardiol J* **26**, 782-789 (2019).
65. Gąsecka, A*., et al.* Role of P2Y Receptors in Platelet Extracellular Vesicle Release. **21**, 6065 (2020).
66. Hankins, H.M., Baldridge, R.D., Xu, P. & Graham, T.R. Role of flippases, scramblases and transfer proteins in phosphatidylserine subcellular distribution. *Traffic* **16**, 35-47 (2015).
67. Mansour, A., Bachelot-Loza, C., Nesseler, N., Gaussem, P. & Gouin-Thibault, I. P2Y12 Inhibition beyond Thrombosis: Effects on Inflammation. **21**, 1391 (2020).
68. Xu, X., Lai, Y. & Hua, Z.C. Apoptosis and apoptotic body: disease message and therapeutic target potentials. *Biosci Rep* **39**(2019).
69. Poon, I.K., Lucas, C.D., Rossi, A.G. & Ravichandran, K.S. Apoptotic cell clearance: basic biology and therapeutic potential. *Nat Rev Immunol* **14**, 166-180 (2014).
70. Battistelli, M. & Falcieri, E. Apoptotic Bodies: Particular Extracellular Vesicles Involved in Intercellular Communication. *Biology (Basel)* **9**(2020).
71. Caruso, S. & Poon, I.K.H. Apoptotic Cell-Derived Extracellular Vesicles: More Than Just Debris. *Front Immunol* **9**, 1486 (2018).
72. György, B*., et al.* Membrane vesicles, current state-of-the-art: emerging role of extracellular vesicles. *Cellular and Molecular Life Sciences* **68**, 2667-2688 (2011).
73. Dang, X.T.T., Kavishka, J.M., Zhang, D.X., Pirisinu, M. & Le, M.T.N. Extracellular Vesicles as an Efficient and Versatile System for Drug Delivery. **9**, 2191 (2020).
74. Lucchetti, D., Fattorossi, A. & Sgambato, A. Extracellular Vesicles in Oncology: Progress and Pitfalls in the Methods of Isolation and Analysis. *Biotechnol J* **14**, e1700716 (2019).
75. Heath, N*., et al.* Rapid isolation and enrichment of extracellular vesicle preparations using anion exchange chromatography. *Sci Rep* **8**, 5730 (2018).
76. Carnino, J.M., Lee, H. & Jin, Y. Isolation and characterization of extracellular vesicles from Broncho-alveolar lavage fluid: a review and comparison of different methods. *Respiratory Research* **20**, 240 (2019).
77. Konoshenko, M.Y., Lekchnov, E.A., Vlassov, A.V. & Laktionov, P.P. Isolation of Extracellular Vesicles: General Methodologies and Latest Trends. *Biomed Res Int* **2018**, 8545347 (2018).
78. Usman, W.M*., et al.* Efficient RNA drug delivery using red blood cell extracellular vesicles. *Nature Communications* **9**, 2359 (2018).

79. Morales-Kastresana, A.*, et al.* Labeling Extracellular Vesicles for Nanoscale Flow Cytometry. *Sci Rep* **7**, 1878 (2017).
80. Théry, C.*, et al.* Minimal information for studies of extracellular vesicles 2018 (MISEV2018): a position statement of the International Society for Extracellular Vesicles and update of the MISEV2014 guidelines. *Journal of Extracellular Vesicles* **7**, 1535750 (2018).
81. Vestad, B.*, et al.* Size and concentration analyses of extracellular vesicles by nanoparticle tracking analysis: a variation study. *J Extracell Vesicles* **6**, 1344087 (2017).
82. Linares, R., Tan, S., Gounou, C. & Brisson, A.R. Imaging and Quantification of Extracellular Vesicles by Transmission Electron Microscopy. *Methods Mol Biol* **1545**, 43-54 (2017).
83. Chuo, S.T.-Y., Chien, J.C.-Y. & Lai, C.P.-K. Imaging extracellular vesicles: current and emerging methods. *Journal of Biomedical Science* **25**, 91 (2018).
84. Robbins, P.D., Dorronsoro, A. & Booker, C.N. Regulation of chronic inflammatory and immune processes by extracellular vesicles. *J Clin Invest* **126**, 1173-1180 (2016).
85. Prado, N.*, et al.* Exosomes from bronchoalveolar fluid of tolerized mice prevent allergic reaction. *J Immunol* **181**, 1519-1525 (2008).
86. Östman, S., Taube, M. & Telemo, E. Tolerosome-induced oral tolerance is MHC dependent. **116**, 464-476 (2005).
87. Kim, S.H., Bianco, N.R., Shufesky, W.J., Morelli, A.E. & Robbins, P.D. MHC class II+ exosomes in plasma suppress inflammation in an antigen-specific and Fas ligand/Fas-dependent manner. *J Immunol* **179**, 2235-2241 (2007).
88. Gatson, N.N.*, et al.* Induction of pregnancy during established EAE halts progression of CNS autoimmune injury via pregnancy-specific serum factors. *J Neuroimmunol* **230**, 105-113 (2011).
89. Njock, M.S.*, et al.* Endothelial cells suppress monocyte activation through secretion of extracellular vesicles containing antiinflammatory microRNAs. *Blood* **125**, 3202-3212 (2015).
90. Yamamoto, S.*, et al.* Inflammation-induced endothelial cell-derived extracellular vesicles modulate the cellular status of pericytes. *Sci Rep* **5**, 8505 (2015).
91. Oggero, S., Austin-Williams, S. & Norling, L.V. The Contrasting Role of Extracellular Vesicles in Vascular Inflammation and Tissue Repair. *Front Pharmacol* **10**, 1479 (2019).
92. Tessandier, N.*, et al.* Platelets Disseminate Extracellular Vesicles in Lymph in Rheumatoid Arthritis. **40**, 929-942 (2020).
93. Milasan, A., Farhat, M. & Martel, C. Extracellular Vesicles as Potential Prognostic Markers of Lymphatic Dysfunction. **11**(2020).
94. Harvey, N.L. The Link between Lymphatic Function and Adipose Biology. **1131**, 82-88 (2008).
95. Montani, J.P.*, et al.* Ectopic fat storage in heart, blood vessels and kidneys in the pathogenesis of cardiovascular diseases. *International Journal of Obesity* **28**, S58-S65 (2004).
96. Bernier-Latmani, J.*, et al.* DLL4 promotes continuous adult intestinal lacteal regeneration and dietary fat transport. *J Clin Invest* **125**, 4572-4586 (2015).
97. Tavakkolizadeh, A., Wolfe, K.Q. & Kangesu, L. Cutaneous lymphatic malformation with secondary fat hypertrophy. *British Journal of Plastic Surgery* **54**, 367-369 (2001).

98. Wadey, R.M.*, et al.* Inflammatory adipocyte-derived extracellular vesicles promote leukocyte attachment to vascular endothelial cells. *Atherosclerosis* **283**, 19-27 (2019).
99. Dini, L.*, et al.* Microvesicles and exosomes in metabolic diseases and inflammation. *Cytokine & Growth Factor Reviews* **51**, 27-39 (2020).
100. Escobedo, N. & Oliver, G. The Lymphatic Vasculature: Its Role in Adipose Metabolism and Obesity. *Cell Metab* **26**, 598-609 (2017).
101. Kuan, E.L.*, et al.* Collecting Lymphatic Vessel Permeability Facilitates Adipose Tissue Inflammation and Distribution of Antigen to Lymph Node–Homing Adipose Tissue Dendritic Cells. **194**, 5200-5210 (2015).
102. Carramolino, L.*, et al.* Platelets Play an Essential Role in Separating the Blood and Lymphatic Vasculatures During Embryonic Angiogenesis. **106**, 1197-1201 (2010).
103. Ali, R.A., Wuescher, L.M. & Worth, R.G. Platelets: essential components of the immune system. *Curr Trends Immunol* **16**, 65-78 (2015).
104. Osada, M.*, et al.* Platelet activation receptor CLEC-2 regulates blood/lymphatic vessel separation by inhibiting proliferation, migration, and tube formation of lymphatic endothelial cells. *J Biol Chem* **287**, 22241-22252 (2012).
105. Lim, L.*, et al.* Hemostasis stimulates lymphangiogenesis through release and activation of VEGFC. *Blood* **134**, 1764-1775 (2019).
106. Tao, S.C., Guo, S.C. & Zhang, C.Q. Platelet-derived Extracellular Vesicles: An Emerging Therapeutic Approach. *Int J Biol Sci* **13**, 828-834 (2017).
107. Flaumenhaft, R., Mairuhu, A.T. & Italiano, J.E. Platelet- and megakaryocyte-derived microparticles. *Semin Thromb Hemost* **36**, 881-887 (2010).
108. Italiano, J.E., Jr., Mairuhu, A.T. & Flaumenhaft, R. Clinical relevance of microparticles from platelets and megakaryocytes. *Curr Opin Hematol* **17**, 578-584 (2010).
109. Antwi-Baffour, S.*, et al.* Understanding the biosynthesis of platelets-derived extracellular vesicles. *Immun Inflamm Dis* **3**, 133-140 (2015).
110. Mause, S.F.*, et al.* Platelet microparticles enhance the vasoregenerative potential of angiogenic early outgrowth cells after vascular injury. *Circulation* **122**, 495-506 (2010).
111. Torreggiani, E.*, et al.* Exosomes: novel effectors of human platelet lysate activity. *Eur Cell Mater* **28**, 137-151; discussion 151 (2014).
112. Ma, Q.*, et al.* Platelet-derived extracellular vesicles to target plaque inflammation for effective anti-atherosclerotic therapy. *Journal of Controlled Release* **329**, 445-453 (2021).
113. Barile, L.*, et al.* Extracellular vesicles from human cardiac progenitor cells inhibit cardiomyocyte apoptosis and improve cardiac function after myocardial infarction. *Cardiovasc Res* **103**, 530-541 (2014).
114. Garcia, N.A., Ontoria-Oviedo, I., González-King, H., Diez-Juan, A. & Sepúlveda, P. Glucose Starvation in Cardiomyocytes Enhances Exosome Secretion and Promotes Angiogenesis in Endothelial Cells. *PLoS One* **10**, e0138849 (2015).
115. Sunderland, N.*, et al.* MicroRNA Biomarkers and Platelet Reactivity: The Clot Thickens. *Circ Res* **120**, 418-435 (2017).
116. Miyazawa, B.*, et al.* Regulation of endothelial cell permeability by platelet-derived extracellular vesicles. *J Trauma Acute Care Surg* **86**, 931-942 (2019).
117. Arias, C.F. & Arias, C.F. How do red blood cells know when to die? *R Soc Open Sci* **4**, 160850 (2017).

118. Kuo, W.P., Tigges, J.C., Toxavidis, V. & Ghiran, I. Red Blood Cells: A Source of Extracellular Vesicles. *Methods Mol Biol* **1660**, 15-22 (2017).
119. Morel, O., Jesel, L., Freyssinet, J.M. & Toti, F. Cellular mechanisms underlying the formation of circulating microparticles. *Arterioscler Thromb Vasc Biol* **31**, 15-26 (2011).
120. Pascual, M., Lutz, H.U., Steiger, G., Stammler, P. & Schifferli, J.A. Release of vesicles enriched in complement receptor 1 from human erythrocytes. *J Immunol* **151**, 397-404 (1993).
121. Donadee, C.*, et al.* Nitric oxide scavenging by red blood cell microparticles and cell-free hemoglobin as a mechanism for the red cell storage lesion. *Circulation* **124**, 465-476 (2011).
122. Li, K.Y., Zheng, L., Wang, Q. & Hu, Y.W. Characteristics of erythrocyte-derived microvesicles and its relation with atherosclerosis. *Atherosclerosis* **255**, 140-144 (2016).
123. Potor, L.*, et al.* Atherogenesis may involve the prooxidant and proinflammatory effects of ferryl hemoglobin. *Oxid Med Cell Longev* **2013**, 676425 (2013).
124. Moxness, M.S., Brunauer, L.S. & Huestis, W.H. Hemoglobin oxidation products extract phospholipids from the membrane of human erythrocytes. *Biochemistry* **35**, 7181-7187 (1996).
125. Smiljić, S., Nestorović, V. & Savić, S. Modulatory role of nitric oxide in cardiac performance. *Med Pregl* **67**, 345-352 (2014).
126. Camus, S.M.*, et al.* Circulating cell membrane microparticles transfer heme to endothelial cells and trigger vasoocclusions in sickle cell disease. *Blood* **125**, 3805-3814 (2015).
127. Loyer, X., Vion, A.C., Tedgui, A. & Boulanger, C.M. Microvesicles as cell-cell messengers in cardiovascular diseases. *Circ Res* **114**, 345-353 (2014).
128. Giannopoulos, G.*, et al.* Red blood cell and platelet microparticles in myocardial infarction patients treated with primary angioplasty. *International Journal of Cardiology* **176**, 145-150 (2014).
129. Bohlen, H.G., Gasheva, O.Y. & Zawieja, D.C. Nitric oxide formation by lymphatic bulb and valves is a major regulatory component of lymphatic pumping. **301**, H1897-H1906 (2011).
130. Gasheva, O.Y., Zawieja, D.C. & Gashev, A.A. Contraction-initiated NO-dependent lymphatic relaxation: a self-regulatory mechanism in rat thoracic duct. **575**, 821-832 (2006).
131. Jean, G., Milasan, A., Boilard, É., Fortin, C. & Martel, C. Extracellular Vesicles Can Be Friends or Foes in Atherosclerosis-related Lymphatic Dysfunction. *Atherosclerosis Supplements* **32**, 93 (2018).
132. Johnson, L.A., Prevo, R., Clasper, S. & Jackson, D.G. Inflammation-induced uptake and degradation of the lymphatic endothelial hyaluronan receptor LYVE-1. *J Biol Chem* **282**, 33671-33680 (2007).
133. Sawa, Y.*, et al.* Effects of TNF-alpha on leukocyte adhesion molecule expressions in cultured human lymphatic endothelium. *J Histochem Cytochem* **55**, 721-733 (2007).
134. Jackson, J.R., Seed, M.P., Kircher, C.H., Willoughby, D.A. & Winkler, J.D. The codependence of angiogenesis and chronic inflammation. *Faseb j* **11**, 457-465 (1997).
135. Ristimäki, A., Narko, K., Enholm, B., Joukov, V. & Alitalo, K. Proinflammatory Cytokines Regulate Expression of the Lymphatic Endothelial Mitogen Vascular Endothelial Growth Factor-C*. *Journal of Biological Chemistry* **273**, 8413-8418 (1998).

136. Hamrah, P., Chen, L., Zhang, Q. & Dana, M.R. Novel expression of vascular endothelial growth factor receptor (VEGFR)-3 and VEGF-C on corneal dendritic cells. *The American journal of pathology* **163**, 57-68 (2003).
137. Baluk, P.*, et al.* Pathogenesis of persistent lymphatic vessel hyperplasia in chronic airway inflammation. *J Clin Invest* **115**, 247-257 (2005).
138. Schoppmann, S.F.*, et al.* Tumor-associated macrophages express lymphatic endothelial growth factors and are related to peritumoral lymphangiogenesis. *Am J Pathol* **161**, 947-956 (2002).
139. Jackson, D.G. Biology of the lymphatic marker LYVE-1 and applications in research into lymphatic trafficking and lymphangiogenesis. *Apmis* **112**, 526-538 (2004).
140. Wigle, J.T.*, et al.* An essential role for Prox1 in the induction of the lymphatic endothelial cell phenotype. *The EMBO journal* **21**, 1505-1513 (2002).
141. Flister, M.J.*, et al.* Inflammation induces lymphangiogenesis through up-regulation of VEGFR-3 mediated by NF-kappaB and Prox1. *Blood* **115**, 418-429 (2010).
142. Hayden, M.S. & Ghosh, S. Regulation of NF-κB by TNF family cytokines. *Semin Immunol* **26**, 253-266 (2014).
143. Lobov, G.I. & Orlov, R.S. [Electrical and contractile activity of the lymphangions of the mesenteric lymphatic vessels]. *Fiziol Zh SSSR Im I M Sechenova* **69**, 1614-1620 (1983).
144. Dougherty, P.J.*, et al.* PKC activation increases Ca^{2+} sensitivity of permeabilized lymphatic muscle via myosin light chain 20 phosphorylation-dependent and -independent mechanisms. *American journal of physiology. Heart and circulatory physiology* **306**, H674-H683 (2014).
145. Szadujkis-Szadurska, K., Grzesk, G., Szadujkis-Szadurski, L., Gajdus, M. & Matusiak, G. Role of nitric oxide and cGMP in the modulation of vascular contraction induced by angiotensin II and Bay K8644 during ischemia/reperfusion. *Exp Ther Med* **5**, 616-620 (2013).
146. Chen, R.*, et al.* Tongmai Yangxin pill reduces myocardial no-reflow by regulating apoptosis and activating PI3K/Akt/eNOS pathway. *Journal of Ethnopharmacology* **261**, 113069 (2020).
147. Scallan, J.P. & Davis, M.J. Genetic removal of basal nitric oxide enhances contractile activity in isolated murine collecting lymphatic vessels. *J Physiol* **591**, 2139-2156 (2013).
148. Gkaliagkousi, E., Ritter, J. & Ferro, A. Platelet-Derived Nitric Oxide Signaling and Regulation. **101**, 654-662 (2007).
149. Azevedo, L.C.*, et al.* Platelet-derived exosomes from septic shock patients induce myocardial dysfunction. *Crit Care* **11**, R120 (2007).
150. Bisoendial, R.*, et al.* Apolipoprotein A-I Limits the Negative Effect of Tumor Necrosis Factor on Lymphangiogenesis. **35**, 2443-2450 (2015).
151. Yang, X.*, et al.* AIBP-CAV1-VEGFR3 axis dictates lymphatic cell fate and controls lymphangiogenesis. 2020.2010.2016.342998 (2020).
152. Sitia, S.*, et al.* From endothelial dysfunction to atherosclerosis. *Autoimmun Rev* **9**, 830-834 (2010).
153. Meier, T.O.*, et al.* Increased Permeability of Cutaneous Lymphatic Capillaries and Enhanced Blood Flow in Psoriatic Plaques. *Dermatology* **227**, 118-125 (2013).
154. Schwager, S. & Detmar, M. Inflammation and Lymphatic Function. **10**(2019).

155. LINDEMANN, S., KRÄMER, B., SEIZER, P. & GAWAZ, M. Platelets, inflammation and atherosclerosis. **5**, 203-211 (2007).
156. Srikanthan, S., Li, W., Silverstein, R.L. & McIntyre, T.M. Exosome poly-ubiquitin inhibits platelet activation, downregulates CD36 and inhibits pro-atherothombotic cellular functions. **12**, 1906-1917 (2014).
157. VAN DER MEIJDEN, P.E.J.*, et al.* Platelet- and erythrocyte-derived microparticles trigger thrombin generation via factor XIIa. **10**, 1355-1362 (2012).
158. Rowley, J.W.*, et al.* Genome-wide RNA-seq analysis of human and mouse platelet transcriptomes. *Blood* **118**, e101-e111 (2011).
159. Tsakiris, D.A., Scudder, L., Hodivala-Dilke, K., Hynes, R.O. & Coller, B.S. Hemostasis in the mouse (Mus musculus): a review. *Thromb Haemost* **81**, 177-188 (1999).
160. Terashita, Z., Imura, Y. & Nishikawa, K. Inhibition by CV-3988 of the binding of [3H]-platelet activating factor (PAF) to the platelet. *Biochem Pharmacol* **34**, 1491-1495 (1985).
161. Nofer, J.R.*, et al.* Impaired platelet activation in familial high density lipoprotein deficiency (Tangier disease). *J Biol Chem* **279**, 34032-34037 (2004).
162. Darrow, A.L.*, et al.* Biological consequences of thrombin receptor deficiency in mice. *Thromb Haemost* **76**, 860-866 (1996).
163. Plé, H.*, et al.* The repertoire and features of human platelet microRNAs. *PLoS One* **7**, e50746 (2012).
164. Gidlöf, O.*, et al.* Platelets activated during myocardial infarction release functional miRNA, which can be taken up by endothelial cells and regulate ICAM1 expression. *Blood* **121**, 3908-3917 (2013).
165. Landry, P.*, et al.* Existence of a microRNA pathway in anucleate platelets. *Nature Structural & Molecular Biology* **16**, 961-966 (2009).
166. Willeit, P.*, et al.* Circulating MicroRNAs as Novel Biomarkers for Platelet Activation. **112**, 595-600 (2013).
167. Kaudewitz, D.*, et al.* Association of MicroRNAs and YRNAs With Platelet Function. **118**, 420-432 (2016).
168. Wang, S.*, et al.* The endothelial-specific microRNA miR-126 governs vascular integrity and angiogenesis. *Dev Cell* **15**, 261-271 (2008).
169. Fish, J.E.*, et al.* miR-126 regulates angiogenic signaling and vascular integrity. *Dev Cell* **15**, 272-284 (2008).
170. Harris, T.A., Yamakuchi, M., Ferlito, M., Mendell, J.T. & Lowenstein, C.J. MicroRNA-126 regulates endothelial expression of vascular cell adhesion molecule 1. **105**, 1516-1521 (2008).
171. Ferrer-Marin, F., Gutti, R., Liu, Z.J. & Sola-Visner, M. MiR-9 contributes to the developmental differences in CXCR-4 expression in human megakaryocytes. *J Thromb Haemost* **12**, 282-285 (2014).
172. Yee, D., Coles, M.C. & Lagos, D. microRNAs in the Lymphatic Endothelium: Master Regulators of Lineage Plasticity and Inflammation. **8**(2017).
173. Angelillo-Scherrer, A. Leukocyte-derived microparticles in vascular homeostasis. *Circ Res* **110**, 356-369 (2012).
174. Baka, Z.*, et al.* Increased serum concentration of immune cell derived microparticles in polymyositis/dermatomyositis. *Immunol Lett* **128**, 124-130 (2010).

175. Ran, S. & Wilber, A. Novel role of immature myeloid cells in formation of new lymphatic vessels associated with inflammation and tumors. **102**, 253-263 (2017).

Figures supplémentaires

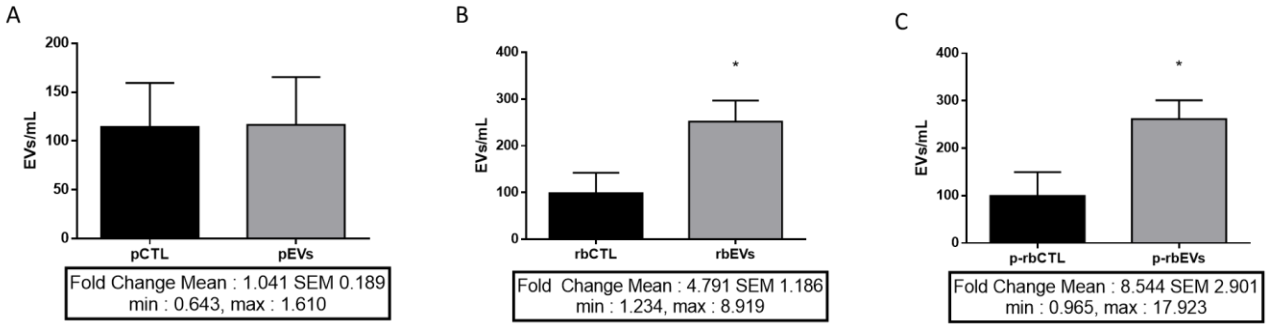

Figure supplémentaire 1 : Les vésicules extracellulaires dérivées de plaquettes et de globules rouges augmentent la production d'Evs dérivées de LECs en conditions inflammatoires.

Les LECs ont d'abord été prétraitées au TNFα (10 ng/mL) dans du milieu sans EVs pendant 24 heures. Suivant l'incubation de concentrations physiologiques de pEVs **(A)**, de rbEVs **(B)** ou des deux sous-types **(C)**, le surnageant a été récolté. Les EVs dérivées de LECs ont été marquées au CFSE et à l'aide de l'anticorps VEGFR3 (PE) avant d'être analysées par cytométrie en flux à l'aide du BD FACSCelesta équipé d'un filtre *bandpass* de 405 nm sur le laser violet. *p<0,05; n=6

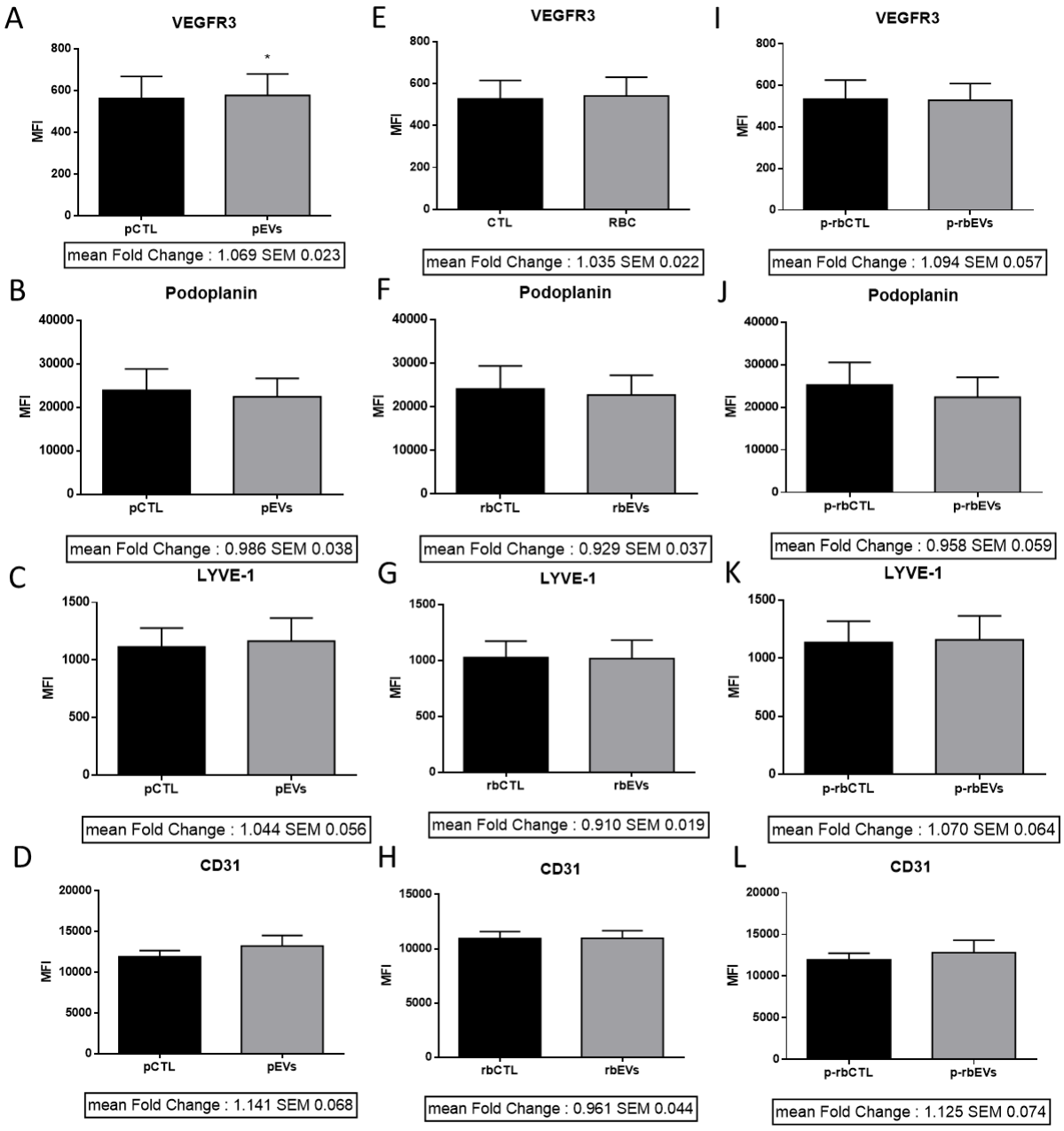

Figure supplémentaire 2 : Peu d'effet des EVs sur l'expression des marqueurs lymphatiques en conditions inflammatoires.

Les LECs ont été prétraitées au TNFα (10 ng/mL) dans du milieu sans EVs pendant 24 heures. Les cellules ont ensuite été incubées avec des pEVs **(A, B, C et D)**, des rbEVs **(E, F, G et H)** ou les deux sous-types **(I, J, K et L)** pendant 24 heures. Les LECs ont été marquées avec l'anticorps VEGFR3 (PE), Podoplanine (PerCP Cy5.5), LYVE-1 (APC), CD31 (APC Cy7) ainsi qu'au DAPI. L'expression des marqueurs lymphatiques a été analysée par cytométrie en flux (BD FACSCelesta). *p<0,05; n=9

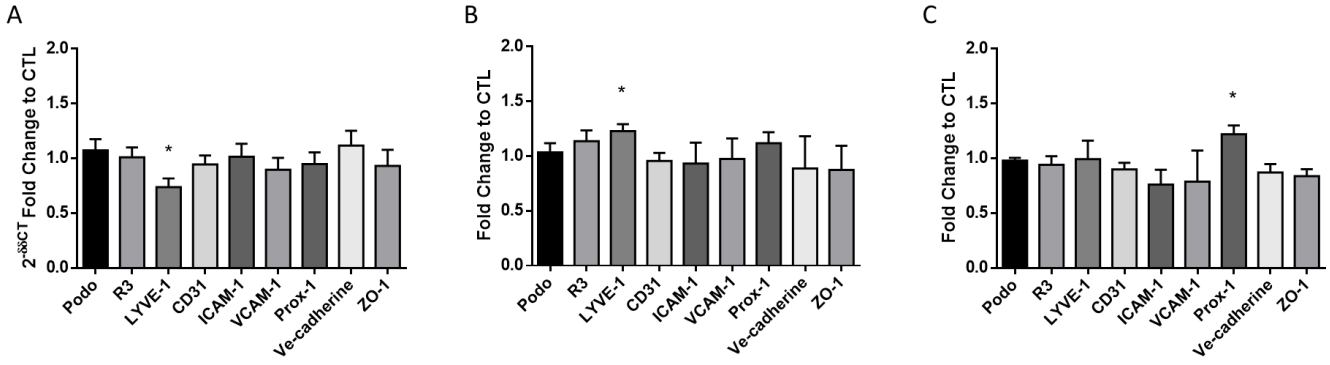

Figure supplémentaire 3 : Régulation des gènes LYVE-1 et Prox-1 par les EVs en conditions inflammatoires.

La régulation de l'ARNm des LECs a été mesurée par qPCR suivant le prétraitement des LECs au TNFα pendant 24 heures et l'incubation des pEVs **(A)**, des rbEVs **(B)** ou des deux sous-types **(C)** pendant 24 heures. *p<0,05; n=5-6 (n=4 pour VCAM-1)

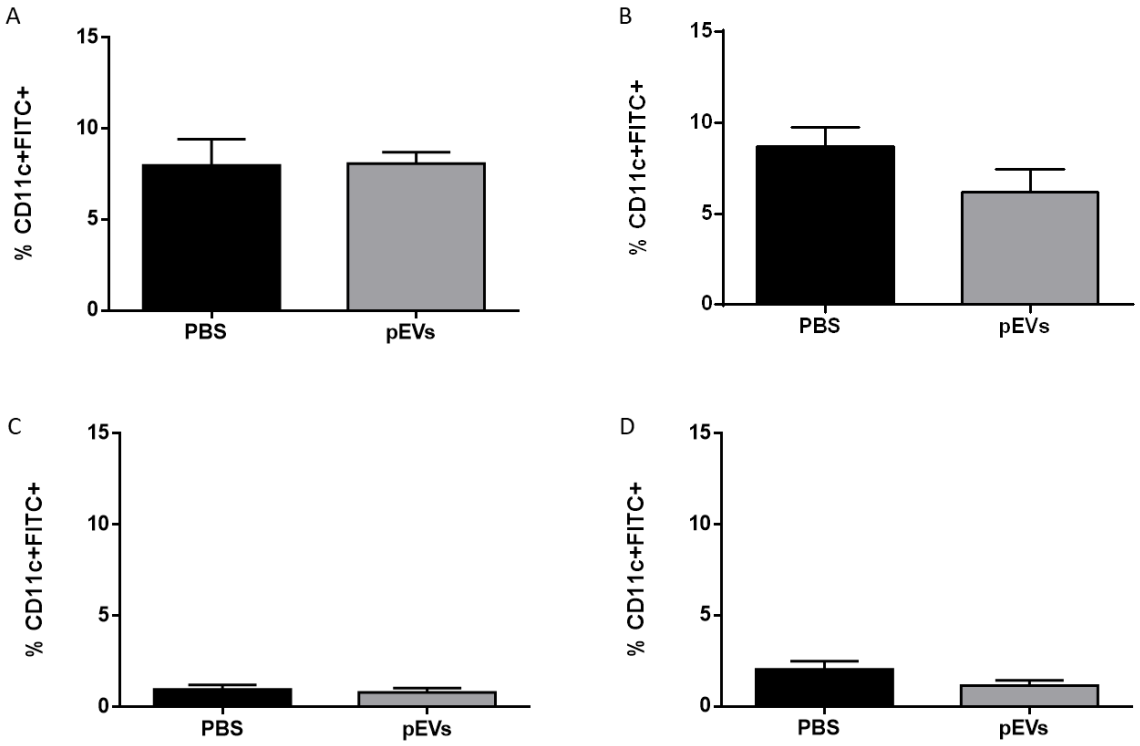

Figure supplémentaire 4 : Une injection de vésicules extracellulaires dérivées de plaquettes n'améliorent pas la fonction lymphatique à priori.

Préalablement à la technique de FITC *painting*, 20 uL de véhicule PBS ou contenant $1x10^7$ pEVs ont été injectés de façon intradermale dans la patte droite des souris. Deux heures suivant l'injection, une solution contenant le marqueur FITC ainsi que du dibutyl phthalate a été appliquée topiquement sur le dos de souris de 10-11 semaines C57BL/6 de type sauvage mâle **(A)** ou femelle **(B)** ainsi que de souris *Ldlr*$^{-/-}$; *hApoB100*$^{+/+}$ mâles **(C)** ou femelles **(D)**. 18 heures après, les ganglions inguinaux droits ont été récupérés puis digérés dans la collagénase D. Les cellules ont été comptées à l'aide du compteur cellulaire Nexcelom puis marquées avec l'anticorps CD11c (BV786), CD11b (PerCP Cy5.5) et CMH II (PE). Les cellules exprimant CD11c, CD11b, CMH II et exprimant le colorant FITC ont été considérées comme des cellules dendritiques migratoires. n=4-5

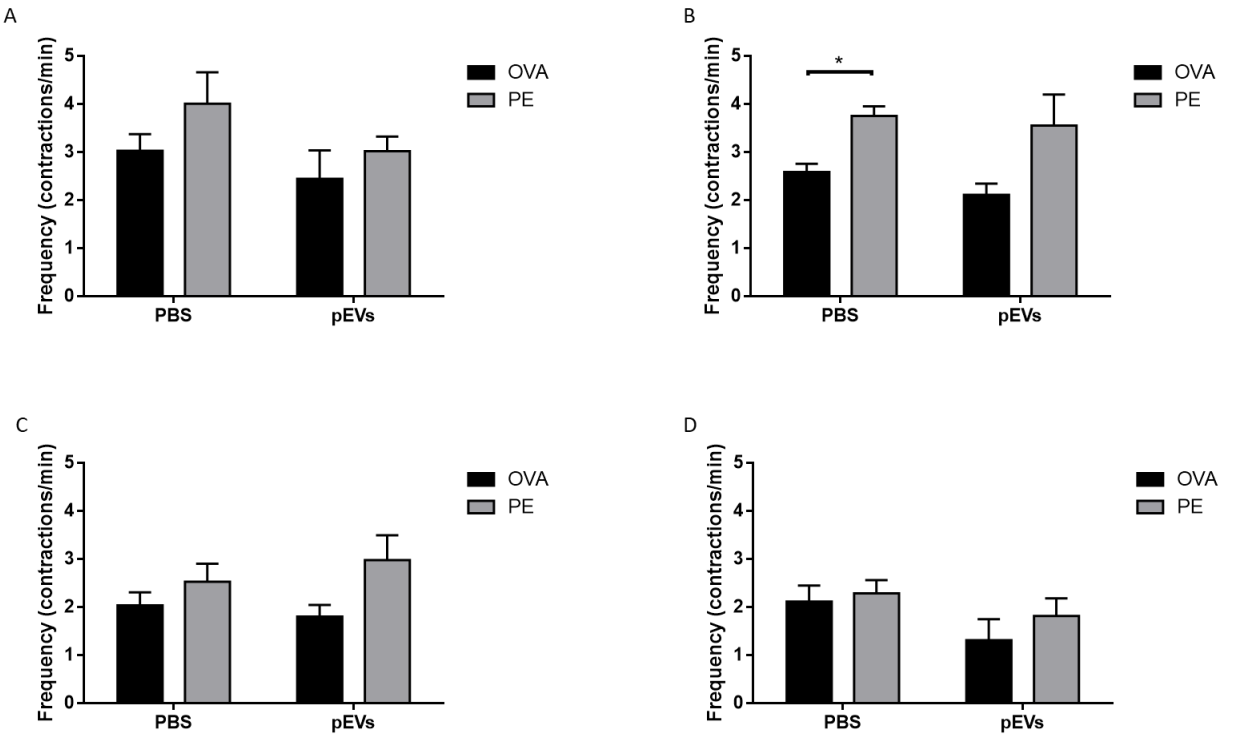

Figure supplémentaire 5 : Une injection simple de vésicules extracellulaires dérivées de plaquettes n'améliorent pas les contractions lymphatiques à priori.

20 uL de véhicule PBS ou contenant 1x10^7 pEVs ont été injectés de façon intradermale dans la patte droite de souris. Deux heures suivant l'injection, les souris C57BL/6 mâles **(A)** ou femelles **(B)** ainsi que *Ldlr*$^{-/-}$; *hApoB100*$^{+/+}$ mâles **(C)** ou femelles **(D)** ont été anesthésiées, la peau recouvrant la patte droite a été retirée puis 10 uL d'ovalbumine (OVA) (AF647) (2 mg/mL) ont été injectés similairement aux pEVs. Après cinq minutes d'équilibre, une vidéo de 10 minutes a été prise à l'aide du microscope à fluorescence AxioCam 5.6 (Zeiss). La réactivité des vaisseaux a été mesurée par l'injection de 10 uL de phényléphrine (PE) (1 µM) en intradermale dans la même patte et la même procédure a été suivie au microscope. Les fréquences de contractions ont été analysées à l'aide du logiciel LymphPulse 3.0. *p<0,05; n=4-7

Annexe

Autre publication

Le système lymphatique joue un rôle clé dans le transport du cholestérol hors de la paroi artérielle et une dysfonction lymphatique des vaisseaux collecteurs à priori précède l'apparition de l'athérosclérose. Chez le modèle murin, cette dysfonction est associée à une diminution de l'expression du récepteur des lipoprotéines de faible densité (LDLR) et est à priori indépendante des taux de cholestérol circulant. De plus, il a été démontré que les souris dépourvues de la proprotéine subtilisine/kexine de type 9 (PCSK9), une proprotéine qui mène à la dégradation du LDLR, ont une fonction lymphatique améliorée, tandis que les souris dépourvues de LDLR développent une dysfonction lymphatique. Ce projet abordant une autre hypothèse quant au potentiel mécanisme instiguant la dysfonction lymphatique a été effectué en parallèle au projet abordé dans ce mémoire. Dans cet article annexé, nous avions pour but de mieux comprendre les mécanismes par lesquels la présence de PCSK9 dans la lymphe ou la modulation du LDLR sur les cellules endothéliales lymphatiques (CEL) peuvent affecter la fonction lymphatique. Les LECs ont été incubées avec du PCSK9 ou traitées avec un ARN inhibant spécifiquement l'expression du LDLR afin d'évaluer comment la présence de PCSK9 ou la modulation du LDLR affecte l'intégrité des LECs. Nos résultats démontrent que le PCSK9 n'induit pas la sécrétion de cytokines inflammatoires et n'affecte pas l'expression des marqueurs lymphatiques. L'inhibition de l'expression du LDLR entraîne une diminution des marqueurs lymphatiques membranaires endothéliaux. La diminution du LDLR a aussi entrainé une diminution des taux de certains lipides intracellulaires et en particulier des phospholipides, des sphingolipides et des triglycérides. Ces résultats suggèrent qu'une perte du LDLR, mais pas la présence de PCSK9 en circulation, pourrait induire l'altération de l'endothélium lymphatique causée par une diminution de l'expression de protéines membranaires essentielles au bon transport de la lymphe.

Soumis (en révision) dans *Theranostics* (2021)

Endothelial-specific low-density lipoprotein receptor knockdown reduces lymphatic contraction capacity through the modulation of lymphatic endothelial cell metabolism

Laurent Vachon*[1,2], Ali Smaani*[1,2], Nolwenn Tessier[1,2], Gabriel Jean[1,2], Andreea Milasan[1,2], Nadine Ardo[2,4], Stéphanie Jarry[1,2], Annie Demers[2], Louis Villeneuve[2], Mary Sorci-Thomas[3], Gaétan Mayer[2,4] Catherine Martel[1,2]

[4] Faculty of Pharmacy, Université de Montréal, Montreal, QC, Canada

**co-first authors*

Corresponding author:

Catherine Martel, PhD

Faculty of Medicine Université de Montréal Montreal Heart Institute

5000, Belanger street, Room S5100 Montreal, Quebec (Canada)

H1T 1C8

Phone: (514) 376-3330 #2977

E-mail: catherine.martel@icm-mhi.org

Introduction. Impairment in lymphatic transport is associated with atherosclerosis onset and progression in animal models. The absence of low-density-lipoprotein receptor (LDLR) expression, rather than increased circulating cholesterol level *per se*, is involved in early atherosclerosis-related lymphatic dysfunction. Enhancing lymphatic function with VEGF-C152s in young *Ldlr*$^{-/-}$ mice successfully delayed atherosclerotic plaque onset when mice were subsequently fed a high-fat diet. However, the specific mechanisms by which LDLR protects against lymphatic function impairment is unknown.

Methods. We herein sought to investigate whether and how a specific knockdown of *Ldlr* gene expression on endothelial cells could reduce lymphatic function in wild-type (WT) and *Pcsk9*$^{-/-}$ mice following an intraperitoneal injection of an adeno-associated virus serotype 1 expressing a shRNA for silencing *Ldlr*. To determine the intracellular mechanisms involved, human dermal LEC were incubated with either exogenous human recombinant PCSK9 or silencing RNA (siRNA) that specifically targets LDLR expression (siLDLR).

Results. LDLR protein expression on lymphatic endothelial cells (LEC) was reduced by at least 70% in both mouse models. Knocking down the expression of LDLR on LEC reduced the capacity of the lymphatics to contract in WT male mice, whereas it had no effect in *Pcsk9*$^{-/-}$ mice. LDLR expression was sensitive to surrounding lipid content, while LEC did not express nor secreted PCSK9. Whereas both treatments decreased LDLR protein expression, only siLDLR treatment enabled a decrease in chromosome duplication phase and a reduction in podoplanin levels, a specific membrane-bound lymphatic marker. Concomitantly, lipidomic analysis revealed that siLDLR led to a reduction in 18 lipid subclasses, including key constituents of lipid rafts.

Conclusion. Treatments that specifically palliate the down regulation of *Ldlr* mRNA by LEC might preserve the integrity of the lymphatic endothelium and sustain lymphatic function.

Keywords: Atherosclerosis, Lymphatic System, Lymphatic dysfunction, LDLR, PCSK9

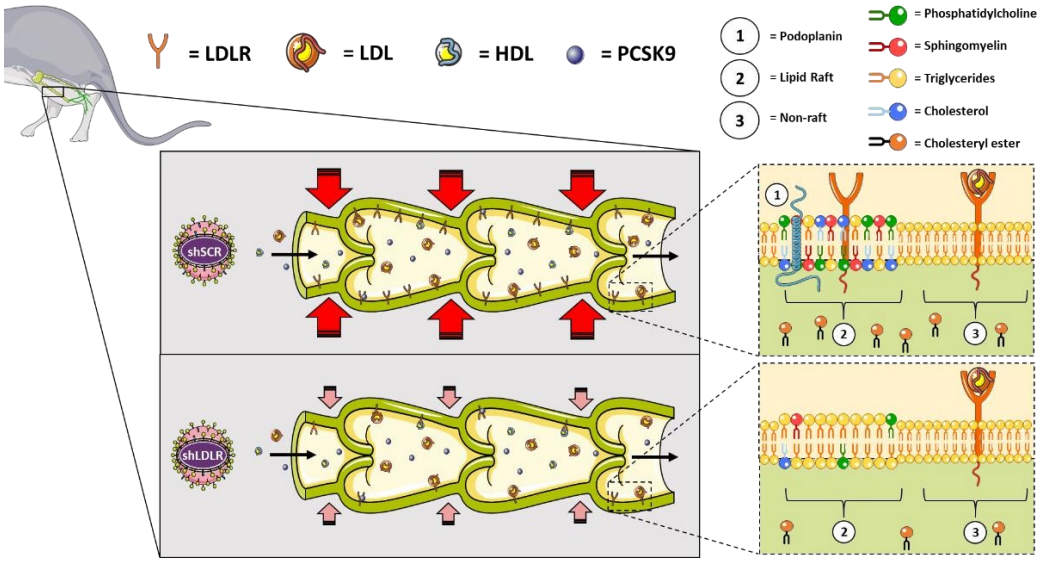
= LDLR
= LDL
= HDL
= PCSK9
1 = Podoplanin
2 = Lipid Raft
3 = Non-raft
= Phosphatidylcholine
= Sphingomyelin
= Triglycerides
= Cholesterol
= Cholesteryl ester
shSCR
shLDLR

INTRODUCTION

Four decades ago, Lemole suggested that intimal vessel thickness was associated with lymphatic vessel blockage. He proposed that enhanced stagnation of the interstitial fluid in the arterial wall could be due to lymphostasis[1, 2]. The lymphatic system is generally known to perform three main functions[3]. First, it allows fluid circulation throughout the body and homeostasis. Any excess fluid that escapes from the bloodstream is collected by the lymphatic system, filtered and returned to the bloodstream, thus preventing the formation of edema. Second, lacteals, which are the lymphatic vessels of the digestive tract, are responsible for dietary fat and fat-soluble vitamins absorption[4]. Third, the lymphatic system defends the body against infections. The vessels displace lymphatic fluid and lymphocytes throughout the body, and the lymph nodes act as a filter to get rid of debris, bacteria, viruses and other foreign bodies. In the past decades, studies analyzing the morphology of lymphatic vessels (LVs) in the artery wall allowed for insights regarding their associations with atherosclerosis[5-8]. Later on, functional studies have proven that the absence of functional adventitial lymphatics is associated to an exacerbated atherosclerotic plaque accumulation in mice, suggesting that preserving lymphatic transport may facilitate cholesterol clearance in therapies aiming at reversing atherosclerosis[9]. Albeit lymphatic dysfunction has first been reported as a consequence rather than a cause of hypercholesterolemia and atherosclerotic lesion development[10-12], a growing number of studies suggest that the interaction between cardiovascular disease (CVD) and lymphatic function is bidirectional. Our team has reported that lymphatic function impairment occurs even before the onset of atherosclerosis in *Ldlr*$^{-/-}$; hapoB100$^{+/+}$ mice[13]. The absence of low-density lipoprotein receptor (LDLR), but not the increase in circulating cholesterol levels, is instigative of the early atherosclerosis-related collecting lymphatic vessel dysfunction[13].

LDLR is ubiquitous and located on the plasma membrane both in and out lipid rafts, which are discrete lipid domains enriched in free cholesterol and glycosphingolipids present in the external leaflet of the plasma membrane[14]. Apolipoprotein (apo) B and apoE-containing particles bind to the LDLR in clathrin-coated pits, rather than LDLR localized in lipid rafts. To decrease cholesterol input from plasma and from endogenous synthesis, as well as to keep the level of unesterified cholesterol in membranes constant, LDLR expression is thoroughly regulated. Decreased 3-

hydroxy-3-methylglutaryl coenzyme A reductase (HMG-CoA reductase) activity, which leads to a decrease in de novo cholesterol synthesis by the cell, upregulates LDLR expression and cholesterol uptake from the circulation to the liver via the activation of sterol regulatory element binding protein (SREBP) [15]. Conversely, when cells contain a surplus of cholesterol, SREBP2 remains in the ER, and cholesterol synthesis and LDLR expression are abrogated[16, 17]. Unlike liver cells that synthesize their cholesterol *de novo*, other cell types, such as endothelial cells, use circulating LDL to meet their cholesterol needs[18]. Whereas hepatic LDL cholesterol is converted to bile acids, LDL cholesterol internalized by non-hepatic cells is used for hormone production and cell membrane synthesis, or stored in the esterified form[19, 20].

In addition to regulating LDL levels *via* LDLR expression, the liver expresses and secretes proprotein convertase subtilisin kexin type 9 (PCSK9), which is capable of binding LDLR and leading to its internalization and degradation in lysosomes[21]. The degradation of this complex is regulated by PCSK9 and LDLR levels themselves, but also by a variety of other proteins[22- 24]. PCSK9 also has pleiotropic effects including in cardiovascular metabolism, and has been reported to promote the internalization and degradation of other receptors and members of the LDLR superfamily[25-29]. As not every cell type throughout the body express PCSK9, circulating PCSK9 produced mainly by the liver would be responsible for the regulation of these cell surface receptors[26]. Albeit PCSK9 has been extensively studied in plasma[30, 31], it is only recently that its accumulation in systemic lymph has been reported[13]. Further, we have demonstrated for the first time that a systemic knockout in PCSK9 improves lymphatic transport in conjunction with increasing LDLR expression on lymphatic endothelial cells (LEC) in six-month-old mice when compared to wild-type mice. As PCSK9 deletion did not affect lymphangiogenesis, these results suggest that collecting lymphatic vessels are primarily involved[13]. We then went on and consequently sought to enhance lymphatic collecting vessel function *per se* in *Ldlr-/-* mice before the administration of a pro-atherogenic diet regimen that would instigate the accumulation of plaque. We administered a mutant form of the vascular endothelial growth factor receptor-C (namely VEGF-C152s) that solely binds to VEGF receptor 3 (VEGFR-3) and reported that enhancing lymphatic contraction capacity early on in the atherosclerotic process protects from subsequent excessive plaque formation[32]. However, the mechanisms by which LDLR is affecting the

lymphatic endothelium integrity is unclear, and whether PCSK9 is involved in the early step of atherosclerosis-related lymphatic dysfunction remains to be studied. Using an *in vivo* model of induced endothelial deletion of LDLR, we will herein determine in both young female and male mice whether PCSK9 deletion is still potentiating lymphatic function when LDLR is downregulated and characterize the cellular mechanisms involved.

MATERIALS AND METHODS

AAV vector constructs. Single-stranded cDNA (sscDNA) containing different short hairpin RNA (shRNA) flanked by HindIII and BamHI sites were purchased from IDT and amplified by PCR using forward and reverse linker primers (Table 1). Double-stranded amplicons were digested, gel-purified and ligated in pU6-ITR, followed by transformation in Stbl3 bacteria. All used clones were confirmed by sequencing and purified by Maxiprep (Qiagen, Catalog No. D4202). All PCR primer pairs are described in Table 1.

AAV1 production and purification. Human embryonic kidney 293T (HEK293T) cells were seeded in sixteen 100 mm plates in DMEM without sodium pyruvate (Wisent cat. 319-015) supplemented with 10% heat-inactivated fetal bovine serum (FBS; Wisent cat. 080-150). Once they have reached 70-80% confluence, cells were transfected with 8.6 ug/plate of the packaging plasmid pXYZ and 2.9 µg/plate of the specific pU6-ITR-sh plasmid (pU6-ITR-AAV1-sh- mLDLR-GFP-C1 or pU6-ITR-AAV1-sh-scramble-GFP) using the polyethylenimine method (46 µl/plate, PEI; Polysciences, cat. 23966). Cells were harvested 72 h post-transfection with a cell scraper, pelleted, resuspended in Tris lysis buffer (150 mM NaCl, 50 mM Tris pH 8.5) and subjected to three freeze/thaw cycles. Cell lysates were treated with 1 mM of MgCl2 and 250 units of benzonase (Santa Cruz cat. sc-202391) for 45 min at 37 °C and then centrifuged 20 min at 6000 g to remove cell debris. The crude lysate was purified by iodixanol gradient. Briefly, 60% iodixanol (OptiPrep; Sigma D1556) was diluted to 40 % and 25% in 5X PBS-MK (5X PBS, 5 mM MgCl2, 12.5 mM KCl). To facilitate distinguishing of

the phase boundaries, 2.5 µL of 0.5% phenol red (Bioshop PHE600.5/5g) was added to the 25 and 60% iodixanol phase. One milliliter of 60, 40, and 25 % iodixanol solutions was successively underlaid in a 5-mL Beckman ultracentrifuge tube (catalog No# 326819), and 1.5 to 2 mL of the processed crude lysate was gently overlaid onto the gradients and centrifuged in a 55Ti rotor for 3 h at 33,000 rpm at 4 °C. After centrifugation, the tubes were punctured at the 60% and 40% interphase (bottom and middle layers) using a 18- gauge needle, to collect ~1-ml/tube of the fraction containing the virus. Pool of collected iodixanol containing virus was cleaned with PBS-0.001% Tween and concentrated with an Amicon Ultra- 15 centrifugal filter unit (MWCO 100kDa; Merck Millipore cat. UFC910024). The virus was then titrated by quantitative PCR using eGFP primers (Table 1) and a standard curve using the corresponding pU6-ITR-sh plasmid in serial dilutions. Finally, viral batches were aliquoted and stored at -80 °C.

Experimental mouse model. C57BL/6 wild-type and *Pcsk*9 knockout (*Pcsk*9$^{-/-}$) mice were obtained from the Jackson Laboratory. The *Pcsk*9$^{-/-}$ mice were backcrossed on a C57BL/6 background for at least 10 generations at our facility. Animals were housed in a pathogen-free environment under 12 h light-dark cycles with free access to water and to standard chow diet. Experiments were carried out on 10-12 week-old male and female mice. Mice were injected into the peritoneal cavity with 1x10^{11} virus genome per milliliter of an Adeno-Associated Virus Serotype 1 (AAV1) expressing mouse LDL-receptor shRNA silencing adenovirus (shLDLR) or a scramble shRNA (shSCR) sequence (Table 1). Mice were euthanized with isoflurane 2% and CO2 two weeks later and perfused with PBS. The liver, aorta and popliteal lymph nodes (LN) were harvested and processed for the assessment of LDLR protein (flow cytometry) or mRNA (qPCR) expression. All experiments were performed in accordance with the Canadian Council on Animal Care guidelines and approved by the Montreal Heart Institute Animal Care Committee.

Measurement of lymphatic function *in vivo*. Migration of dendritic cells to LN was evaluated following a contact sensitization assay[13]. Briefly, the animals were sacrificed 18 h after an epicutaneous application of a solution containing fluorescein isothyiocyanate (FITC) (Sigma

Aldrich cat. #F7250-250MG), dibutyl phtalate and acetone (Sigma Aldrich), and corresponding skin-draining LNs were collected and enzymatically digested in collagenase D (Cedarlane cat. #11088882001) for 25 min at 37 °C. Cells were passed through a 70 µM strainer, washed, counted and stained for analysis by flow cytometry (BD FACSCelesta™). The following fluorescence-conjugated antibodies were used: anti-mouse CD11b PerCp-Cy5.5 (BioLegend cat. #101228), anti-mouse CD11c BV786 (BD Biosciences cat. #563735) and anti-mouse MHCII PE (Tonbo Biosciences cat. #35-5321-U100). The percentage of FITC-positive dendritic cells that migrated to the corresponding draining lymph nodes was analyzed with FlowJo™ software (Tree Star Inc.).

***In vivo* measurement of lymphatic vessel contraction.** Mice were anesthetized with isoflurane (2%) and oxygen, placed in abdominal decubitus on a heat pad at 40 °C and the contraction capacity of the popliteal lymphatic measured as previously described[32, 33], with minor modifications. Briefly, the mouse right hind was shaved and an incision was made all around the knee allowing the gentle removal of the skin down to the ankle. Skin was removed and 10 uL of Alexa-Fluor 647-conjugated ovalbumin (2 mg/mL, Thermofisher Scientific cat. #O34784) was injected in the dermis of the footpad followed by three manual contractions of the leg and a smooth massage of the injection site. After a 5 min wait and the regular hydration of the leg with PBS saline (Gibco), the contractions and massage were repeated before the lymphatic function assessment. The contraction imaging was performed for a duration of 10 min with the Axiozoom V.16 microscope (Zeiss). Following the first imaging session, 10 uL of phenylephrine (1 µM, Sigma Aldrich cat. #P6126-5G) was injected in the dermis of the footpad as a vasoactive agent and the protocol was repeated as mentioned above. A total of 326 pictures per imaging session were taken with an exposure time of 1 s. Images were stabilized using the Template Matching Imagej™ plugin and analyzed with the LymphPulse 3.0 Matlab™ based software (Figure S1). Five regions of interest (ROI) were manually sketched on each lymphatic vessel and the background intensity was subtracted. The projected curves displayed peaks and valleys with a detection threshold placed at 40 arbitrary units (AU) by the user. The contractions frequency was then computed from each curve with our Matlab algorithm following the formula (Np+Nv)/(2*dt) where Np et Nv are the number of peaks and number of valleys, respectively, and dt is the analysis time. The

contraction amplitude was calculated as the mean fluorescence intensity (MFI) change within each contraction out of the maximum fluorescence intensity reached from each ROI and expressed in percentage.

Cell culture. Primary human dermal lymphatic microvascular endothelial cells-adult (HMVEC-dLyAd) were cultured according to the manufacturer's protocol (Lonza cat. #CC-2810) in EBM- 2 medium containing the EGM-2 MV SingleQuots (PromoCell). Cells were seeded in 6-well cell culture plates at 80-90% confluence, incubated in FBS-free media for 1 h and treated with either human recombinant PCSK9 or vehicle control in FBS-free media (6.5 ug/mL, ProSci cat. #96- 577) for 16 h or transfected with human LDLR siRNA (25 nM, Qiagen Hs_LDLR_2 cat. #SI00011172 or Hs_LDLR_3 cat. #SI00011179) or non-targeting siRNA (Qiagen cat. #1027280) for 48 h in EGM-2 MV using TransIT-X2® Dynamic Delivery System (MirusBio cat. #MIR6003). Human hepatoma cell lines HepG2 and Huh7 cells were cultured in Dulbecco's Modified Eagle's Medium (DMEM, Wisent cat. 319-005-CL) containing 10% FBS (Wisent cat. 080-350) in a 5% CO2 atmosphere at 37 °C. Cells were used at 70-90% confluency for all experiments.

Flow cytometry and antibodies. HMVEC-dLyAd (or human hepatoma Huh7 cells) were harvested from the cell culture plates and centrifuged at 430 g for 5 min. All sample cells were suspended in PBS supplemented with 0.1% (vol/vol) bovine serum albumin (BSA) and 0.1% sodium azide. Flow cytometry was performed using the BD FACSCelesta™ and data were analyzed using FlowJo™ software (Tree Star Inc.). The following fluorescence-conjugated antibodies were used in this study: anti-human LDLR (clone ID 301, SinoBiological cat. #10231- R301-A), anti-human VEGFR3 (clone ID 9D9F9, BioLegend cat. #356204), anti-human LYVE- 1 (Invitrogen cat. #PA5-22782) and anti-human podoplanin (clone ID NC-08, BioLegend cat. #337012). For cell cycle distribution, cells were fixed in cold 70% ethanol, washed and stained with a propidium iodide (PI) solution (Biotium cat. #40017) (containing Ribonuclease I), which is fluorogenic and binds to nucleic acids in a stoichiometric manner to allow the assessment of the proportion of cells in each phase of the cell cycle (pre-replicative (G0/G1), replicative (S) and post-replicative and mitotic

cells (G2/M))[34]. LDL internalization by HMVEC-dLyAd was determined following a 4-hour incubation with 10 µg/ml of Dil-LDL (Alfa Aesar™ cat. #J5330AMH). Unless indicated otherwise, results are expressed as mean fluorescence intensity (MFI) and each treatment was normalized to its respective control. Cells were harvested, washed and analyzed by flow cytometry. For the *in vivo* experiment, the efficiency of the LDLR shRNA to downregulate the LDLR protein expression was determined by measuring the percentage of LDLR-positive lymphatic endothelial cells within the popliteal lymph node following a 25 min enzymatic digestion with collagenase D at 37 °C. The decrease in LDLR was also assessed in the $CD45^+$ cells.

Immunofluorescence. LDLR expression was also determined by immunofluorescence on HMVEC-dLyAd seeded in glassbottom culture dishes chamber (Mattek). Live cells were stained for 30 min at 37 °C with anti-LDL receptor Alexa Fluor 647 Conjugate (Bioss cat. #bs-0705R), Cholera Toxin Subunit B Alexa Fluor 555 Conjugate (Invitrogen cat. #C-34776) and nuclei marker DAPI (4',6-diamidino-2-phenylindole, BioShop cat. #DAP444.5). Live images were acquired at 37 °C, 5% CO2 with a LSM 710 Confocal Microscope (Zeiss) equipped with a 63/1.4 oil DIC objective. Z-stacks were deconvolved with Huygens Professional (Scientific Volume Imaging,SVI, Netherlands) using a theoretical spread function (PSF). Three-dimensional rendering and quantitative colocalization (whole volume) analysis of LDLR and cholera toxin was estimated (Colocalization Analyzer, SVI) using Pearson's correlation coefficient, for which an absolute value of one indicates a perfect linear relationship, whereas a correlation close to 0 indicates no linear relationship between the variables.

Immunoblotting. Proteins were extracted from either HMVEC-dLyAd, human embryonic kidney 293 cells (HEK-293) or human liver cell lines (HepG2 or Huh7) using ice-cold radioimmunoprecipitation (RIPA) assay buffer and the protein concentration of the supernatants were established using MicroBCA™ Protein Assay Kit (ThermoFisher). Protein samples were diluted in 4X Laemmli buffer, heated at 95 °C for 5 min, separated by electrophoresis on a 10% SDS-PAGE and then transferred on a poly(vinylidene fluoride) (PVDF) membrane for 90 min at 4

°C. The membranes were blocked with 5% nonfat dry milk in Tris-buffered saline (TBST, 0.1% Tween 20) for 1 h at room temperature, then incubated with anti-PCSK9 (Abcam cat. #AB95478), anti-LDLR (R&D Systems cat. #AF2148-SP), or anti-beta-actin (Abcam, AB8227) overnight at 4°C. The membranes were washed with TBST and incubated with horseradish peroxidase (HRP)-conjugated secondary antibodies (Abcam, AB6721 or AB6741) for 90 min at room temperature. A Clarity™ Western ECL Blotting Substrates Kit (BioRad) was used for detection.

ELISA. PCSK9 was measured according to the manufacturer's instructions (Human Proprotein Convertase 9/PCSK9 Quantikine ELISA Kit) in HMVEC-dLyAd, HuH7 and HEK293 supernatants that were concentrated using the Amicon® Ultra-2 centrifugal filter device (Milipore).

Messenger RNA analysis by RT-qPCR. Treated cells were harvested, suspended in RiboZol™ RNA Extraction Reagent and stored at -80 °C for at least 24 h. The RNA was extracted using the PureLink RNA Mini Kit extraction kit (Invitrogen) according to the manufacturer's protocol and quantified on a NanoDrop™ 1000 Spectrophotometer (ThermoFisher). Reverse transcription of RNA was performed using the iScript kit cDNA synthesis kit (Bio-Rad). Quantitative PCR was performed on the QuantStudio™ 3 (ThermoFisher Scientific) using 2 µg of complementary DNA (cDNA) mixed with TransStart TipGreen qPCR SuperMix 2X and Passive Reference Dye II (Transgen Biotech cat. #AQ141-01). The primers used are displayed in Table 1. The amplification cycles were performed at 94 °C for 10 s and at 60 °C for 45 s. The relative expression was calculated by the comparative method of (2-ΔΔCT) and normalized to the control gene β2- microglobulin (B2M).

Non-targeted lipidomic by liquid chromatography quadrupole time-of-flight mass spectrometry (LC-QTOF-MS). The LC-QTOF-MS was performed by the Montreal Heart Institute Metabolomics core facility as previously described [35]. Cells were seeded in 60 mm glass petri dishes (Pyrex™ cat. #C316060) to avoid polymer (polyethylene glycol, PEG) contamination, and treated as described above. Cells were then harvested, washed, and suspended in 1 mL of serum-free

medium. Lipids were extracted using internal standards (monoacylglycerosphosphocholine (LPC) 13:0, diacylglycerophosphocholine (PC) 14:0/14:0 and 19:0/19:0, phosphatidylserine (PS) 12:0/12:0, diacylglycerophosphoethanolamine (PE) 17:0/17:0, and diacylglycerophosphoglycerol (PG) 15:0/15:0)) and injected into a high performance liquid chromatograph (1290 Infinity HPLC) coupled to quadrupole time-of-flight mass spectrometry (Agilent Technologies Inc.) equipped with a dual electrospray ionization source and analyzed in positive and negative mode. The lipid elution was carried out on a Zorbax Eclipse plus column (C18, 2.1 mm × 100 mm, 1.8 µm, Agilent Technologies Inc.) for 83 min at a constant temperature of 40 °C in a gradient of solvent A (0.2% Methanoic acid and 10 mM ammonium formate in water) and B (0.2% methanoic acid and 5 mM ammonium formate in methanol/acetonitrile/methyl tert- butyl ether [MTBE], 55:35:10 [v/v/v]). Mass spectrometry data analysis was performed with the Mass Hunter Qualitative Analysis software and lipids were identified by Tandem Mass Spectrometry (MS/MS). Statistical analyzes were carried out by unpaired Student's t-test followed by Benjamini-Hochberg correction with the program Mass Professional Pro version 12.6.1 (Agilent Technologies Inc.).

Extracellular vesicle production in cell culture media. Following the 48-hour treatment with siLDLR (or control), the cell culture supernatant was collected and the concentration of lymphatic-endothelial cell-derived extracellular vesicles (EV) determined by flow cytometry (BD FACSCelesta™). For EV analysis, the 450/40 bandpass filter (BV421, violet laser) was manually swapped after cytometer setting and tracking (CS&T) calibration with a 1 mm-thick magnetron sputtered 405/10 bandpass filter (Chroma Technology, Bellows Falls, VT, USA), which is referred as V-SSC in this manuscript. Plots and histograms are showing all parameters in height (indicated as –H), as recommended for EV detection[36]. For a more precise calibration for assessment of biological vesicle size (refractive index in the range 1.36 to 1.42), the flow cytometer was calibrated for EV detection using the ApogeeMix (#1493, Apogee Flow Systems, Hemel Hempstead, UK), which consists of a mixture of non-fluorescent silica beads (180, 240, 300, 590, 880, and 1300 nm) and FITC-fluorescent latex beads (110 and 500 nm) (Figure S2A). The EV gate was set to contain events ranging from 100 to 1000 nm using the size of the non-fluorescent silica beads in the ApogeeMix, whose refractive index is close to that of cellular membranes[37]. The

threshold for the forward scatter (FSC) detector was set at the lowest possible value (200 V) in FACS Diva software (BD Biosciences). Events were acquired at a flow rate of 12 µL/minute, which is the lowest flow rate on the FACSCelesta. The flow rate during acquisition was kept to the minimum to avoid swarming effects and coincident detection[38]. EV were stained with CFSE (esterase activity, eBioscience cat. #65-0850-84)[39] and antibodies against CD31 (clone ID WM59, BD Biosciences cat. #563653) and VEGFR3 (clone ID 9D9F9, BioLegend cat. #356204). The background in the EV gate was determined by running samples containing all reagents and antibodies except EV-containing culture media and was subtracted from the values obtained for samples with EV-containing culture media. To confirm the cellular origin of the vesicles detected, 0.1% Triton X-100 (0.05% final concentration) was added to the samples for 30 min, and the decrease in EV count denoted. The absolute concentration of EV/mL was calculated using count beads (#7804, Biocytex, Marseille, France, Figure S2B) and the formula: (# of events in EV gate/ # of events in count beads gate)*(total number of beads in sample/sample volume)*dilution factor.

Total cholesterol measurement. Total cholesterol measurement was performed according to the manufacturer's protocol (Cholesterol E-Test, Wako Pure Chemicals Industries) in cell culture media as well as in HMVEC-dLyAd-derived EV (elicited with Triton X-100) following the 48 h treatment with LDLR siRNA or non-targeting siRNA.

Statistics. Data are expressed as mean ± standard error of the mean (SEM). Statistical significance was evaluated by unpaired t test or, for multiple comparisons, one-way ANOVA using appropriate corrections when data was not normally distributed, or for unequal variances. Each in vitro experiment was performed in triplicate. All calculations were done with GraphPad Prism v8 software (GraphPad Software, La Jolla, CA, USA), and p-values <0.05 were considered statistically significant.

RESULTS

Endothelial cell-specific knockdown of LDLR expression in mice reduced lymphatic contraction capacity in wild-type mice. LDLR deficiency has been associated to early lymphatic dysfunction in pre-atherosclerotic mice and a systemic knockout in PCSK9 improves lymphatic transport in aged mice[13]. As enhancing lymphatic function in *Ldlr-/-* mice before the administration of a pro-atherogenic regimen protects from subsequent excessive plaque formation through the improvement of lymphatic contraction capacity[32], we used an *in vivo* model of induced endothelial deletion of LDLR to determine whether PCSK9 deletion is potentiating lymphatic function when LDLR is downregulated on LEC in 3-month-old mice. Two weeks post- injection of AAV1, popliteal lymph nodes were harveste and analyzed by flowcytometry, and endothelial cells were selected based on CD31 and CD45 expression (Figure 1A). ShLDLR efficiently decreased LDLR expression in $CD45^{-}CD31^{+}Podoplanin^{+}$ cells in popliteal lymph nodes by 70% (Figure 1B, 1E), whereas it had no effect on LDLR $CD45^{+}$ cells (Figure 1C, 1D). Using intravital imaging, the capacity of the popliteal collecting vessel to contract was evaluated following the injection of fluorescent ovalbumin. Knocking down LDLR expression on lymphatic endothelial cells significantly decreased the number of contractions observed per min in 12-week- old wild-type male mice (Figure 2A), whereas it had no effect in wild type females or *Pcsk9*$^{-/-}$ mice (Figure 2B). Neither *Pcsk9*$^{-/-}$ nor wild-type mice had changes in contraction amplitude (Figure 2C- D). We have previously reported that *Pcsk9*$^{-/-}$ mice displayed improved dendritic cell migration through the lymphatics at 6 months of age compared to wild-type mice, whereas it had a similar magnitude of trafficking in 3-month-old mice[13]. We herein also report that the efficiency of dendritic cells to migrate from the skin to the draining lymph nodes following an 18 h contact sensitization assay remained unchanged in both 3-month-old male and female wild-type (Figure S3A) and *Pcsk9*$^{-/-}$ mice (Figure S3B). Decreasing LDLR expression on endothelial cells had no effect on cell migration through lymphatics in these mice (Figure S3).

LDLR expression is tightly regulated on lymphatic endothelial cells. We have previously demonstrated that LDLR is expressed on mice LEC, but not on lymphatic muscle cells[13]. We herein sought to understand how LDLR expression is regulated on LEC and might be responsible for lymphatic contraction impairment when hypercholesterolemia is not causal. The expression of LDLR was first confirmed by immunoblotting in whole cell lysates of HMVEC-dLyAd either treated or not with siLDLR and compared with hepatocytes (Huh7) and human embryonic kidney cells (HEK293) (Figure 3A). Flow cytometry allowed for the detection of membrane LDLR on HMVEC-dLyAd (Figure 3B). Immunofluorescence images revealed that LDLR is mostly likely located in the lipid rafts (Figure 3C), as it is positively correlating with the presence of GM1 gangliosides labeled by cholera toxin subunit B (Pearson coefficient, 0.804; Figure 3D) within the cells. When incubated for 4 hours with Dil-LDL, flow cytometry data (Figure 3E) indicated that LEC could efficiently internalize LDL (Figure 3F), albeit the levels of membrane LDLR were not impacted (Figure 3G). LEC were next incubated with fetal bovine serum (FBS)-free media for 24 h and cell surface expression of LDLR was measured by flow cytometry. Decreasing surrounding lipid content increased LDLR levels on the cell membrane (Figure 3H). As hepatic and extra-hepatic cells such as fibroblasts are also known to overexpress LDLR when incubated with serum-depleted medium[40, 41], we then investigated whether LDLR levels on LEC were also modifiable through the action of PCSK9.

Human lymphatic endothelial cells do not express PCSK9. Our laboratory has demonstrated that PCSK9 is circulating in mouse lymph and that lymphatic function is improved in 6-month- old *Pcsk9*$^{-/-}$ mice[13]. The source of PCSK9 in lymph remains unknown, and whether PCSK9 by itself can affect lymphatic function in aged mice needs to be determined. We therefore measured PCSK9 in whole cell lysate by immunoblotting of HMVEC-dLyAd and compared it with its expression in HepG2 and HEK293 cells (Figure 4A). Whereas hepatocytes strongly express PCSK9, LEC, just like HEK293 cells[28], do not express PCSK9. In addition, we performed an ELISA to assess whether HMVEC-dLyAd in culture can secrete PCSK9 (Figure 4B). Our results

suggest that PCSK9 present in lymph was neither expressed nor secreted by LEC. PCSK9 is typically recognized for its role in the regulation of cholesterol metabolism; it binds hepatic LDLR and induces its degradation in lysosomes leading lower cell surface LDLR and to an increase in plasma LDL-cholesterol[42]. In the past decade, PCSK9 has been studied for its role in atherosclerosis through pleiotropic effects on diverse cell types[43-45]. For instance, it has been reported that circulating PCSK9 contributes directly to the progression of atherosclerosis by suppressing the inflammatory response induced by oxLDL through inhibition of NF-kappaB activation in THP-1-derived macrophages[46] and by enhancing blood endothelial cells dysfunction independent of its effect on the LDLR[47]. The main role of PCSK9 on lymphatic endothelial cells is unknown, and we herein sought to define whether PCSK9 can control LDLR expression or if it rather acts through an LDLR-independent mechanism. We have thus optimized a treatment to determine whether PCSK9 can decrease LDLR expression on HMVEC-dLyAd. We incubated LEC for 16 hours with recombinant PCSK9 (6.5 µg/mL) and observed a decrease in total LDLR protein by immunoblotting (Figure 4C) and a 90% decrease of the membrane-bound LDLR protein by flow cytometry (Figure 4D). Further, exogenous PCSK9 did not affect the Pearson coefficient assessing the colocalization between LDLR and cholera toxin subunit B (average of 0.694 with exogenous PCSK9 vs. 0.804 for control; Figure 4E). Next, we used these conditions to study the effect of PCSK9 on lymphatic endothelial cell integrity.

PCSK9 *per se* does not decrease the expression of lymphatic markers nor affect the cell cycle. Signaling by vascular endothelial growth factors (VEGFs) through VEGF receptors (VEGFRs) plays important roles in vascular development[48]. PCSK9 inhibitors have been shown to increase VEGFR-2^{+} endothelial progenitor cells[49] and increase VEGF release into supernatants of blood endothelial cells *in vitro*[50]. Several lymphatic endothelial markers, such as VEGFR-3, but also lymphatic vessel endothelial hyaluronic acid receptor-1 (LYVE-1), prospero-related homeobox-1 (Prox-1) and podoplanin are widely used in the detection of lymphangiogenesis and proper lymphatic vessel function. We herein wanted to assess whether PCSK9 treatment would decrease VEGFR-3 and other lymphatic markers on HMVEC-dLyAd *in vitro*. Albeit it decreased LDLR protein expression (Figure 4C-D) without however altering the transcription of the protein[51],

exogenous PCSK9 had no effect on VEGFR-3 (Figure 5A), LYVE-1 (Figure 5B) or podoplanin (Figure 5C) protein expression. Cholesterol synthesis is tightly related to cell proliferation[52, 53].

In general, proliferating cells show increased cholesterol synthesis and LDL receptor activity, which reflects the cellular lipid storage[54]. Contrariwise, cholesterol synthesis inhibitors can block cell proliferation[55-58]. Suppressing PCSK9 has recently been shown to significantly alter the cell cycle and induce apoptosis of human keratinocytes[59]. Luan et al. reported that when topically applied for either 24 h or 72 h, siRNA targeting PCSK9 increased significantly the percentage of keratinocytes in S phase compared to control treatment[59]. To explore whether PCSK9 could exert its effect on lymphatic function by altering lymphatic endothelial cell cycle, we used the classical DNA fragmentation assay and analyzed the data by flow cytometry (Figure 5D)[34]. Our data revealed that exogenous PCSK9 did not alter the lymphatic endothelial cell cycle *in vitro* (Figure 5E). Our results thus suggest that decreasing LDLR expression at the protein level might not be sufficient to alter LEC replication and integrity.

Small interfering RNA targeting LDLR reduces the cell replication phase in LEC. HMVEC- dLyAd were treated for 48 h with 25 nM siRNA targeting LDLR (siLDLR) or non-targeting siRNA in complete medium. The expression of LDLR protein in whole cell lysate (Figure 6A) and on the cell membrane (Figure 6B), as well as at the mRNA level (Figure 6C) were blunted following siLDLR treatment. Knocking down LDLR, however, did not affect the Pearson coefficient assessing the colocalization between LDLR and cholera toxin subunit B (average of 0.688 with siLDLR vs. 0.766 for control; Figure 6D). Whereas VEGFR-3 (Figure 6E) and LYVE-1 (Figure 6F) membrane expression were not altered by LDLR mRNA downregulation, membrane-bound podoplanin was reduced (Figure 6G), albeit podoplanin mRNA levels were unchanged (Figure 6C) compared to control. Furthermore, the assessment of the cell cycle by flow cytometry[34] revealed that the replication phase was significantly reduced in siLDLR-treated HMVEC-dLyAd compared to the non-targeting siRNA treatment (Figure 6H).

Small interfering RNA targeting LDLR blunts lipids contained in lipid rafts. As podoplanin resides in lipid rafts in the plasma membrane[60], we then turn our attention to the membrane of LEC to explain how LDLR downregulation might decrease podoplanin at the protein level but not at the mRNA level. We thus performed non-targeted lipidomic and first described that total cholesterol was decreased in cells treated with siLDLR compared to non-targeting siRNA (Figure 7A). In total, among the 2139 MS signals (or features) obtained following data processing, 80 features significantly discriminated siLDLR-treated cells from control cells (Figure 7B), among which we identified 18 unique lipids (Figure 7C). As the lipids identified were mostly contained in the membrane of the cells, we therefore sought to investigate siLDLR could mediate these changes by increasing the production of extracellular vesicles (EV) derived from the plasma membrane. Using a flow cytometer equipped with a 405/10 bandpass filter that allows the cell scatter detection on the violet laser with a better acuteness, we next assessed the number of EV produced upon siLDLR (or si-control) treatment. Downregulating LDLR on LEC had no effect on the production of LEC-derived EV, nor on the total cholesterol content of these EV (Figure 7D- E).

DISCUSSION

Efficient lymphatic drainage is crucial for atherosclerosis regression[9, 61, 62]. For a long time, hypercholesterolemia was defined as the corner stone between cardiovascular disease and lymphatic function[10-12]. Recently the role of the lymphatics has been refined throughout the development of the atherosclerosis process, placing front stage this network in the early phase of the disease[13, 32]. However, the exact mechanism underlying this chronological process that appears to be independent of circulating cholesterol level remains unclear.

In the present article, we sought to pinpoint the key element(s) that could be instigating the lymphatic dysfunction that occurs before the onset of atherosclerosis. As previous data suggest that LDLR and PCSK9 might be involved in the impaired collecting lymphatic transport in mice that are predisposed to develop atherosclerosis[13], we are herein aiming at determining whether and how a specific knockdown of *Ldlr* gene expression on endothelial cells could reduce lymphatic

function in mice either systemically lacking PCSK9 or not. Using an AAV1-shLDLR, we showed that knocking down the expression of LDLR by over 50% on LEC degraded the capacity of the lymphatics to contract in wild-type male mice, whereas it had no effect in *Pcsk9*$^{-/-}$ mice. Albeit the amplitude of the contractions did not significantly differ between groups, wild-type male mice tend to display larger amplitude when treated with AAV1-shLDLR. We have previously reported that wild-type and *Pcsk9*$^{-/-}$ mice had a similar magnitude of dendritic cell transport through their lymphatics after a contact sensitization assay at three months of age, while 6-month-old *Pcsk9*$^{-/-}$ mice displayed an improved lymphatic transport compared to wild-type mice[13]. The results we report herein on 12-week-old mice are no exception, suggesting that a specific defect in the contraction capacity of the collecting lymphatic vessels is the primary underlying instigating mechanism of lymphatic transport impairment. These differences in lymphatic contractility could be, at least in part, attributable to the more modest LDLR expression on LEC and the slight increase in lymph PCSK9 concentration in wild-type mice compared to *Pcsk9*$^{-/-}$ mice[13].

Mice systemically lacking LDLR are displaying impaired endothelial function and an altered redox balance associated with reduced nitric oxide (NO) bioavailability, which contributes to the accelerated atherosclerosis[63]. Similarly to blood vessels, NO is a fine regulator of lymphatic function, mainly through the regulation of collecting lymphatic vessel contractions[64]. Whereas the lymphatic system can uptake fluid and macromolecules from the interstitial tissue through the capillaries (also called initial lymphatics), collecting lymphatic vessels are responsible for the propulsion of lymph through lymph nodes to the lymphovenous junctions, where the network connects with the blood circulation. When there is a change in surrounding interstitial pressure, lymphatic vessels either expand in order to fill with lymph or rather contract to push lymph forward[65]. One of the major driving forces of lymphatic pumping is the surrounding layer of muscle cells whose activity largely depends on intracellular Ca^{2+} levels, which are modulated by NO levels produced by the endothelial nitric oxide synthase (eNOS) under physiological conditions. Under inflammatory conditions, lymphatic contraction frequency is reduced due to the increase secretion of NO from the inducible NOS (iNOS) produced by immune cells and inflamed endothelium[66]. PCSK9 might influence the vascular wall and atherosclerotic plaque locally, as it is expressed in cellular components of the blood vessel wall, such endothelial cells

and smooth muscle cells[67, 68], as well as inflammatory cells[69, 70]. The PCSK9-reactive oxygen species (ROS) interaction is involved in vascular aging and atherosclerosis propagation[71]. We believe that it may be able to modulate lymphatic function as well, as the formation of ROS negatively influences lymphatic contractile function[72]. Given this evidence, PCSK9 may exert pro- atherogenic effects beyond its activity on hepatic LDLR and we hypothesized that PCSK9, through LDLR modulation or *via* pleiotropic effects, might affect one of the newly identified player in atherosclerosis, the lymphatic network.

The reason why a decreased collecting lymphatic vessel contractility could be observed in wild-type male but not in female could reside in several combined answers. First, it is known that the intraluminal lymphatic pumping pressure that decreases with age is significantly worse in female patients[73]. This observation could be partially explained by the fact that a decrease in estrogen production with age might limit NO-dependent contractile forces in the lymphatic endothelium. Thus, we assume it is why the wild-type female mice included in our study start off with a tendency to have lower contraction frequency than male. Mansukhani et al. reported that an increase in atherosclerosis over time is more important in females *Ldlr*$^{-/-}$ mice rather than in male mice[74]. The underlying mechanism of this differential phenotype of atherosclerosis is not clear yet, and do not exclude a direct role for LDLR *per se*. Few years back, Roubtsova et al. elegantly showed that total LDLR protein levels in liver, pancreas and small intestine extracts were increased compared to wild-type animals in both male and female *Pcsk9*$^{-/-}$ mice[75]. However, systemic deletion of PCSK9 results in a sex- and tissue-specific subcellular distribution of the LDLR in an estradiol-dependent manner[75]. In our hands, shLDLR decreased LDLR expression on lymph node LEC in a similar magnitude in wild-type and *Pcsk9*$^{-/-}$ mice, but the effect on lymphatic function appeared only in wild-type male mice, suggesting that PCSK9 could be an active player in modulating LDLR-dependent lymphatic function. However, when digging into the mechanisms involved, we showed that PCSK9 is not produced nor secreted by LEC, and that LDLR is located mostly in lipid rafts, whereas on other cell types, LDL binds to the LDLR in clathrin-coated pits, rather than LDLR associated with lipid rafts[14]. Exogenous PCSK9 and siLDLR did not affect the Pearson correlation coefficient between LDLR and cholera toxin subunit B. Therefore, LDLR modulation on LEC could have completely different physiological functions than on any other cell

type and affect lymphatic function in a mechanism that is independent of its LDL binding properties. Whereas FBS depletion in the media could efficiently increase LDLR expression on LEC, exogenous (DiI-)LDL had no impact on LDLR membrane levels overall despite a clear internalization of the lipoprotein. This might also suggest that apolipoprotein (apo) B and apoE-containing particles other than LDL might bind to the LDLR, which could mediate their internalization in LEC. Lymph is rich in high-density lipoprotein (HDL) and chylomicron, as it returns the peripheral fluid to the bloodstream via the subclavian vein, but a much smaller proportion of LDL can be retrieved in lymph. Therefore, albeit a recent publication indicated that acute exposure of collecting lymphatic vessels to LDL increases contraction frequency and lymph flow[76], we do not think that this mechanism would be happening significantly physiologically or at least affect lymphatic function *per se*. The modulation of LDLR on LEC might be happening through another mechanism to in turn affect lymphatic endothelial cell metabolism and lymphatic transport. To test whether PCSK9 might account for these changes, either *via* the LDLR or through pleiotropic effects, we tested whether this convertase is expressed by LEC. Whereas PCSK9 is present in mouse lymph[13], LEC did not expressed PCSK9, meaning that circulating lymph PCSK9 originates from other cell types.

Incubating human dermal LEC with either exogenous human recombinant PCSK9 or a silencing RNA (siRNA) that specifically targets *Ldlr* expression both decreased LDLR protein expression. However, only siLDLR treatment enabled a decrease in chromosome duplication phase and a reduction in podoplanin protein levels, a specific membrane-bound lymphatic marker involved in lymphatic function. Specific residues on podoplanin can mediate interactions with other proteins that are crucial in lymphatic function[77], including for the formation of the lymphovenous junction and for the lymphatic vessel integrity *per se*, during development and throughout life[78, 79]. Podoplanin signaling has intrinsic effects on the proliferation, migration, and tube formation of LEC[80, 81], which could explain the decrease the S-phase of the cell cycle of LEC. The fact that podoplanin is modulated by the downregulation of LDLR mRNA could be a key element in our comprehension of the mechanism underlying the premature defect in lymphatic transport early in the atherosclerosis process. As popoplanin decreased at the protein but not mRNA level, we suggest that a reduction in membrane cholesterol (consequence of a reduction in LDLR) could

increase the turnover of podoplanin on cell membrane. We thus went on and studied the effect of LDLR mRNA modulation on the LEC lipid raft content. Podoplanin is most likely expressed in lipid rafts of the plasma membrane of lymphatic endothelial cells[60]. Lipid rafts have lifetimes on the plasma membrane that range from seconds to minutes[82]. Albeit very labile, these segregations of lipids are typically enriched in free cholesterol and glycosphingolipids and regulate important cellular functions such as cellular polarity, vesicular traffic and signaling pathways[83]. Our lipidomic analysis revealed that *Ldlr* downregulation decreased total cholesterol within the cells and a reduction in 18 lipid subclasses, including key constituents of lipid rafts. Of all the lipids detected that have decreased following siLDLR treatment, phosphatidylcholines, sphingomyelins and ceramides were identified. Phosphatidylcholines are lipids which account for about 40% of phospholipids in cells[84]. Their suppression in blood endothelial cells prevents normal functioning of apoptosis signaling pathways[85]. Disturbance in the ratios of membrane lipids (phosphatidylcholines to phosphatidylethanolamines) leads to the development of organ failure in mice caused by loss of membrane integrity of hepatocytes[86] and affects the normal processes of cell proliferation and viability[87]. Ceramides are important for the stability of the lipid bilayer[88] and they participate in the regulation of cell proliferation by inducing apoptosis under normal conditions[89, 90]. Whereas how lipid rafts are formed remains unclear, we sought to determine whether siLDLR could modulate the plasma membrane composition by releasing lymphatic endothelial cell-derived extracellular vesicles (EV). We thus quantified EV produced following cell treatment and reported that LDL modulation had no impact on the concentration of EV retrieved in the cell culture supernatant. As we could not exclude that the EV production rate might remain unchanged but its composition different, we measured the total cholesterol content of these EV and showed that it was also unchanged compared to the control-treated group, suggesting that plasma membrane cholesterol is not mobilized out of the cell through the production of extracellular vesicles.

CONCLUSIONS

Efficient lymphatic drainage is crucial for atherosclerosis regression[9, 61, 62]. Whereas hypercholesterolemia has previously been defined as the corner stone between cardiovascular disease and lymphatic function[10-12], we herein confirm that lymphatic function is rather tightly regulated throughout the development of the atherosclerosis process and highlight the crucial role of the LDLR in that chronological process. Using an *in vivo* model of induced endothelial deletion of LDLR and human cell lines, we are reporting that knocking down the expression of LDLR on lymphatic endothelial cells degrades the capacity of the lymphatics to contract in mice where PCSK9 levels are abundant. Our *in vitro* findings show that LDLR needs to be modulated at the mRNA level to in turn affect membrane lymphatic markers expression and the cellular replication phase of lymphatic endothelial cells, a process in which changes in lipid rafts appear to be involved. Albeit more studies are needed on the role of lipid rafts in lymphatic function during atherosclerosis, our results suggest that treatments that specifically palliate the down regulation of *Ldlr* mRNA by LEC might preserve the integrity of the lymphatic endothelium and sustain lymphatic function in subjects at higher risk of atherosclerosis.

ABBREVIATIONS

AAV1: Adeno-Associated Virus Serotype 1 CVD: cardiovascular disease

EV: extracellular vesicles FBS: fetal bovine serum

FITC: fluorescein isothyiocyanate HEK: human embryonic kidney HuH7: hepatocytes

LDL: low-density lipoprotein

LDLR: low-density lipoprotein receptor LEC: lymphatic endothelial cell

LN: lymph node

LVs: lymphatic vessels

LYVE-1: lymphatic vessel endothelial hyaluronic acid receptor-1 MFI: mean fluorescence intensity

PCSK9: proprotein convertase subtilisin kexin type 9 ROI: region of interest

shRNA: short hairpin RNA shSCR: sramble short hairpin RNA siRNA: short-interfering RNA

VEGF-C152s: vascular endothelial growth factor receptor-C VEGFR3: vascular endothelial growth factor receptor 3

Wt: C57BL/6 wild-type

AUTHOR CONTRIBUTIONS

LV* and AS* conducted experiments, acquired and analyzed data and edited the manuscript; GJ and AM acquired and analyzed data; NT and SJ performed the *in vivo* injections and organs harvesting; NA and AD conducted the AAV1 constructions; LV performed the confocal microscopy experiments; MST provided scientific insights and edited the manuscript; GM provided the *Pcsk9*$^{-/-}$ mice and edited the manuscript; CM designed research studies, acquired and analyzed data and wrote the manuscript.

ACKNOWLEDGEMENTS

We would like to thank Vincent Finnerty for developing the LymphPulse 3.0 software, Azadeh Alikashani for her help with qPCR analysis, Carl Fortin for his technical support with flow cytometry analysis and Dr Matthieu Ruiz, Caroline Daneault and Isabelle Robillard Frayne from the MHI Metabolomics core facility for performing the untargeted lipidomic analysis.

CONFLICT OF INTEREST

The authors have no conflict of interest to disclose.

FINANCIAL SUPPORT

This work was supported by the Canadian Institutes of Health Research (Project scheme,

C.M. ; MSc training grant, L.V.) and by the Fonds de Recherche du Québec – Santé (doctoral training grant, A.M.).

REFERENCES

1. Lemole GM, Sr. The Role of Lymphstasis in Atherogenesis Revisited. Ann Thorac Surg. 2016; 101: 2029.

2. Lemole GM. The role of lymphstasis in atherogenesis. Ann Thorac Surg. 1981; 31: 290-3.

3. Cueni LN, Detmar M. The lymphatic system in health and disease. Lymphat Res Biol. 2008; 6: 109-22.

4. Iqbal J, Hussain MM. Intestinal lipid absorption. Am J Physiol Endocrinol Metab. 2009; 296: E1183-94.

5. Nakano T, Nakashima Y, Yonemitsu Y, Sumiyoshi S, Chen YX, Akishima Y, et al. Angiogenesis and lymphangiogenesis and expression of lymphangiogenic factors in the atherosclerotic intima of human coronary arteries. Hum Pathol. 2005; 36: 330-40.

6. Eliska O, Eliskova M, Miller AJ. The absence of lymphatics in normal and atherosclerotic coronary arteries in man: a morphologic study. Lymphology. 2006; 39: 76-83.

7. Kholova I, Dragneva G, Cermakova P, Laidinen S, Kaskenpaa N, Hazes T, et al. Lymphatic vasculature is increased in heart valves, ischaemic and inflamed hearts and in cholesterol-rich and calcified atherosclerotic lesions. Eur J Clin Invest. 2011; 41: 487-97.

8. Drozdz K, Janczak D, Dziegiel P, Podhorska M, Patrzalek D, Ziolkowski P, et al. Adventitial lymphatics of internal carotid artery in healthy and atherosclerotic vessels. Folia Histochem Cytobiol. 2008; 46: 433-6.

9. Martel C, Li W, Fulp B, Platt AM, Gautier EL, Westerterp M, et al. Lymphatic vasculature mediates macrophage reverse cholesterol transport in mice. J Clin Invest. 2013; 123: 1571-9.

10. Vuorio T, Nurmi H, Moulton K, Kurkipuro J, Robciuc MR, Ohman M, et al. Lymphatic vessel insufficiency in hypercholesterolemic mice alters lipoprotein levels and promotes atherogenesis. Arterioscler Thromb Vasc Biol. 2014; 34: 1162-70.

11. Lim HY, Thiam CH, Yeo KP, Bisoendial R, Hii CS, McGrath KC, et al. Lymphatic vessels are essential for the removal of cholesterol from peripheral tissues by SR-BI-mediated transport of HDL. Cell Metab. 2013; 17: 671-84.

12. Lim HY, Rutkowski JM, Helft J, Reddy ST, Swartz MA, Randolph GJ, et al. Hypercholesterolemic mice exhibit lymphatic vessel dysfunction and degeneration. Am J Pathol. 2009; 175: 1328-37.

13. Milasan A, Dallaire F, Mayer G, Martel C. Effects of LDL Receptor Modulation on Lymphatic Function. Sci Rep. 2016; 6: 27862.

14. Munro S. Lipid rafts: elusive or illusive? Cell. 2003; 115: 377-88.

15. Goldstein JL, Brown MS. Familial hypercholesterolemia: identification of a defect in the regulation of 3-hydroxy-3-methylglutaryl coenzyme A reductase activity associated with overproduction of cholesterol. Proc Natl Acad Sci U S A. 1973; 70: 2804-8.

16. Brown MS, Goldstein JL. A proteolytic pathway that controls the cholesterol content of membranes, cells, and blood. Proc Natl Acad Sci U S A. 1999; 96: 11041-8.

17. Gil G, Faust JR, Chin DJ, Goldstein JL, Brown MS. Membrane-bound domain of HMG CoA reductase is required for sterol-enhanced degradation of the enzyme. Cell. 1985; 41: 249-58.

18. Goldstein JL, Brown MS. The low-density lipoprotein pathway and its relation to atherosclerosis. Annu Rev Biochem. 1977; 46: 897-930.

19. Daniels TF, Killinger KM, Michal JJ, Wright RW, Jr., Jiang Z. Lipoproteins, cholesterol homeostasis and cardiac health. Int J Biol Sci. 2009; 5: 474-88.

20. Hu J, Zhang Z, Shen WJ, Azhar S. Cellular cholesterol delivery, intracellular processing and utilization for biosynthesis of steroid hormones. Nutr Metab (Lond). 2010; 7: 47.

21. Abifadel M, Varret M, Rabes JP, Allard D, Ouguerram K, Devillers M, et al. Mutations in PCSK9 cause autosomal dominant hypercholesterolemia. Nat Genet. 2003; 34: 154-6.

22. Nassoury N, Blasiole DA, Tebon Oler A, Benjannet S, Hamelin J, Poupon V, et al. The cellular trafficking of the secretory proprotein convertase PCSK9 and its dependence on the LDLR. Traffic. 2007; 8: 718-32.

23. Mayer G, Poirier S, Seidah NG. Annexin A2 is a C-terminal PCSK9-binding protein that regulates endogenous low density lipoprotein receptor levels. J Biol Chem. 2008; 283: 31791-801.

24. Poirier S, Mamarbachi M, Chen WT, Lee AS, Mayer G. GRP94 Regulates Circulating Cholesterol Levels through Blockade of PCSK9-Induced LDLR Degradation. Cell Rep. 2015; 13: 2064-71.

25. Demers A, Samami S, Lauzier B, Des Rosiers C, Ngo Sock ET, Ong H, et al. PCSK9 Induces CD36 Degradation and Affects Long-Chain Fatty Acid Uptake and Triglyceride Metabolism in Adipocytes and in Mouse Liver. Arterioscler Thromb Vasc Biol. 2015; 35: 2517- 25.

26. Roubtsova A, Munkonda MN, Awan Z, Marcinkiewicz J, Chamberland A, Lazure C, et al. Circulating proprotein convertase subtilisin/kexin 9 (PCSK9) regulates VLDLR protein and triglyceride accumulation in visceral adipose tissue. Arterioscler Thromb Vasc Biol. 2011; 31: 785-91.

27. Levy E, Ben Djoudi Ouadda A, Spahis S, Sane AT, Garofalo C, Grenier E, et al. PCSK9 plays a significant role in cholesterol homeostasis and lipid transport in intestinal epithelial cells. Atherosclerosis. 2013; 227: 297-306.

28. Canuel M, Sun X, Asselin MC, Paramithiotis E, Prat A, Seidah NG. Proprotein convertase subtilisin/kexin type 9 (PCSK9) can mediate degradation of the low density lipoprotein receptor- related protein 1 (LRP-1). PLoS One. 2013; 8: e64145.

29. Poirier S, Mayer G, Benjannet S, Bergeron E, Marcinkiewicz J, Nassoury N, et al. The proprotein convertase PCSK9 induces the degradation of low density lipoprotein receptor (LDLR) and its closest family members VLDLR and ApoER2. J Biol Chem. 2008; 283: 2363-72.

30. Lakoski SG, Lagace TA, Cohen JC, Horton JD, Hobbs HH. Genetic and metabolic determinants of plasma PCSK9 levels. J Clin Endocrinol Metab. 2009; 94: 2537-43.

31. Baass A, Dubuc G, Tremblay M, Delvin EE, O'Loughlin J, Levy E, et al. Plasma PCSK9 is associated with age, sex, and multiple metabolic markers in a population-based sample of children and adolescents. Clin Chem. 2009; 55: 1637-45.

32. Milasan A, Smaani A, Martel C. Early rescue of lymphatic function limits atherosclerosis progression in Ldlr(-/-) mice. Atherosclerosis. 2019; 283: 106-19.

33. Chong C, Scholkmann F, Bachmann SB, Luciani P, Leroux JC, Detmar M, et al. In vivo visualization and quantification of collecting lymphatic vessel contractility using near-infrared imaging. Sci Rep. 2016; 6: 22930.

34. Riccardi C, Nicoletti I. Analysis of apoptosis by propidium iodide staining and flow cytometry. Nat Protoc. 2006; 1: 1458-61.

35. Forest A, Ruiz M, Bouchard B, Boucher G, Gingras O, Daneault C, et al. Comprehensive and Reproducible Untargeted Lipidomic Workflow Using LC-QTOF Validated for Human Plasma Analysis. J Proteome Res. 2018; 17: 3657-70.

36. Poncelet P, Robert S, Bailly N, Garnache-Ottou F, Bouriche T, Devalet B, et al. Tips and tricks for flow cytometry-based analysis and counting of microparticles. Transfus Apher Sci. 2015; 53: 110-26.

37. Beuthan J, Minet O, Helfmann J, Herrig M, Muller G. The spatial variation of the refractive index in biological cells. Phys Med Biol. 1996; 41: 369-82.

38. Poncelet P, Robert S, Bouriche T, Bez J, Lacroix R, Dignat-George F. Standardized counting of circulating platelet microparticles using currently available flow cytometers and scatter-based triggering: Forward or side scatter? Cytometry A. 2016; 89: 148-58.

39. Morales-Kastresana A, Telford B, Musich TA, McKinnon K, Clayborne C, Braig Z, et al. Labeling Extracellular Vesicles for Nanoscale Flow Cytometry. Sci Rep. 2017; 7: 1878.

40. Brown MS, Goldstein JL. Regulation of the activity of the low density lipoprotein receptor in human fibroblasts. Cell. 1975; 6: 307-16.

41. Shimomura I, Bashmakov Y, Shimano H, Horton JD, Goldstein JL, Brown MS. Cholesterol feeding reduces nuclear forms of sterol regulatory element binding proteins in hamster liver. Proc Natl Acad Sci U S A. 1997; 94: 12354-9.

42. Burke AC, Dron JS, Hegele RA, Huff MW. PCSK9: Regulation and Target for Drug Development for Dyslipidemia. Annu Rev Pharmacol Toxicol. 2017; 57: 223-44.

43. Bittner V. Pleiotropic Effects of PCSK9 (Proprotein Convertase Subtilisin/Kexin Type 9) Inhibitors? Circulation. 2016; 134: 1695-6.

44. Cheng JM, Oemrawsingh RM, Garcia-Garcia HM, Boersma E, van Geuns RJ, Serruys PW, et al. PCSK9 in relation to coronary plaque inflammation: Results of the ATHEROREMO-IVUS study. Atherosclerosis. 2016; 248: 117-22.

45. Lambert G, Petrides F, Chatelais M, Blom DJ, Choque B, Tabet F, et al. Elevated plasma PCSK9 level is equally detrimental for patients with nonfamilial hypercholesterolemia and heterozygous familial hypercholesterolemia, irrespective of low-density lipoprotein receptor defects. J Am Coll Cardiol. 2014; 63: 2365-73.

46. Tang Z, Jiang L, Peng J, Ren Z, Wei D, Wu C, et al. PCSK9 siRNA suppresses the inflammatory response induced by oxLDL through inhibition of NF-kappaB activation in THP-1- derived macrophages. Int J Mol Med. 2012; 30: 931-8.

47. Ferri N, Marchiano S, Tibolla G, Baetta R, Dhyani A, Ruscica M, et al. PCSK9 knock-out mice are protected from neointimal formation in response to perivascular carotid collar placement. Atherosclerosis. 2016; 253: 214-24.

48. Hamada K, Oike Y, Takakura N, Ito Y, Jussila L, Dumont DJ, et al. VEGF-C signaling pathways through VEGFR-2 and VEGFR-3 in vasculoangiogenesis and hematopoiesis. Blood. 2000; 96: 3793-800.

49. Schuster S, Rubil S, Endres M, Princen HMG, Boeckel JN, Winter K, et al. Anti-PCSK9 antibodies inhibit pro-atherogenic mechanisms in APOE*3Leiden.CETP mice. Sci Rep. 2019; 9: 11079.

50. Safaeian L, Vaseghi G, Jabari H, Dana N. Evolocumab, a proprotein convertase subtilisin/kexin type 9 inhibitor, promotes angiogenesis in vitro. Can J Physiol Pharmacol. 2019; 97: 352-8.

51. Maxwell KN, Breslow JL. Adenoviral-mediated expression of Pcsk9 in mice results in a low-density lipoprotein receptor knockout phenotype. Proc Natl Acad Sci U S A. 2004; 101: 7100- 5.

52. Brown MS, Goldstein JL. Suppression of 3-hydroxy-3-methylglutaryl coenzyme A reductase activity and inhibition of growth of human fibroblasts by 7-ketocholesterol. J Biol Chem. 1974; 249: 7306-14.

53. Chen HW, Kandutsch AA, Waymouth C. Inhibition of cell growth by oxygenated derivatives of cholesterol. Nature. 1974; 251: 419-21.

54. Vitols S, Norgren S, Juliusson G, Tatidis L, Luthman H. Multilevel regulation of low- density lipoprotein receptor and 3-hydroxy-3-methylglutaryl coenzyme A reductase gene expression in normal and leukemic cells. Blood. 1994; 84: 2689-98.

55. Martinez-Botas J, Suarez Y, Ferruelo AJ, Gomez-Coronado D, Lasuncion MA. Cholesterol starvation decreases p34(cdc2) kinase activity and arrests the cell cycle at G2. FASEB J. 1999; 13: 1359-70.

56. Corsini A, Mazzotti M, Raiteri M, Soma MR, Gabbiani G, Fumagalli R, et al. Relationship between mevalonate pathway and arterial myocyte proliferation: in vitro studies with inhibitors of HMG-CoA reductase. Atherosclerosis. 1993; 101: 117-25.

57. Jakobisiak M, Bruno S, Skierski JS, Darzynkiewicz Z. Cell cycle-specific effects of lovastatin. Proc Natl Acad Sci U S A. 1991; 88: 3628-32.

58. Chakrabarti R, Engleman EG. Interrelationships between mevalonate metabolism and the mitogenic signaling pathway in T lymphocyte proliferation. J Biol Chem. 1991; 266: 12216-22.

59. Luan C, Chen X, Zhu Y, Osland JM, Gerber SD, Dodds M, et al. Potentiation of Psoriasis-Like Inflammation by PCSK9. J Invest Dermatol. 2019; 139: 859-67.

60. Barth K, Blasche R, Kasper M. T1alpha/podoplanin shows raft-associated distribution in mouse lung alveolar epithelial E10 cells. Cell Physiol Biochem. 2010; 25: 103-12.

61. Martel C, Randolph GJ. Atherosclerosis and transit of HDL through the lymphatic vasculature. Curr Atheroscler Rep. 2013; 15: 354.

62. Yeo KP, Lim HY, Thiam CH, Azhar SH, Tan C, Tang Y, et al. Efficient aortic lymphatic drainage is necessary for atherosclerosis regression induced by ezetimibe. Sci Adv. 2020; 6.

63. Zadelaar S, Kleemann R, Verschuren L, de Vries-Van der Weij J, van der Hoorn J, Princen HM, et al. Mouse models for atherosclerosis and pharmaceutical modifiers. Arterioscler Thromb Vasc Biol. 2007; 27: 1706-21.

64. Gasheva OY, Zawieja DC, Gashev AA. Contraction-initiated NO-dependent lymphatic relaxation: a self-regulatory mechanism in rat thoracic duct. J Physiol. 2006; 575: 821-32.

65. Wang Y, Oliver G. Current views on the function of the lymphatic vasculature in health and disease. Genes Dev. 2010; 24: 2115-26.

66. Liao S, Cheng G, Conner DA, Huang Y, Kucherlapati RS, Munn LL, et al. Impaired lymphatic contraction associated with immunosuppression. Proc Natl Acad Sci U S A. 2011; 108: 18784-9.

67. Ferri N, Tibolla G, Pirillo A, Cipollone F, Mezzetti A, Pacia S, et al. Proprotein convertase subtilisin kexin type 9 (PCSK9) secreted by cultured smooth muscle cells reduces macrophages LDLR levels. Atherosclerosis. 2012; 220: 381-6.

68. Schulz R, Schluter KD, Laufs U. Molecular and cellular function of the proprotein convertase subtilisin/kexin type 9 (PCSK9). Basic Res Cardiol. 2015; 110: 4.

69. Ding Z, Wang X, Liu S, Zhou S, Kore RA, Mu S, et al. NLRP3 inflammasome via IL- 1beta regulates PCSK9 secretion. Theranostics. 2020; 10: 7100-10.

70. Giunzioni I, Tavori H, Covarrubias R, Major AS, Ding L, Zhang Y, et al. Local effects of human PCSK9 on the atherosclerotic lesion. J Pathol. 2016; 238: 52-62.

71. Ding Z, Liu S, Wang X, Deng X, Fan Y, Sun C, et al. Hemodynamic shear stress via ROS modulates PCSK9 expression in human vascular endothelial and smooth muscle cells and along the mouse aorta. Antioxid Redox Signal. 2015; 22: 760-71.

72. Zawieja DC, Greiner ST, Davis KL, Hinds WM, Granger HJ. Reactive oxygen metabolites inhibit spontaneous lymphatic contractions. Am J Physiol. 1991; 260: H1935-43.

73. Unno N, Tanaka H, Suzuki M, Yamamoto N, Mano Y, Sano M, et al. Influence of age and gender on human lymphatic pumping pressure in the leg. Lymphology. 2011; 44: 113-20.

74. Mansukhani NA, Wang Z, Shively VP, Kelly ME, Vercammen JM, Kibbe MR. Sex Differences in the LDL Receptor Knockout Mouse Model of Atherosclerosis. Artery Res. 2017; 20: 8-11.

75. Roubtsova A, Chamberland A, Marcinkiewicz J, Essalmani R, Fazel A, Bergeron JJ, et al. PCSK9 deficiency unmasks a sex- and tissue-specific subcellular distribution of the LDL and VLDL receptors in mice. J Lipid Res. 2015; 56: 2133-42.

76. Solari E, Marcozzi C, Bartolini B, Viola M, Negrini D, Moriondo A. Acute Exposure of Collecting Lymphatic Vessels to Low-Density Lipoproteins Increases Both Contraction Frequency and Lymph Flow: An In Vivo Mechanical Insight. Lymphat Res Biol. 2020; 18: 146- 55.

77. Martin-Villar E, Megias D, Castel S, Yurrita MM, Vilaro S, Quintanilla M. Podoplanin binds ERM proteins to activate RhoA and promote epithelial-mesenchymal transition. J Cell Sci. 2006; 119: 4541-53.

78. Osada M, Inoue O, Ding G, Shirai T, Ichise H, Hirayama K, et al. Platelet activation receptor CLEC-2 regulates blood/lymphatic vessel separation by inhibiting proliferation, migration, and tube formation of lymphatic endothelial cells. J Biol Chem. 2012; 287: 22241-52.

79. Hess PR, Rawnsley DR, Jakus Z, Yang Y, Sweet DT, Fu J, et al. Platelets mediate lymphovenous hemostasis to maintain blood-lymphatic separation throughout life. J Clin Invest. 2014; 124: 273-84.

80. Navarro A, Perez RE, Rezaiekhaligh MH, Mabry SM, Ekekezie, II. Polarized migration of lymphatic endothelial cells is critically dependent on podoplanin regulation of Cdc42. Am J Physiol Lung Cell Mol Physiol. 2011; 300: L32-42.

81. Navarro A, Perez RE, Rezaiekhaligh M, Mabry SM, Ekekezie, II. T1alpha/podoplanin is essential for capillary morphogenesis in lymphatic endothelial cells. Am J Physiol Lung Cell Mol Physiol. 2008; 295: L543-51.

82. Pralle A, Keller P, Florin EL, Simons K, Horber JK. Sphingolipid-cholesterol rafts diffuse as small entities in the plasma membrane of mammalian cells. J Cell Biol. 2000; 148: 997-1008.

83. Sorci-Thomas MG, Thomas MJ. Microdomains, Inflammation, and Atherosclerosis. Circ Res. 2016; 118: 679-91.

84. van der Veen JN, Kennelly JP, Wan S, Vance JE, Vance DE, Jacobs RL. The critical role of phosphatidylcholine and phosphatidylethanolamine metabolism in health and disease. Biochim Biophys Acta Biomembr. 2017; 1859: 1558-72.

85. Miao JY, Kaji K, Hayashi H, Araki S. Suppression of apoptosis by inhibition of phosphatidylcholine-specific phospholipase C in vascular endothelial cells. Endothelium. 1997; 5: 231-9.

86. Li Z, Agellon LB, Allen TM, Umeda M, Jewell L, Mason A, et al. The ratio of phosphatidylcholine to phosphatidylethanolamine influences membrane integrity and steatohepatitis. Cell Metab. 2006; 3: 321-31.

87. Cui Z, Houweling M, Chen MH, Record M, Chap H, Vance DE, et al. A genetic defect in phosphatidylcholine biosynthesis triggers apoptosis in Chinese hamster ovary cells. J Biol Chem. 1996; 271: 14668-71.

88. Simons K, Toomre D. Lipid rafts and signal transduction. Nat Rev Mol Cell Biol. 2000; 1: 31-9.

89. Hannun YA, Obeid LM. Ceramide: an intracellular signal for apoptosis. Trends Biochem Sci. 1995; 20: 73-7.

90. Obeid LM, Linardic CM, Karolak LA, Hannun YA. Programmed cell death induced by ceramide. Science. 1993; 259: 1769-71.

AAV1-shRNA	
shSCR	5'-CGAGGGCGACTTAACCTTAGG-3'
shLDLR	5'-TATTAAGGGAGAATGGCGACT-3'
Primers	
Human LDLR	Forward: 5'-TGAGGTCCACATTTGCCACA-3' Reverse: 5'-TCCTCCAGACTGACCATCTGT-3'
Human Lyve-1	Forward: 5'-GCCGACAGTTTGCAGCCTATTG-3' Reverse: 5'-CCGAGTAGGTACTGTCACTGAC-3'
Human FOXC2	Forward: 5'-TCACCTTGAACGGCATCTACCAG-3' Reverse: 5'-TGACGAAGCACTCGTTGAGCGA-3'
Human Podoplanin	SinoBiological, Cat : HP100937
Human Prox1	Forward: 5'-CTGAAGACCTACTTCTCCGACG-3' Reverse: 5'-GATGGCTTGACGTGCGTACTTC-3'
Human VEGFR3	Forward: 5'-GAGCAGATAGAGAGCAGGCAT-3' Reverse: 5'-ACATTCTGGCCAGGTCCTTTAC-3'
Human B2M	Forward: 5'-CCACTGAAAAAGATGAGTATGCCT-3' Reverse: 5'-CCAATCCAAATGCGGCATCTTCA-3'

Table 1. List of sequences for primers and AAV1-shRNA used throughout the study.

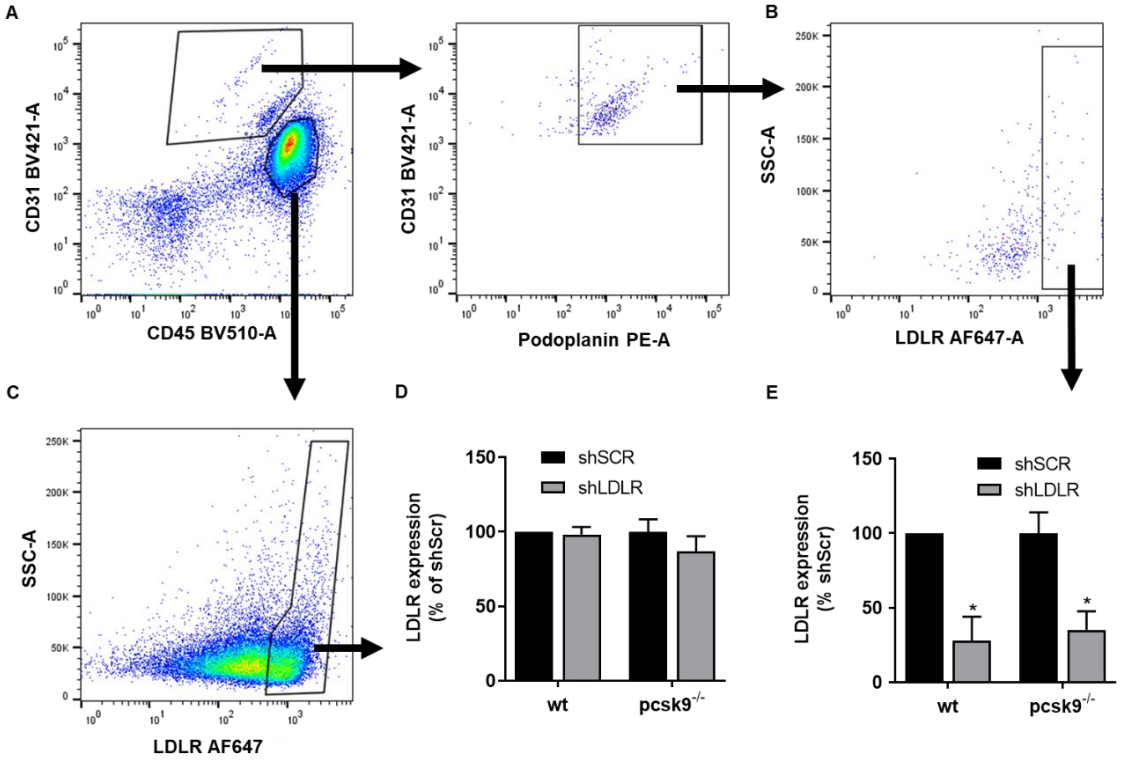

Figure 1. Endothelial cell-specific knockdown of LDLR expression in mice. Two weeks following the intraperitoneal injection of an associated-adenovirus (AAV1) containing a shRNA targeting LDLR in WT and Pcsk9-/- mice, popliteal lymph nodes were harvested, digested and analyzed by flow cytometry. (A) Endothelial cells and leukocytes were selected based on CD31 and CD45 expression, and LDLR levels were measured on (B, E) $CD45^{-}CD31^{+}Podoplanin^{+}$ and (C, D) CD45+ cells. (n=3-4 ; *p<0.05)

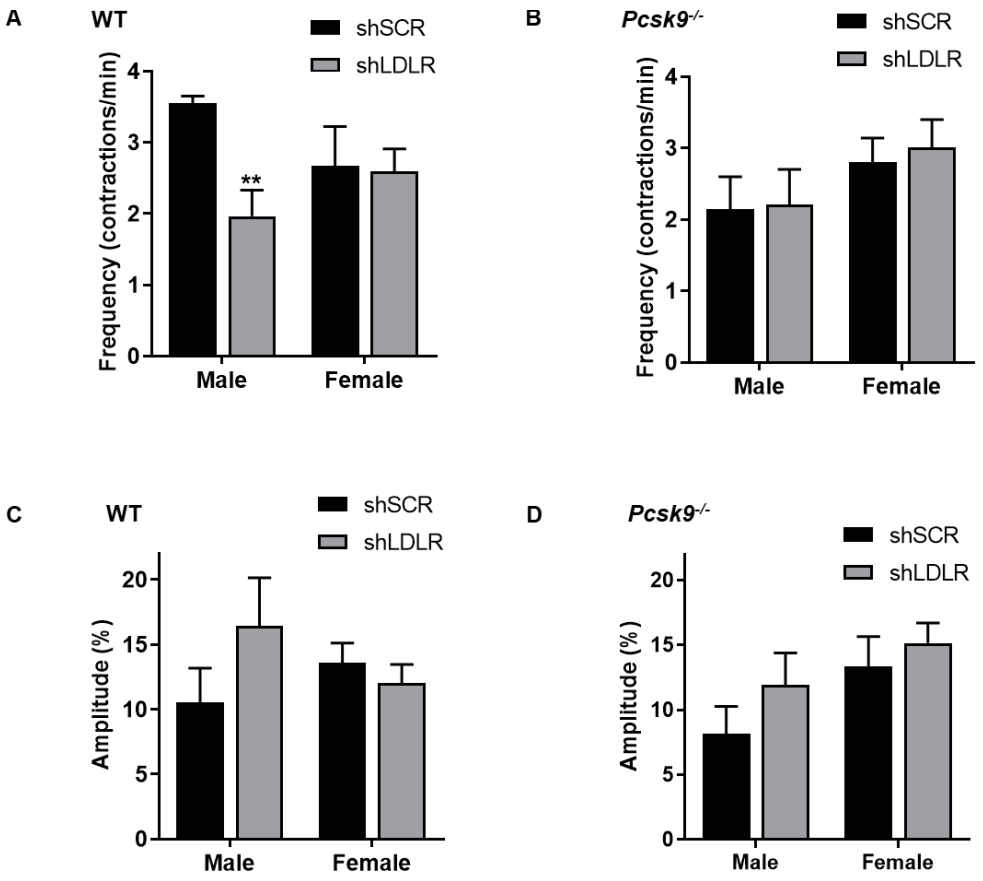

Figure 2. Lymphatic function assessment in mice following a specific knockdown of LDLR in murine endothelial cells. Two weeks after the intraperitoneal injection of an AAV1 containing a shLDLR, lymphatic contraction capacity was assessed by fluorescent *in vivo* imaging in **(A)** WT and **(B)** *Pcsk9*$^{-/-}$ mice. The mean fluorescent amplitude of contraction was also assessed in **(C)** WT and **(D)** *Pcsk9*$^{-/-}$ mice. (n=4-9 ; **p<0.01 vs. shSCR)

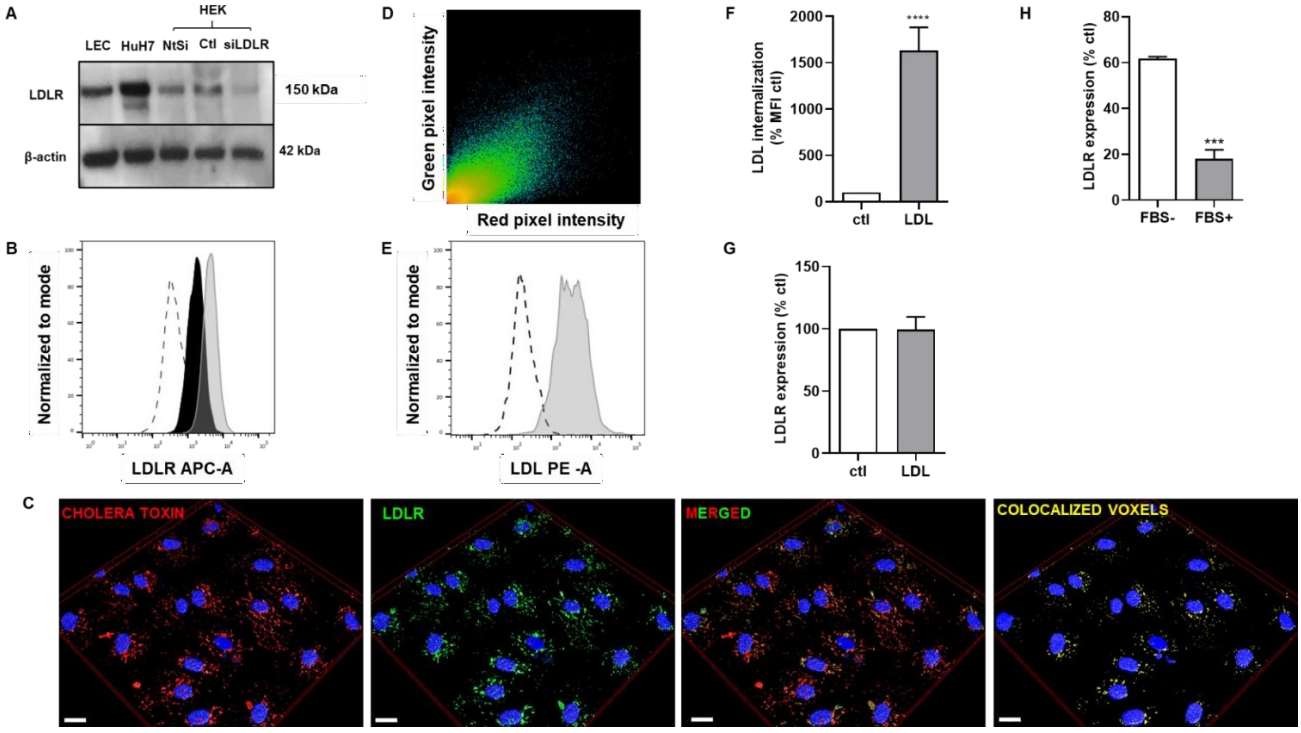

Figure 3. LDLR expression and regulation in human LEC. (A) Expression of LDLR was detected in protein lysates by immunoblotting of HMVEC-dLyAd. Huh7 were used as a positive control and HEK293 cells treated with siLDLR were used as a negative control. LDLR protein expression on LEC was measured by **(B)** flow cytometry after extracellular staining of LEC (black line) and Huh7 (grey line) and by **(C)** immunofluorescence (Blue, DAPI ; red, cholera toxin ; green, anti-LDLR; yellow, colocalized voxels; scale bar, 20 µM). **(D)** Scatterplot of red and green pixel intensities of cholera toxin (red) and anti-LDLR (green) in lymphatic endothelial cells. **(E)** LEC were incubated with Dil-LDL and LDL uptake was measured by flow cytometry (dotted line, no LDL ; grey line, Dil-LDL) and **(F)** results were expressed as % of LDL internalization compared to control. **(G)** Cell surface of expression of LDLR was also determined by flow cytometry. **(H)** Cell surface expression of LDLR was measured by flow cytometry after a 24 h incubation with or without FBS (n=3 ; **p<0.01, ***p<0.001, ****p<0.0001)

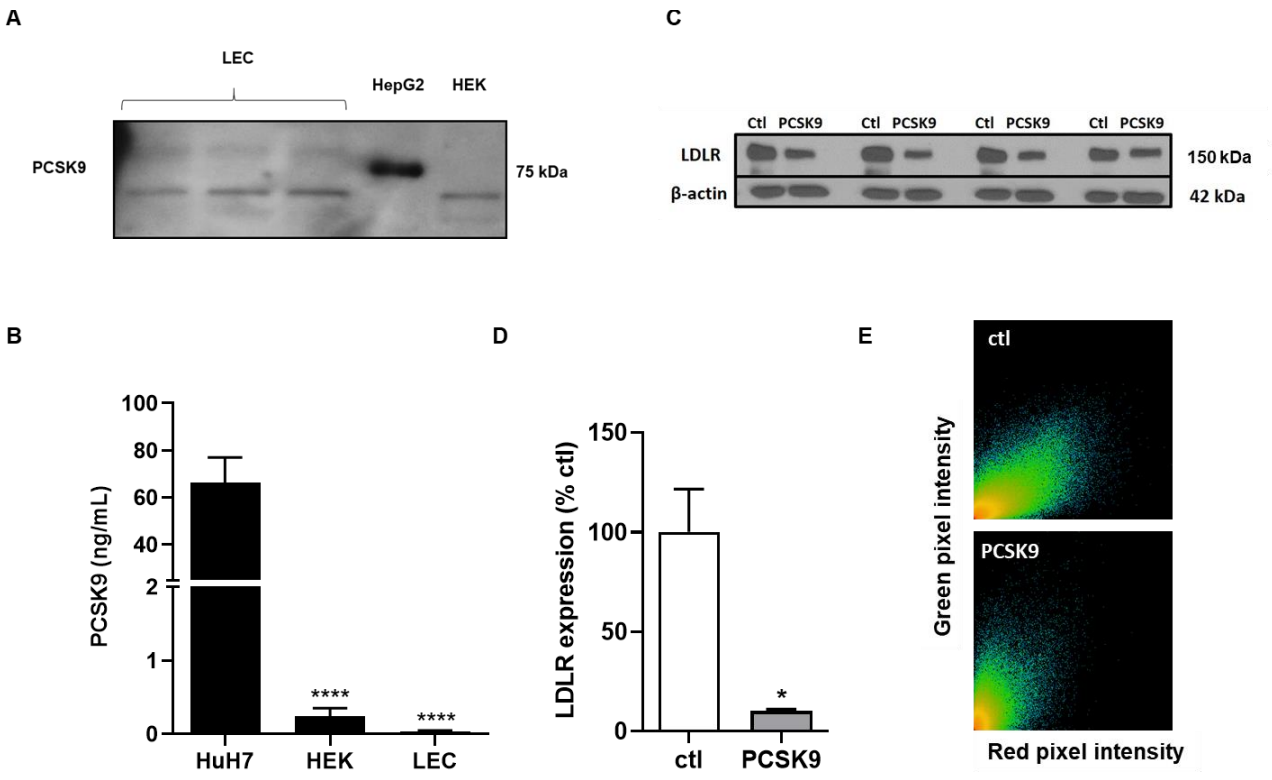

Figure 4. Assessment of PCSK9 expression and secretion by human LEC. (A) PCSK9 expression was measured by immunoblotting in either LEC, HepG2 or HEK293 cell lysates. (B) ELISA was used to measure PCSK9 levels in the cell culture supernatant of Huh7, HEK293 and LEC. Exogenous PCSK9 (6.5 µg/mL) was added to LEC culture media for 16 h and LDLR expression was detected and quantified by (C) immunoblotting and (D) flow cytometry. Data are normalized to control cells without PCSK9 treatment. (E) Representative scatter plot of red and green pixel intensities of cholera toxin subunit B (red) and anti-LDLR (green) in lymphatic endothelial cells. (n=3-5; *****p<0.0001, *p<0.05)

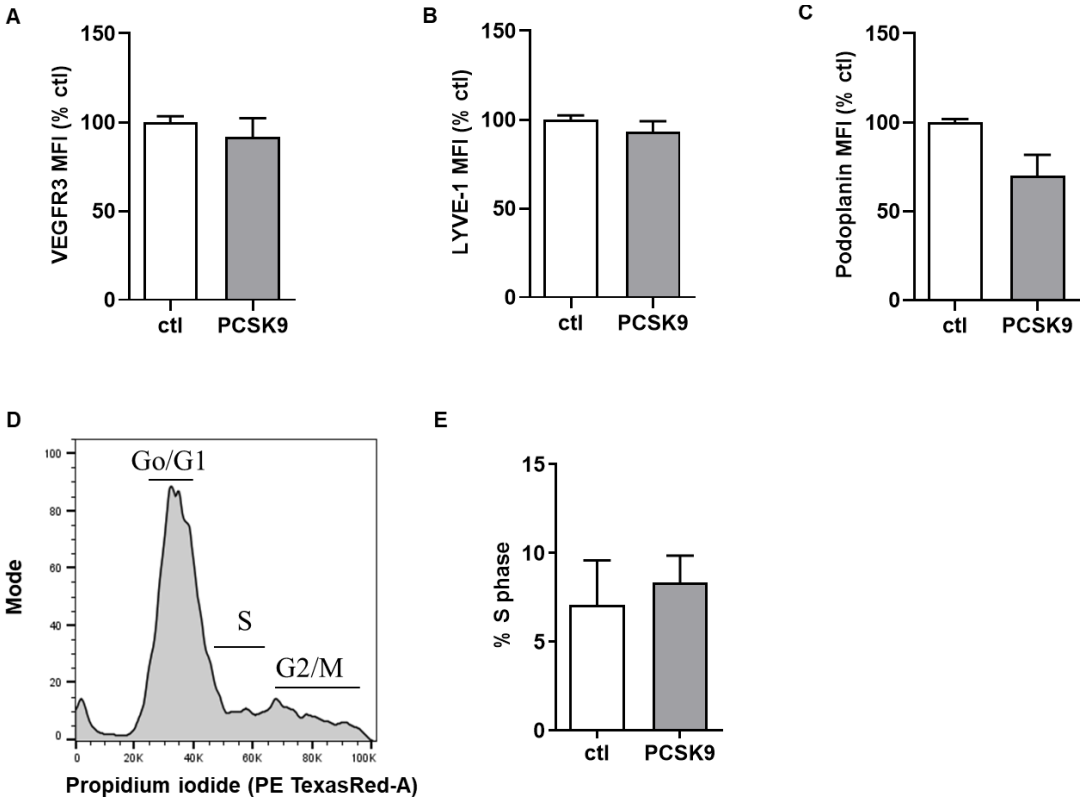

Figure 5. Effect of PCSK9 on LEC integrity. Protein expression of (A) VEGFR3, (B) LYVE-1 and (C) podoplanin was measured in HMVEC-dLyAd following a 16 h incubation with 6.5 µg/ml human recombinant PCSK9. (D) Representative histogram of the assessment of DNA fragmentation performed by flow cytometry, and (E) quantification of the proportion of cells in the S phase following exogenous PCSK9 treatment. (n=3)

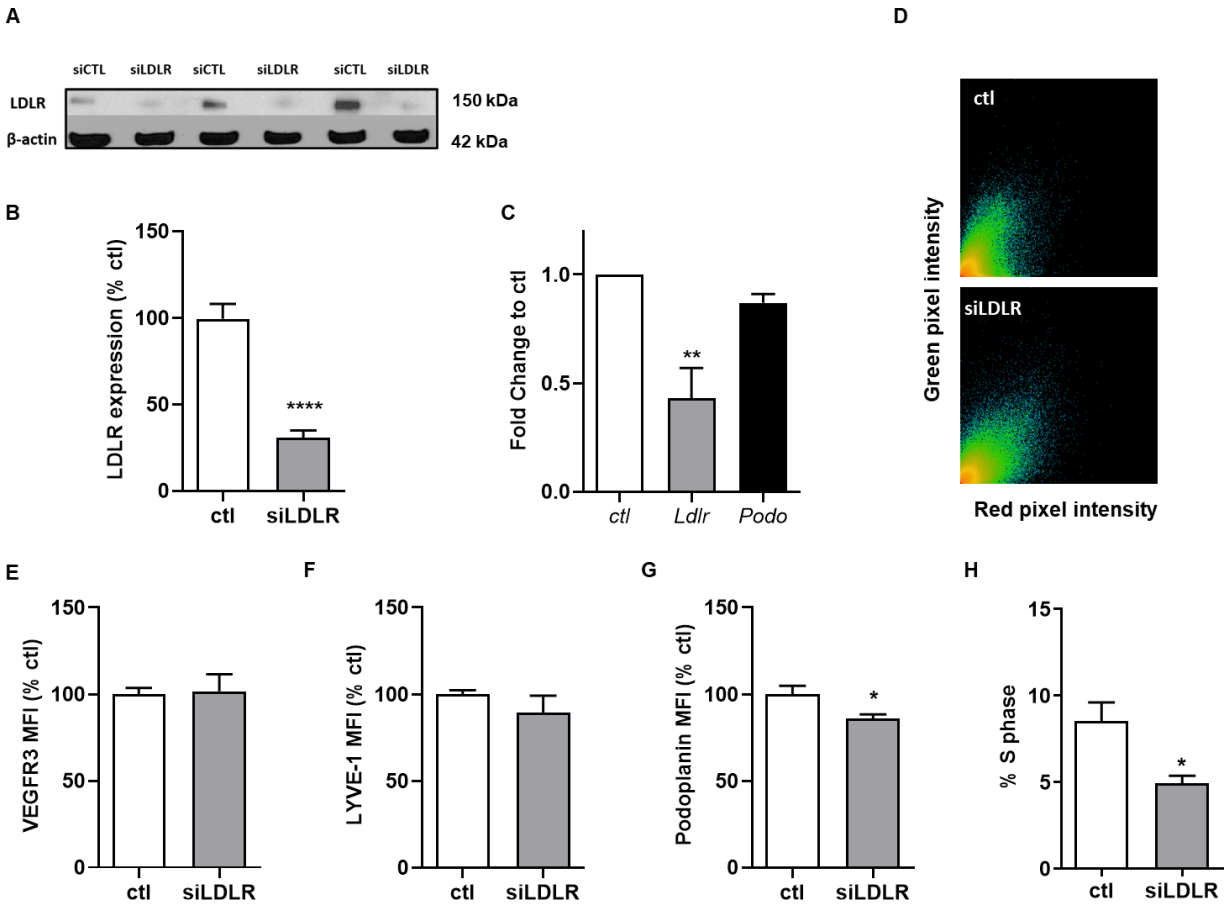

Figure 6. LDLR modulation with a specific siRNA. LDLR expression was measured in LEC in vitro by (A) immunoblotting and (B) flow cytometry following treatment with 25 nM of non- targeting siRNA or siLDLR for 48 h. (C) LDLR and podoplanin mRNA expression in LEC was assessed by qPCR. (D) Representative scatterplot of red and green pixel intensities of cholera toxin (red) and anti-LDLR (green) in lymphatic endothelial cells. Protein expression of (E) VEGFR-3,

(F) LYVE-1 and (G) podoplanin were measured by flow cytometry following treatment with 25 nM of siCTL or siLDLR. (H) Quantification of the proportion of cells in the S phase following 25 nM of siCTL or siLDLR. (n=3-4 ; *p<0.05,**p<0.01, ****p<0.0001)

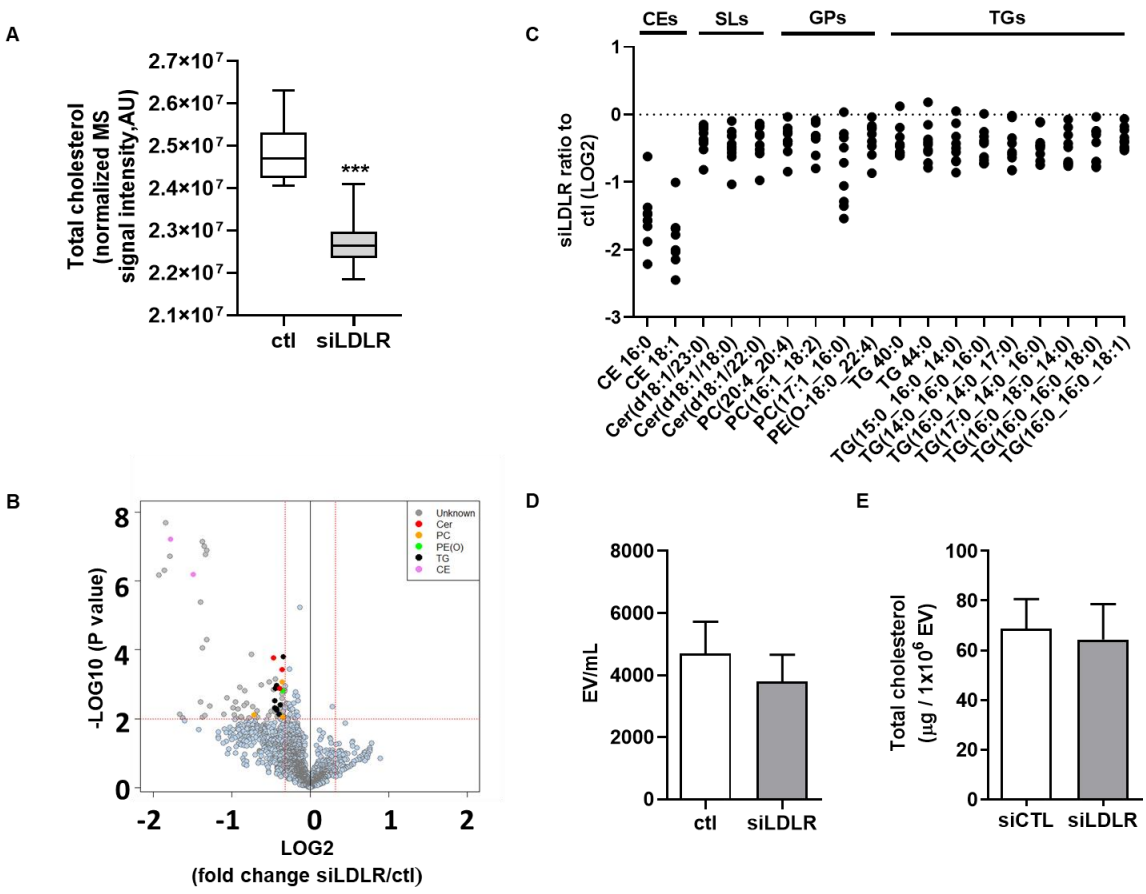

Figure 7. Untargeted lipidomics in siLDLR-treated LEC. LEC were treated *in vitro* with 25 nM of siLDLR or siCTL for 48 h and MS-based lipidomics analysis of cellular extracts from siLDLR and control-treated cells was performed. **(A)** Total cholesterol and **(B)** 2139 MS features were obtained using p-values expressed as -log10 (threshold p-value<0.01), and **(C)**18 unique lipid (sub)classes discriminating siLDLR- and siCTL- treated cells were identified. Each dot represents a log2-tranformed siLDLR/siCTL signal intensity ratio. **(D)** Extracellular vesicles derived from LEC *in vitro* were quantified by flow cytometry and **(E)** their total cholesterol content was measured following a 30 min incubation with a detergent (triton X-100) by colorimetry. EV, extracellular vesicles; CE, cholesteryl esters; Cer, ceramides; GPs, glycerophospholipids; PC, phosphatidylcholine; PE(O-), phosphatidylethanolamine (plasmanylethanolamine); SLs, sphingolipids; TGs, triglycerides. "_" in TGs refers to acyl chains for which the position remains to be ascertained. (n=3-9 ; ***p<0.001)

SUPPL.
FIGURES

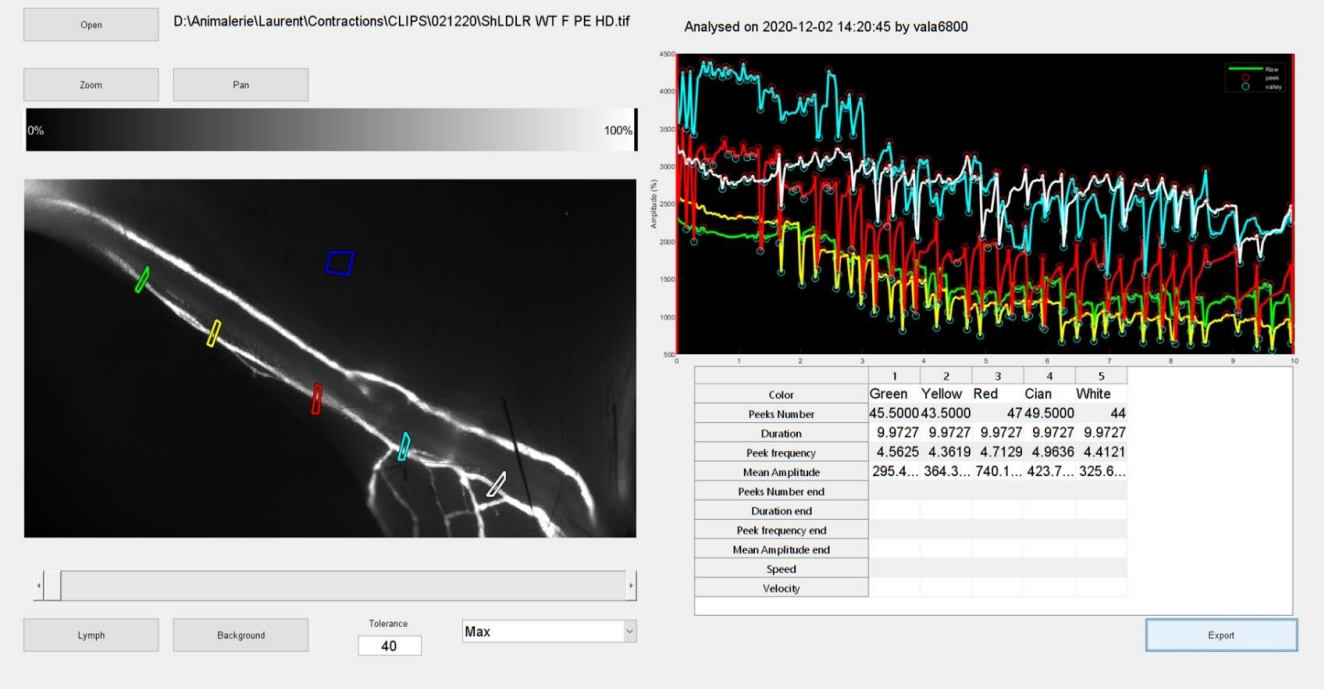

	1	2	3	4	5
Color	Green	Yellow	Red	Cian	White
Peeks Number	45.5000	43.5000	47	49.5000	44
Duration	9.9727	9.9727	9.9727	9.9727	9.9727
Peek frequency	4.5625	4.3619	4.7129	4.9636	4.4121
Mean Amplitude	295.4...	364.3...	740.1...	423.7...	325.6...
Peeks Number end					
Duration end					
Peek frequency end					
Mean Amplitude end					
Speed					
Velocity					

Figure S1. Representative screenshot of the LymphPulse 3.0 Matlab™ based software.

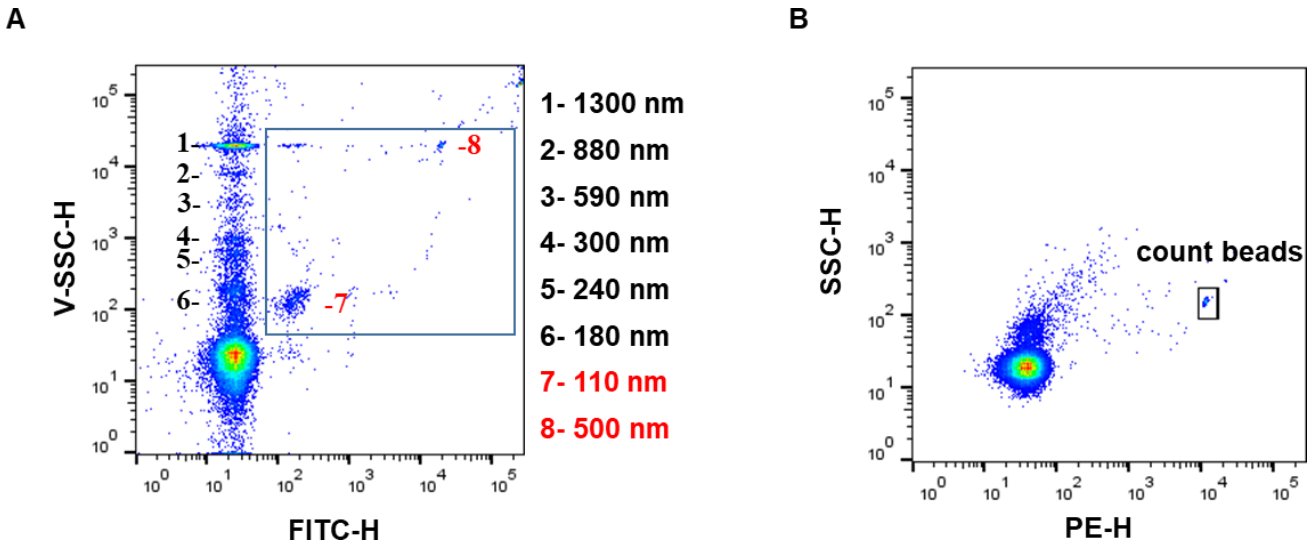

Figure S2. Cytometer setup for the measurement of extracellular vesicles in cell culture media. (A) The flow cytometer was calibrated for EV detection using the ApogeeMix containing non-fluorescent silica beads (black; 180, 240, 300, 590, 880, and 1300 nm) and FITC-fluorescent latex beads (red; 110 and 500 nm). **(B)** PE-fluorescent count beads (3 µM in diameter) were used to quantify the concentrationof beads per sample.

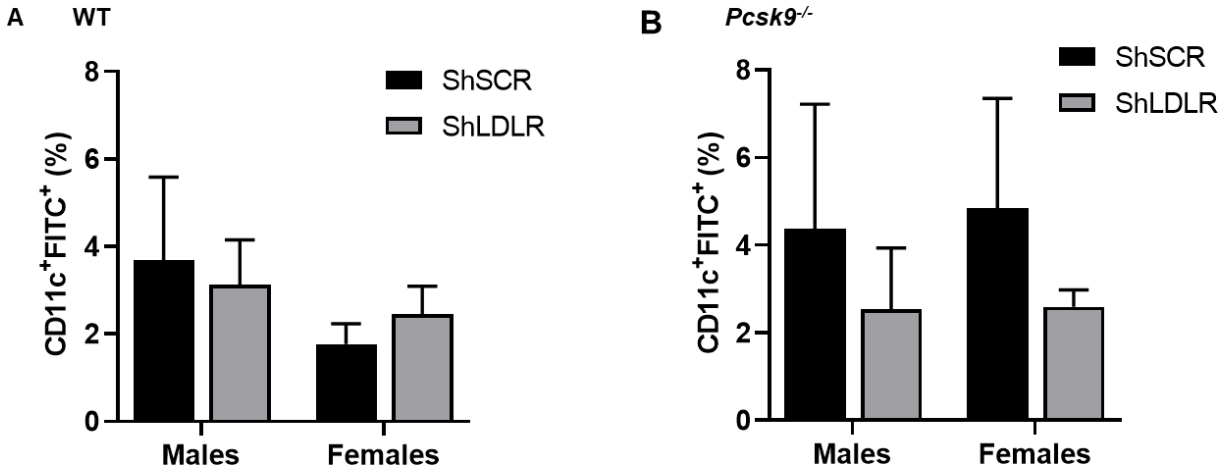

Figure S3. Dendritic cell migration from the skin to draining lymph nodes following a specific knockdown of LDLR in mouse endothelial cells. Dendritic cell migration was determined following a18 h contact sensitization assay in 3-month-old **(A)** WT and **(B)** *Pcsk9*$^{-/-}$ mice.